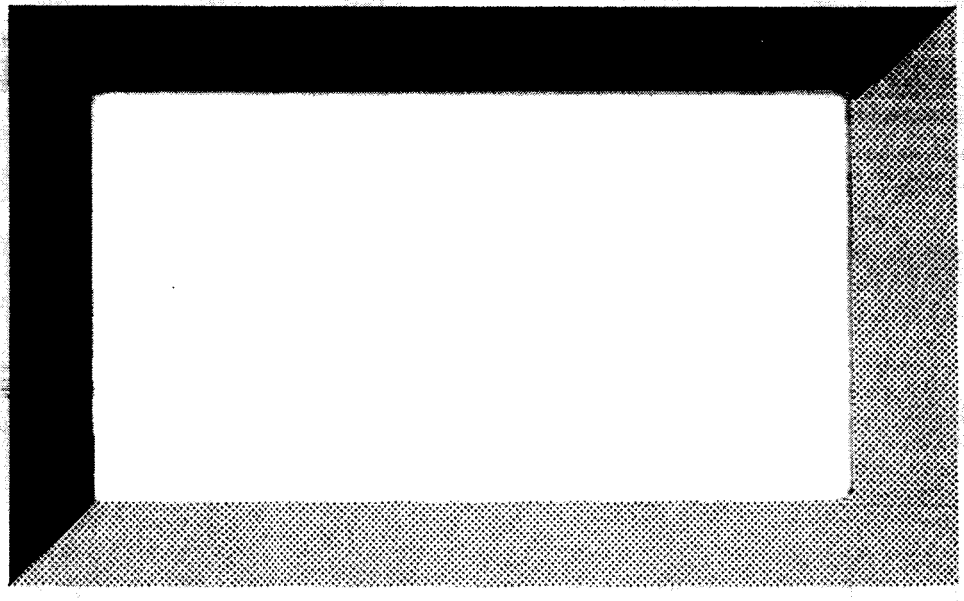

GAS TURBINE LABORATORY
MASSACHUSETTS INSTITUTE OF TECHNOLOGY
CAMBRIDGE, MASSACHUSETTS

DESIGN AND EVALUATION OF A PULSING JET INJECTOR FOR ROTATING FAN EXCITATION

by

Gregory P. Buliavac
Edward F. Crawley

GTL Report No. 185 October 1985

This research was sponsored under NASA Lewis Research Center grant NSG-3079, monitored by Mr. Donald Boldman and Mr. Calvin Ball.

Acknowledgements

This research was sponsored under NASA Lewis Research Center grant NSG-3079, monitored by Mr. Donald Boldman and Mr. Calvin Ball.

Abstract

The feasiblity of using injected pulsing jets to excite the aeroelastic modes of a rotating fan was investigated. An unsteady velocity deficit is created in the wake behind a circumferentially injected jet at the frequency of jet pulsation. Adjacent jets are phased so that their interaction and diffusion with the mean flow creates a spatially sinusoidal wake. This spatially sinusoidal wake rotates around the flow annulus, resulting in the excitation of traveling wave vibration modes in the fan.

A prototype jet injector was designed and constructed which produces high frequency pulsing jets, which meet the requirements of a fan aerodynamic damping experiment to be performed at the NASA Lewis Research Center Multistage Compressor Test Facility. This prototype was first used to produce a single steady jet in the absence of a cross flow to determine its flow characteristics. These jets conformed to classical jet models. Pulsing jets were then produced to evaluate the ability of the injector to produce high frequency pulsing jets. No acoustic limitations to the maximum jet pulsing frequency were discovered.

The prototype was then installed in a low turbulence wind tunnel. The behavior of a single steady jet in a cross flow was studied. The jets produced behaved similarly to classical studies of steady jets injected into a cross flow. Pulsing jets were then studied to determine if the fan to be excited would experience a periodic excitation, and to evaluate the ability of the phased jets to form a spatially sinusoidal wake for traveling wave excitation. Results indicate that the excitation force on the fan will remain periodic if the jet injection point is close enough to the plane of the fan and that spatially sinusoidal wakes are formed. It was therefore concluded that there are no fundamental fluid mechanical obstacles to using pulsing jets to excite traveling wave vibrations in a rotating fan. A preliminary design and design criteria for such a device are given.

Contents

List of Figures

1. Introduction

Increasing the efficiency and performance of fans and compressors is a continuing focus of gas turbine research. One of the factors which limits both the efficiency and performance of a fan is its flutter speed. The flutter boundary limits the speed at which the fan can operate, thus influencing the maximum stage pressure ratio which can be achieved. The need to design against flutter also influences the blade thickness, chord, and inclusion of mid span shrouds, all of which can adversely affect efficiency.

Throughout the development of a new fan, extensive flutter testing is performed. When a typical flutter test is performed only one piece of information, the location of the flutter boundary on the compressor map, is obtained. It would be advantageous to obtain more information about the aeroelastic behavior of the fan as this boundary is approached. In particular, it wouldbe desirable to measure the aerodynamic damping in the system as the rotor speed approaches the flutter boundary. Since the ability to accurately predict flutter is of extreme importance in engine design, this additional information could be used to better correlate the analytical model of flutter onset with the experimental measurement. Additionally, this information could be used to determine the sensitivity of the aerodynamic damping to the rotor speed as the flutter boundary is approached. This information could be invaluable in making

redesign decisions during fan development.

To determine the extra information desired, the sub-flutter aerodynamic damping, it is necessary to use system identification techniques. System identification consists of two parts. The first part is the excitation of the system to be studied. The second part is the analysis of the response of the system to that excitation in order to extract the system parameters of interest, in this case the aerodynamic damping data. This report will focus on the development of a method to excite the vibrational modes of interest in a rotating fan, for the ultimate objective of system identification of the aerodynmic damping.

In order for an excitation system to be useful it must meet several requirements. First, it must have sufficient amplitude to excite the rotor in the working environment. Second, it must function at an arbitrary frequency or over a broad band of frequencies. Third, it must be able to excite an arbitrary interblade phase angle or a broad band of interblade phase angles. Finally, it must either be explicitly known, in order to allow determination of the transfer function between excitation and response, or it must possess the capability to be turned off instantaneously, in order to allow measurement of the transient decay of the system.

Several methods of fan excitation have been proposed and used in previous experiments. These include the use of piezoelectric crystals, electromagnetic drivers, injected steady jets, and

screens placed in the upstream flow.

The first excitation method mentioned above involves the use of piezoelectric crystals attached directly to the blades to apply a driving force [1,2]. This allows very accurate control of the phasing of the forcing applied to each blade, thus allowing precise control of the frequency and interblade phase angle. However, piezoelectrics are limited in the power they can provide, and may be inadequate for excitation of fans operating in high speed flows.

A second method of fan excitation entails the use of an electromagnetic coil system to drive ferromagnetic fan blades [3]. In principle precise control over frequency and interblade phase is possible. However, this method can only be implemented easily for excitation of a non-rotating fan, and strength of the possible excitation is again in question.

A third method to provide excitation is to use steady jets injected into the tunnel flow [4]. The injected jets form disturbances in the flow at predetermined circumferential locations, thus causing the fan blades to feel an unsteady forcing as they rotate. Although this method has been successfully used in previous experiments to provide strong excitation to the rotor, it cannot be used to excite traveling wave modes in a rotating fan, and thus fails the requirement for control of the excitation interblade phase angle.

Another method involves placing screens or rods into the flow

at various circumferential locations [2,3]. The screens or rods form velocity defects in the flow which excite the rotating fan downstream. This method also has been used successfully for simulation of upstream disturbances, but lacks the ability to excite arbitrary traveling wave modes in a rotating fan. Thus, of the four existing methods for fan excitation, two, piezoelectrics and electromagnetics, lack sufficient power, and two, steady jets and screens, lack sufficient versatility.

The purpose of this study is to examine the feasibility of an alternate method of fan excitation. This method involves using pulsating jets injected into the axial flow just upstream of the rotor. The circumferentially injected jets interact with the mean flow creating a wake. The blades respond to this unsteady wake. Ideally it would be desirable to inject a spatially sinusoidal continuous circumferential jet into the flow. However, this is quite difficult to implement in a simple way. It is hoped that by properly phasing the pulsation of circumferentially discrete jets the interaction of the jets and their subsequent diffusion in the mean flow will simulate a spatially sinusoidal disturbance. It is expected that this method would be capable of producing the necessary excitation while remaining versatile enough to excite a wide range of frequencies and interblade phase angles.

In order to practically implement pulsing jet excitation in a fan, a device must be designed and constructed which is capable of producing jets which are valved at high frequencies. A large

number of these jets, all pulsed in the proper relative phase, are needed around the circumference of the flow annulus.

In order to evaluate this excitation method, it was necessary to design and build a prototype device capable of producing these pulsing jets and to make detailed measurements of the jet injection interacting with the mean flow in a wind tunnel. It was also necessary that the prototype jet injector be designed to be physically representative of the mechanical design of the actual device intended for fan excitation.

The prototype injector used in this experiment was designed specifically to meet the excitation requirements for an experiment to be performed in the NASA Lewis Research Center Multistage Compressor Test Facility (W8). This experiment involves the measurement of aerodynamic damping in a tuned, structurally mistuned, and aerodynamically detuned, shroudless rotor. Structural mistuning and aerodynamic detuning are both methods of increasing the stability of a shroudless rotor [5,6].

The design and evaluation of such a prototype injector requires a detailed understanding of the behavior of pulsing jets injected into a cross flow. To acquire this understanding it is beneficial to first understand the behavior of steady jets entering a cross flow. These flows have been the subject of several classic experiments, motivated by studies of thrust vectored jets of vertical take-off aircraft, secondary jet cooling in gas turbine combustors, and atmospheric plumes from chimneys.

These studies generally involve injecting jets into cross flows at various angles of incidence and then determining the jet trajectory. Callaghan and Ruggeri [7] investigated the penetration distance of a jet injected perpendicularly to the air stream at a variety of flow conditions and obtained an empirical equation for the penetration in terms of the other flow parameters. Jordinson [8] measured total pressure distributions of a jet injected normal to the cross flow and determined the path of the jet and the shape of the jet cross-section. Kamotani and Greber [9] took velocity, temperature, and turbulence intensity measurements of a jet directed perpendicularly to the free stream and determined the functional relationships between the penetration depth and the momentum ratio of the jet to the freestream. Margason [10] has also made measurements of the path and shape of the wake of a single jet exiting at large angles to the free stream and developed equations to describe the jet path. Margason's results were then compared with equations for the jet path from other investigations.

Relatively little research has been done on unsteady jets, and none found on the injection of unsteady jets into a cross flow. Work by Curtet and Girard [1] involved flow visualization of a pulsating jet in the absence of a cross flow to show its time evolution. Kovasznay, Fujita and Lee [12] examined discrete and unsteady puffs and attempted to develop theoretical representations of such unsteady turbulent flows using ensemble

averaging to obtain mean values of velocity and turbulence levels within the puffs.

This report will explore the behavior of periodically pulsing jets injected into a cross flow in an attempt to determine the feasibility of using them to excite controlled vibrations in a rotating fan. A series of conceptual questions must be answered. The first is whether there are any acoustic limitations to the frequency attainable by a pulsating jet, due to the length of the jet plenum. It is possible that the Helmholtz frequency of the jet plenum may limit the jet frequency which can be achieved. It is also necessary to know if, at high frequencies, the pulses will remain discrete until they reach the rotor, or will they mix and simply create a turbulent flow with no discrete temporal periodicity. The next conceptual question is whether or not a phasing of neighboring jets can be used to form a pattern of forcing which varies sinusoidally spatially as well as temporally. The last conceptual concern is to determine if the jet will penetrate far enough into the flow to create a sufficiently deep wake to excite the blades.

The second goal of this study is to show the feasibility of the mechanical design of such an injector. This involves the design and construction of a prototype which is capable of producing jets which satisfy the needs of the real experiment as well as simulating a design which is a feasible configuration for the planned tests at NASA Lewis. The operation of the prototype

must properly simulate the operating conditions of this experiment to adequately determine its potential for success. Potential problems include pressure losses in tubing, leakage, and crosstalk between neighboring jets.

In Chapter 2 the principle behind the use of pulsating jets to excite vibrations in rotating fans will be discussed. Then the basic calculations for determining the jet pulsing frequency, the jet spacing, and the jet diameter will be presented. Finally, the potential fluid dynamic limitations and mechanical difficulties, to be evaluated in this report, will be introduced.

A discussion of the behavior of steady jets injected into a cross flow will be presented in Chapter 3 to provide a foundation for acquiring an understanding of the behavior of pulsing jets. A summary of investigations into the behavior of steady jets and models that have been developed is also presented. Finally, the additional complicating factors associated with the unsteadiness of a pulsating jet, and the reduced frequencies of importance, will be introduced.

In Chapter 4 the design of the prototype experiment is presented with the calculations upon which the design is based. The testing procedure and the test objectives are then outlined. Finally, the methods used for data reduction and analysis are presented.

The experimental results of the testing program will be presented and discussed in Chapter 5. The behavior of steady jets

both in the absence and presence of a cross flow is observed and compared to classic analysis. Then, the behavior of pulsing jets both in the absence and presence of a cross flow is observed and compared to the behavior of steady jets. Conclusions are then drawn concerning the feasibility of using pulsing jets to excite vibrations in rotating fans.

2. Design Considerations for a Jet Injector for Fan Excitation

This chapter outlines a proposed design for a device capable of injecting pulsing jets into the test section of a compressor test facility for the purpose of the controlled excitation of vibration in a rotating fan. The success of this design depends upon several fundamental fluid dynamic considerations, as well as several practical design and implementation considerations. These design considerations are enumerated in this chapter and will be resolved by the testing program presented in Chapter 5.

The fundamental concept of using pulsing jets for fan excitation is presented in Section 2.1. The specific design calculations are presented in Sections 2.2 and 2.3, based on the demands of the mistuned fan experiment planned at the NASA Lewis Research Center. The fundamental fluid dynamic considerations of the design will be discussed in Section 2.4. Finally, the practical implementation considerations will be discussed in Section 2.5.

2.1 Conceptual Design

A steady jet injected into a cross flow causes a blockage, which results in a decrease in total pressure and velocity in the region directly behind the jet. The jet is turned by this pressure difference, carrying a total pressure excess along the jet trajectory. Downstream then, the net result of the transverse

jet is a total pressure deficit near the wall surface pierced by the injected jet and a smaller total pressure excess due to the residual jet velocity at a height above the wall surface. This behavior will be discussed in more detail in Chapter 3. It is postulated that by pulsing the jet these total pressure and velocity defects and excesses can likewise be made to pulsate.

These pulsing velocity defects will in turn be felt by the blades just downstream of the injector. This nonuniform inflow velocity will cause an unsteady loading on the blading which will provide the excitation force to the fan. By pulsing the jets sinusoidally in time, a temporally periodic excitation force should result. The desired frequency of the pulsing jet will depend on the rotor configuration, speed, and the number of blades, as will be discussed in Section 2.2

However, pulsing the jets sinusoidally in time alone is not sufficient to excite the aeroelastic vibration modes in a rotating fan. The natural vibration modes take the form of traveling waves with an interblade phase angle β_n which depends on the number of blades, N, and the number of nodal diameters, n, in the particular mode. This relationship is:

$$\beta_n = \frac{2\pi n}{N} \qquad (2.1)$$

where β_n is expressed in radians. The pattern of nodal diameters is defined as the locus of points on which the blades have no deflection. This pattern is not stationary, but rotates around the fan as the blades oscillate. In order to excite pure

aeroelastic modes it is therefore necessary to use a traveling wave which is spatially sinusoidal. In principle this would entail using a continuous jet injected around the circumference of the wind tunnel which is throttled to produce a wake which is spatially sinusoidal. Since it is nearly impossible to produce such a continuous jet, it is hoped that a series of discrete jets which are phased properly can be used to approximate a continuous throttled gust. This concept is illustrated in Fig. 2.1 As the jets pulsate, the result will be an approximately spatially sinusoidal velocity deficit at the rotor tip which rotates around the circumference of the compressor test section.

Thus the concept can be summarized as follows. The result of pulsing each jet sinusoidally with an appropriate difference in phasing between adjacent jets is to produce an excitation force which varies sinusoidally both spatially and temporally, and which forms a traveling wave of velocity deficit around the annulus. The temporal variation will excite the blades at a fixed frequency, and the spatial variation will cause the blades to vibrate with a specific interblade phase angle. The interblade phasing is determined by the number of nodal diameters desired in the vibration mode and the number of blades on the fan. The pulsing frequency of a given jet is determined by the rotation speed of the fan, the number of nodal diameters of the mode to be excited, and the blade frequency in the rotating frame which is to be excited.

2.2 Calculation of Desired Pulsing Frequency

The required pulsing frequency of an individual jet depends on several factors. These include the number of nodal diameters in the mode to be excited, the rotational speed of the rotor, and the natural frequency of the blades in the rotating frame to be excited. To find this relationship, it is necessary to start from the expression for the excitation forcing pattern as viewed in the nonrotating (test section) frame. The forcing is a function of the circumferential position Ψ measured in the nonrotating frame as shown in Fig. 2.2 and time, and can be expressed as:

$$f_N(\Psi,t) = f\cdot\cos(n\Psi - \omega_N t) \qquad (2.2)$$

where f_N is the magnitude of the forcing at a given circumferential position Ψ and time t, f is the maximum amplitude of the forcing, n is the number of nodal diameters in the particular mode, and ω_N is the frequency of the jet in the nonrotating frame. This assumes the jet pattern is perfectly sinusoidal both temporally and spatially. The jet frequency in the nonrotating frame can also be expressed as:

$$\omega_N = n\Omega_N \qquad (2.3)$$

where Ω_N is the jet pattern rate of rotation as viewed in the nonrotating frame. Equation 2.2 now becomes:

$$f_N(\Psi,t) = f\cdot\cos(n\Psi - n\Omega_N t) \qquad (2.4)$$

It is then necessary to make a transformation from the nonrotating

frame to the rotating frame by letting:

$$\Psi = \theta + \Omega t \tag{2.5}$$

where θ is the circumferential position of a point measured with respect to the rotating frame attached to the fan as shown in Fig. 2.2. Substituting into equation 2.4 gives:

$$f_R(\theta,t) = f\cdot\cos(n\theta + n\Omega t - n\Omega_N t) \tag{2.6}$$

where f_R is now the magnitude of the forcing as observed in the rotating frame. Equation 2.6 can be reduced to:

$$f_R(\theta,t) = f\cdot\cos[n\theta + n(\Omega - \Omega_N)t] \tag{2.7}$$

Equation 2.7 is the expression for the forcing magnitude in the rotating frame, and is analogous to equation 2.4, the expression for the forcing in the nonrotating frame. The pattern still has n nodal diameters, but they are observed at a frequency ω_R:

$$\omega_R = n(\Omega - \Omega_N) \tag{2.8}$$

where ω_R is the effective jet frequency as observed in the rotating frame, i.e., the frequency in the rotating frame at which a blade is to be excited. This should correspond to the blade natural frequency, since flutter in fans occurs most commonly at a blade natural frequency. Equation 2.8 can also be expressed as:

$$\Omega_N = \Omega - \frac{\omega_R}{n} \tag{2.9}$$

Combining equations 2.3 and 2.9 yields:

$$\omega_N = n\Omega - \omega_R \tag{2.10}$$

This expression now gives the jet frequency as observed in the nonrotating frame in terms of the known values n, Ω, and ω_R, where ω_R is the desired excitation frequency in the rotating frame.

Note that by the sign convention chosen in equation 2.8 if $\omega_R>0$, we find that $(\Omega-\Omega_N)>0$, or $\Omega>\Omega_N$. Thus the excitation moves more slowly than the rotor, and as viewed in the rotating frame of reference is a backward moving excitation. If $\omega_R<0$, then $(\Omega-\Omega_N)<0$ and $\Omega<\Omega_N$, and a forward moving excitation in the rotating frame occurs.

Table 1 shows values of ω_N for various values of n at the design parameters for the planned mistuned fan experiment. For a value of $\omega_R<0$, that is, forward excitation, ω_N is always positive, thus forcing is always forward in the nonrotating frame. For $\omega_R>0$, that is, backward excitation, we have backward excitation in the nonrotating frame for small n. This results in ω_N having a value that is negative. Since the concept of negative frequency has no physical meaning, these values for ω_N are plotted in Fig. 2.3 as positive. For larger n, we have forward excitation in the non-rotating frame. The data from this table is plotted in Fig. 2.3

Table 1. Ω_N and ω_N as functions of n for the rotor parameters of the planned mistuned fan experiment.

n	F_R (w_R < 0)		B_R (w_R > 0)	
	Ω_N	w_N	Ω_N	w_N
0	∞	1100	∞	-1100
2	817	1633	-283	-567
4	542	2167	-8	-33
6	450	2700	83	500
10	377	3767	157	1567
15	340	5100	193	2900
20	322	6433	212	4233
25	311	7767	223	5567
30	303	9100	230	6900

It is important to note that for nodal diameters above half the number of blades, aliasing occurs and the backward excitation again looks like forward excitation in the rotating frame. In other words, above $n = \frac{N}{2}$, where N is the number of blades on the rotor, backward excitation cannot be identified. The backward excitation branch folds back, and recrosses the forward excitation branch. This joining occurs at:

$$n = \frac{N}{2} + \frac{\omega_R}{\Omega} \tag{2.11}$$

ω_R having its negative value. At this value of n, Equation 2.10 becomes:

$$\begin{aligned} \omega_N &= \left[\frac{N}{2} + \frac{\omega_R}{\Omega} \right] \Omega - \omega_R \\ &= \frac{N\Omega}{2} + \omega_R - \omega_R \\ &= \frac{N\Omega}{2} \end{aligned} \tag{2.12}$$

which is half the blade passing frequency. Therefore the maximum frequency necessary for ω_N, the jet pulsing frequency, is half the blade passing frequency. If the jets can be pulsed at this frequency, the entire range of interblade phase angles can be excited.

Thus the frequency of jet pulsing has been completely determined. Given ω_R, the desired frequency of excitation (positive for backward moving waves and negative for forward moving waves) and n, the number of nodal diameters, Equation 2.10 defines ω_N except when n is larger than $\frac{N}{2}$. In this case the design is on the branch where backward excitation in the rotating

frame is aliased to forward excitation. On this branch:

$$\omega_N = -\Omega n + \left[2 \cdot \left[\frac{N}{2}\Omega - \omega_R\right] + \omega_R\right] \qquad (2.13)$$

or the jet pulsing frequency is given by:

$$\omega_N = -\Omega n + N\Omega - \omega_R \qquad (2.14)$$

2.3 Calculation of Jet Spacing and Diameter

Now that an expression for the jet pulsing frequency has been obtained, it is necessary to determine an appropriate size and spacing for the jets. The objective is to create an approximately continuous spatially sinusoidal pattern using discrete jets. This merging into a continuous pattern will occur due to the diffusion of the jets into the mean flow.

The choice of jet spacing depends in part on the distance the jet injector is located upstream of the rotor face. Since jets diffuse as they are convected downstream, the further the distance to the rotor the greater the allowable spacing becomes. Of course the further the downstream distance from jets to rotor face, the weaker the velocity deficit becomes, also due to diffusion with the axial flow. A good compromise is to locate the injector holes approximately ten jet diameters upstream.

Previous investigations [8] determined that a jet will diffuse by approximately a factor of four at a station eleven jet diameters downstream. Therefore, to insure that neighboring jet wakes would appear merged at the rotor face, it was decided to space the jets three jet diameters apart.

In order to insure that a particular blade would perceive a smooth spatial excitation force in modes with a large number of nodal diameters, it was decided to use four jets per blade spacing. For the experiment to be performed at the NASA Lewis Research Center the blade spacing is 1.5". This indicated a jet spacing around the circumference of the wind tunnel of about .375". For this distance to be three jet diameters, a jet diameter of .125" was required. To achieve the desired magnitude of mixing diffusion, over the converted distanceof ten jet diameters, this dictated that the jets should be located approximately 1.375" upstream from the rotor. It was estimated from the jet penetration depth equations presented in Chapter 3 that these conditions will produce a jet penetration distance capable of producing a sufficient excitation amplitude. These design rules are illustrated in Fig. 2.4

Having determined the frequency at which the jets must be pulsed, the spacing, and the axial location, there remains only the relative phasing of the adjacent jets to determine. If the J jets are spaced uniformly around the circumference of the test section, the circumferential angle α between them is:

$$\alpha = \frac{2\pi}{J} \tag{2.15}$$

where α is expressed in radians. The relative phase between two jets depends on the number of nodal diameters in the pattern to be excited:

$$\beta_j = n\alpha = \frac{2\pi n}{J} \tag{2.16}$$

where β_j is the relative phase angle between jets also expressed in radians. Note that in order to excite different spatial patterns (nodal diameter modes) it is necessary to provide a means to change β_j, the relative phase of adjacent jets.

The design requirements for the injector are now completely specified. The injector must be capable of creating pulsing jets at frequencies up to one half the blade passing frequency, with relative phase between jets given by expression 2.16 above. It should be located such that the size, phasing, and axial location of the jets follow the rules oultlined above.

2.4 Fundamental Fluid Mechanical Considerations

The feasibility of using pulsating jets to excite vibrations in rotating fans depends upon the answers to some fundamental questions of fluid mechanics. The purpose of this study is to determine whether or not the system of jets proposed in the previous section will behave as anticipated. The first potential problem to be resolved is to determine if there is an acoustic limit to the frequency at which a jet can be pulsed. It is expected that the maximum pulsing frequency of half the blade passing frequency will be quite high, on the order of several kilohertz. If this frequency is above the Helmholtz resonant frequency of the jet plenum, it is possible that the flow will be attenuated. This would limit the jet pulsing frequency which could be obtained for a given injector, or would necessitate

changes in the mechanical design of the jet injector system.

The second concern is over whether the jet pulses will maintain their integrity and be felt by the rotor as discrete gusts. It is thought that entrainment of the jet into the mean flow may cause the pulsing jet to lose its periodicity at the plane of the fan, thus causing the jet to lose its ability to excite blade vibrations at discrete frequencies.

The third fundamental problem is whether the jets will actually diffuse to form a continuous and smooth spatially sinusoidal pattern, or will they remain relatively discrete as they are convected downstream by the mean axial flow. The success of exciting particular modes will depend on the ability to form these spatially sinusoidal wake patterns.

The final fundamental concern is whether or not the pulsing jets will be able to penetrate far enough into the flow to effectively excite the blades. It is possible that a pulsing jet may diffuse more rapidly than a steady jet due to its fluctuating mass flow rate. This might result in a smaller penetration distance and a decrease in the velocity defect produced, thus decreasing the excitation force on the blades.

2.5 Implementation Considerations

In addition to the fundamental fluid mechanical concerns, the feasibility of the proposed injector also depends on several mechanical implementation considerations. The first problem is

that of how to valve the jets so they turn on and off at the necessary high frequencies. Typically a pulsing frequency of up to five to six kilohertz will be necessary. The method developed for this study involves placing a rotating hollow steel drum inside an aluminum housing. This design is illustrated in Fig. 2.5 The drum would be pressurized with a gas supply and would be turned with a connecting electric motor. A series of holes in the housing will provide the passageway for the jet from the inner drum to the test section wall. At each jet exit location the drum will be drilled with a series of evenly spaced holes. As the drum turns, these holes become aligned with the holes in the housing to provide the path for the jet flow. As the drum rotates, these pathways will open and close very quickly, resulting in the required high frequency jets. The resulting time history of the jet open area is shown in Fig. 2.6.

The next problem is phasing the jets properly. Equation 2.16 gives the relationship for the interjet phasing in terms of the number of equally spaced jets and the number of nodal diameters in the mode to be excited. This phasing can be achieved by offsetting the locations of each circumferential set of holes in the inner drum. This procedure is illustrated in Fig. 2.7. The result of this design is to produce pulsing jets, each of which opens and closes at a slight phase difference from its neighbors. To excite modes with different numbers of nodal diameters it will be necessary to devise a way in which this phase difference

between adjacent injected jets can be varied. One approach to this problem is to closely couple the injector drum to the test section wall and to construct drums with different offsets between the axial locations of hole circles. Fig. 2.8a shows this close-coupled concept. Another option involves using longer, flexible tubes to connect the injector to the tunnel walls. This method is illustrated in Fig. 2.8b. If these longer tubes can be used while still producing acceptable pulsing jets, it may be possible to use "pneumatic logic" to reduce the number of drums needed. Fig. 2.9 illustrates how a single drum can be used to excite three different modes.

Ideally, jets should be located around the entire circumference of the test section. However, since it is impossible to curve a constant radius rotating drum around the test section, it was decided to use four separate units located on the test section as shown in Fig. 2.8. Each injector spans 60° of the test section circumference.

There remains the exercise of specifying the precise parameters for the design of an injector for the planned mistuning experiment and the prototype injector. The desired jet spacing in the test section wall was determined in Section 2.3 to be .375". The NASA Lewis Research Center Multistage Compressor Test Facility has a diameter of 20", with a resulting jet spacing of $\alpha = 2.15^{\circ}$. This was rounded to $\alpha = 2^{\circ}$ to simplify machining of the test section casing. The result will be 31 jets in a single injector

unit spanning 60° of the test section circumference.

The speed at which the drum is turned for a particular jet frequency depends on the number of holes at each valving station on the injector drum. A drum diameter of 2.5" was selected as the largest which could be used while maintaining the jet placement at approximately 1.5" upstream of the rotor. The injector placement in the NASA Lewis testing facility is shown in Fig. 2.10 Ideally it is desired to place the .125" diameter jets .25" center to center around the drum. However, this would result in 31.4 holes at each valving station on the drum. Therefore the drums are designed with 30 holes at each axial station located 12° (or approximately .26") apart. This design will yield a jet pulsing frequency of 30 times the drum rotation frequency. This design will also insure that each jet pulse terminates completely before the next pulse begins.

In order to determine the maximum frequency, the details of the fan to be tested must be examined. The fan to be used in the mistuned rotor experiment has 42 blades and is designed to operate at 16,000 rpm. From Equation 2.12 the maximum required pulsing pulsing frequency is 5600 hz. The injector valve drum speed to produce this jet pulsing frequency will be 11,200 rpm. The 42 bladed rotor has 42 aeroelastic traveling wave modes associated with its first blade torsional frequency of approximately 1100 Hz. In principle, to excite all the aeroelastic modes, 21 different nodal diameter patterns would be required. Each pattern can

excite a forward or backward wave, depending on the direction of drum rotation in the injector mechanism. In practice, if 10 traveling wave modes could be identified, requiring only 5 drum hole patterns, a great deal of information could be derived.

In this chapter the conceptual design for a device to excite vibrations in a rotating fan by injecting pulsing jets into the flow has been presented. Calculations were performed to determine the maximum jet pulsing frequency which will be required. This was found to be equal to half the blade passing frequency. Calculations were also performed to determine the appropriate jet spacing, size, and location in the test section. It was determined that for the planned mistuning experiment the jets should be .125" in diameter and be spaced .375" apart. The jets should be located approximately eleven jet diameters upstream from the fan. Calculations for the proper phasing between adjacent jets to excite different aeroelastic modes were also presented. The fundamental fluid mechanic and practical implementation questions to be answered in this report were also posed.

3. Models of Transverse Jet Behavior

Before analyzing the behavior of unsteady jets in a cross flow, it is first necessary to understand the behavior of steady jets in a cross flow. This chapter will discuss the general behavior of steady jets and summarize the results of research in this area. The additional effects due to the unsteadiness of the jet will then be discussed.

The general characteristics of steady jets in a cross flow such as the penetration, diffusion, and the turning of the jet will be presented in Section 3.1. Past research into steady jets will be discussed, including empirical predictions of the jet trajectories. The additional factors due to unsteadiness of a pulsating jet will be discussed in Section 3.2 and the reduced frequencies of importance will be defined.

3.1 Steady Jet Behavior

As a transversly injected jet enters the cross flow, two effects begin to cause the jet's direction to change and turn with the flow. The first effect is a pressure difference occurring across the jet. The injected jet blocks the flow and causes a pressure defect to form in the wake of the jet. The resulting pressure difference causes the jet to begin to turn downstream. This pressure difference is the dominating effect in determining the downstream curvature in the early portion of the jet

trajectory. The second effect is the entrainment of the jet into the mean cross flow. This effect dominates the latter portion of the jet trajectory [8].

Just as in the classic model of a jet in the absence of a cross flow, diffusion of the jet flow occurs, affecting its shape and velocity. The jet expands so that its defining boundaries become larger. The momentum of the jet begins to diffuse, and the peak velocity along its center line decreases. This effect is illustrated in Fig. 3.1.

Furthermore, a secondary flow interaction develops with the mean flow. As the jet travels it loses its initial round shape and takes on a horseshoe shape. This effect is illustrated in Fig 3.2. This change in shape is due to the fact that the fluid particles at the edges of the jet have less momentum and are entrained into the mean flow more rapidly. This results not only in the characteristic horseshoe shape, but in the formation of two shed vortices in the wake which grow and eventually dominate the downstream flow.

The effect of the injected jet is therefore to introduce both a velocity deficit and excess into the mean flow. At a short distance downstream from the injected jet, the net effect is seen as a pressure defect directly behind the jet close to the exit wall. Further from the wall the excess at the jet centerline is seen, and still further from the exit wall the flow is largely undisturbed by the presence of the injected jet. This is

illustrated in Fig. 3.3.

Various studies have confirmed this model of steady jet behavior [7,8,9,10]. Margason [10] has derived an empirical relationship for the penetration distance of a steady jet injected into a cross flow from flow visualization studies and has compared it to relationships developed in other studies by both analytic techniques and experimental curve fit procedures. In general, the penetration depth normalized by the jet diameter is dependent only on the effective velocity ratio and the angle at which the jet is injected relative to the free stream. The effective velocity ratio is defined as:

$$V_e = \sqrt{\frac{\rho_\infty U_\infty^2}{\rho_j U_j^2}} \qquad (3.1)$$

where ρ is density , U is velocity, and the subscrpts ∞ and j refer to the free stream and jet respectively. V_e is an effective measure of the relative kinetic energy of the mean flow to the injected jet flow. All the relationships reviewed by Margason are very similar. The penetration distance depends on a power of the velocity ratio and a power of the downstream distance. For a jet injected at an angle of 90° to the flow Margason's empirically derived relation is:

$$\frac{x}{D} = \frac{-1}{4} \cdot \left[\frac{z}{D}\right]^3 \cdot V_e^2 \qquad (3.2)$$

where z is the vertical penetration distance, x is the distance downstream, D is the jet diameter, and V_e is the effective

velocity ratio. Margason derived this relationship from an empirical fit to flow visualization data. The negative sign is due to the coordinate system used in his experiment, where z was defined as positive downward. Changing to a convention defining z as positive upward, Equation 3.2 can also be solved for the penetration distance as:

$$\frac{z}{D} = \sqrt[3]{\frac{4(x/D)}{V_j^2}} \tag{3.3}$$

Jordinson [#] formed a similar empirical relationship by assuming the same functional form and using maximum total pressure measurements in the curve fit. The resulting relationship is:

$$\frac{x}{D} = -2.3 \cdot \left[\frac{z}{D}\right]^3 \cdot V_j^3 \tag{3.4}$$

This equation also defines z as positive downward. After changing this convention to one defining z as positive upward and solving for the penetration distance, Equation 3.4 can be expressed as:

$$\frac{z}{D} = \sqrt[3]{\frac{\frac{1}{2.3}\left[\frac{x}{D}\right]}{V_j^3}} \tag{3.5}$$

Callaghan and Ruggeri [7] use a slightly different functional form to develop an empirical curve fit for their data. They used a temperature probe to determine the penetration distance of a heated jet and developed the equation:

$$\frac{x}{D} = 0.118\left[\frac{\rho_\infty U_\infty}{\rho_j U_j}\right]^2 \left[\frac{z}{D}\right]^{3.3} \tag{3.6}$$

Solving for the penetration distance, equation 3.6 becomes:

$$\frac{z}{D} = \sqrt[3.3]{\frac{\frac{1}{0.118}\left[\frac{x}{D}\right]}{\left[\frac{\rho_\infty U_\infty}{\rho_j U_j}\right]^2}} \qquad (3.7)$$

As a practical matter, Equations 3.3, 3.5, and 3.7 all yield comparable jet trajectories. They are plotted together for a number of cases by Margason [10]. Equation 3.3 will be used in this report for calculation of jet penetration distances.

3.2 Effects of Unsteadiness

The fact that the jet is pulsing fundamentally changes the character of the jet. The mass flow rate is no longer constant, but varies from zero to some maximum value. The effect this will have on the behavior of the jet and the nature of its interaction with the mean flow is unknown. A thorough understanding of these effects of unsteadiness is the goal of this study.

However, it is possible to define two non-dimensional parameters of importance in the study of a pulsing jet. Both are identifiable as reduced frequencies, but are based on different reference lengths. The first reduced frequency is based on the hole diameter, so that:

$$K_D = \frac{fD}{U_\infty} \qquad (3.8)$$

where K_D is the reduced frequency based on the jet diameter, f is the jet pulsing frequency in hertz, D is the jet diameter, and U_∞ is the velocity of the cross flow. This reduced frequency relates

the convection time of the mean flow across the jet opening to the period of the jet. It is therefore a measure of the unsteadiness of the injection process occurring at the jet orifice. If this reduced frequency is less than unity, the mean flow will feel the jet injection in the vicinity of the injector as a quasi-steady process. Typical values for K_D in the experiment described ranged from 0.02 to 0.66. Thus this injection reduced frequency was always less than unity, and the injection phenomena was therefore quasi-steady.

The second reduced frequency is based on the distance downstream from the jet at which measurements are made or the wake structure is being studied. It is defined as:

$$K_x = \frac{fx}{U_\infty} \tag{3.9}$$

where K_x is the reduced frequency based on the distance downstream from the jet, and x is the downstream distance. This reduced frequency relates the convection time of the jet flow to a fixed downstream station to the period of the jet. It is therefore a measure of the unsteadiness of the interaction or mixing of the jet and the mean flow, as observed at a downstream station. If the value of K_x is less than unity, the effects of a given pulse will have been carried past the measurement station before the next jet pulse begins. Thus the interaction will be quasi-steady. If K_x is greater than unity the effects of several jet pulses will be contributing to the downstream flow at any one time, and the

process will be highly unsteady. Typical values for K_x in these experiments ranged from 0.26 to 6.4. Thus a range of behavior of the injection process from largely quasi-steady to unsteady was studied.

In this chapter the known behavior of steady jets in a cross flow based on past studies has been discussed as a preliminary step toward understanding the behavior of a pulsing jet in a cross flow. The additional effects of the unsteadiness of a pulsing jet were then introduced and the reduced frequencies of importance were defined.

4. Design of Prototype Experiment

In order to test the feasibility of the injected pulsing jet method of fan excitation, it was necessary to design and build a prototype device. This prototype was designed with the jet diameter, spacing, and pulsing frequency which matched the requirements for the fan excitation system to be used in the actual aerodynamic measurement experiment, to be performed in the Multistage Compressor Test Facility at the NASA Lewis Research Center. The prototype was then tested in a low speed wind tunnel at MIT in order to determine if the use of injected pulsating jets is a practical means of exciting vibrations in rotating fans.

In this chapter, the design of the prototype experiment will be discussed. In Section 4.1, the hardware used in the experiment is described. The testing procedure is presented in Section 4.2. The data reduction and analysis methods are discussed in Section 4.3.

4.1 Hardware

The design and fabrication of the injector itself and the measurement instrumentation will be discussed in this section. The full size injector for the close coupled injector concept discussed in Section 2.5 covers 60° of the test section circumference. For a 20 inch test section, this would require a drum of approximately 13 inches in length. The prototype jet

injector was made shorter than the actual injector in order to minimize manufacturing difficulties. The prototype design is shown in Fig. 4.1. The prototype had a 6.5" long drum within an 8" housing. A close tolerance was required between the drum and housing in order to reduce jet crosstalk. Because of the possibility of contact between the drum and housing at the high drum rotation speeds involved, a steel drum and aluminum housing were built. It was believed that rubbing in a steel-aluminum system would not result in catastrophic welding if a seizure occurred. An aluminum-aluminum device would experience more severe binding problems in the event of contact and might weld if a seizure occurred at high speeds. Steel was avoided for use in the housing due to the relative difficulty in boring a long hole in steel. Also, since aluminum has a higher coefficient of thermal expansion than steel, as the system heats up the separation between the drum and the housing will increase rather than decrease, reducing the possibility of seizure due to thermal growth.

In order to determine the cold clearance between the inner steel drum and the outer aluminum housing it was necessary to account for three factors. These included the expansions of the drum due to rotation, thermal expansion, and the radial play of the support bearings.

The drum expansion due to rotation is governed by the expression:

$$\Delta r = \frac{\Omega_D^2 r^3 \rho}{E} \qquad (4.1)$$

where Δr is the change in drum radius due to its rotation, r is the mean radius of the drum, Ω_D is the rotational speed of the drum, ρ is the density of the drum material, and E is the Young's modulus of the drum material. For values expected in this experiment, that is, Ω_D = 11,200 rpm, r = 1.25", ρ = .283 lb/in^3, and E = 29 x 10^6 lb/in^2, Δr has a value of 7 x 10^{-5} in.

The thermal expansion of the steel drum is governed by the relation:

$$\Delta r = r\alpha\Delta T \qquad (4.2)$$

where α is the coefficient of thermal expansion for the drum material and ΔT is the change in temperature. This calculation is a worst case analysis, since it is assumed that only the steel drum undergoes a temperature change. In actuality, the aluminum housing will also expand and for the same change in temperature will actually expand more than the steel drum. Selecting a ΔT of 100°F at the thermal pinch point, and setting α = 6.6 x $10^{-6}/°F$, Δr has a value of .00083".

The radial play of the support bearings used in this device is rated at .0002-.0004". Thus summing the contributions of the mechanical, thermal, and bearing play deflections, the maximum Δr expected is .0013". Therefore clearance between the inner steel drum and the aluminum housing was chosen to be .002". This is 1.5 times the maximum expected growth in radius.

The diameter of the drum was therefore ground to 2.496", and the housing was bored with a diameter of 2.500". The drum was mounted on a .5" diameter precision steel shaft. The shaft was suspended in the housing on two precision Barden^{tm} ball bearings. Tolerances on these bearings met ABEC-7 standards, with the best radial play tolerances available. The shaft was in turn connected to a 1/4 horsepower drive motor through a flexible coupling to eliminate the possibility of applied transverse forces due to motor misalignment. This arrangement is shown in Fig. 4.2. The motor speed was controlled by a variable transformer.

A bank of twelve prepurified nitrogen bottles was used as a gas supply for the jet injector. Prepurified nitrogen was chosen since its density is very near to the density of air and it has very few impurities. The bottles were hooked to a common manifold equipped with a high mass flow pressure regulator to control delivery pressure. A pressure gauge in the supply line was used for the monitoring of the delivery pressure. A flexible copper tube with an inner diameter of 7/16" delivered the flow from the regulator to one end of the injector housing. This diameter was chosen to keep the cross sectional area of the supply line greater than the total area of the open jets. This insures that sonic flow would first occur at the jet orifices. The gas supply system is diagrammed in Fig. 4.3.

In order to introduce the gas supply into the inside of the drum, the injector housing was machined with a slot passing

through 60° of arc at the axial location of the gas inlet. The drum was perforated with eight equally spaced 3/8" diameter holes at this axial location. This resulted in one or more of the holes in the drum being open to the slot at all times. This arrangement provided a continuous passage for the gas supply to the interior of the drum, which acted as a plenum. This design is illustrated in Fig. 4.4.

The remaining length of the drum was drilled with a series of 1/8" diameter holes which encircle the tube. At each axial location, there were thirty equally spaced holes. The axial stations are 3/8" apart, as in the actual injector. There were eleven such axial locations in the drum. The housing was drilled with eleven 1/8" diameter holes which lined up with the holes in the drum. Each row of holes in the drum was offset 2° from the preceeding one. Since there are 30 holes at any station of the drum, this causes the interjet phasing β_j to be 60 degrees. Said another way, this causes there to be six holes in a cycle of the spatially sinusoidal envelope formed by the injected jets. This was chosen as the most severe test of the ability of discrete jets to form a sinusoidal envelope. By comparison, in the actual injector design the greatest interjet phase required is only 42 degrees, based on Equation 2.16.

The rotation speed of the injector drum was monitored by a tachometer made up of a photosensitive transistor and a light emitting diode. A small metal trigger attached to the shaft

interrupted the path between the transistor and the diode once per revolution. The result was a pulse in the output voltage of the circuit which was used as a clock as described in Section 4.2.

The wind tunnel used in this experiment was a low turbulence wind tunnel with a 12" x 12" test section. The test section speed was monitored by a pitot-static probe attached to an alcohol monometer. This probe was located near the top center of the test section three inches upstream from the jet injection point. The jets were injected upward into the mean flow and the surface of the injector was placed flush with the tunnel wall. No attempt was made to bleed off the boundary layer. The measurement probes were inserted into the flow from the side of the tunnel. A diagram of the wind tunnel testing arrangement is shown in Fig. 4.5. The maximum tunnel speed used was 60 mph.

In order to make time accurate measurement, a probe designed around a Kulite pressure transducer, model number XCQ-062, was used to measure the total pressure of the flow downstream from the jet. This transducer is rated to 50 psi and has a frequency range of 600 kHz. These characteristics made it suitable for measuring the high frequency pressure fluctuations involved in the experiment. The transducer was recessed into a probe with an L-shaped head, and the bore of the tube forward of the transducer face was machined with a 15° angle according to standard probe design technique to minimize the probe's sensitivity to slight misalignments to the flow. Fig. 4.6 shows the probe designed.

The tubing was 0.085" stainless steel, and the length of the tube section forward of the bend was 1.5", or approximately 17.6 tube diameters. The probe was attached to a traversing mechanism with micrometer movements for locating the probe at a desired point for data collection. An attachment head was made for the probe which allowed it to be used as a static pressure probe. This attachment is shown in Fig. 4.9. The probe was calibrated by evacuating the reference pressure tube and determining the transducer guage factor by comparing the output voltage to the known atmospheric pressure.

4.2 Testing Procedure

Before the prototype was tested in the wind tunnel, base line tests were performed on the lab bench in the absence of cross flow. The test setup is shown in Fig. 4.8. This was done in order to examine the velocity distribution of steady jets to confirm that the jets produced behaved as expected, and to allow comparison with classical experiments and theory. First, the injector was operated with one hole in an open position and all other holes covered. The Kulite pressure transducer was mounted on a traversing device with micrometer movements. Total pressure measurements were made across the jet at a number of heights from 0.5" to 2" at a delivery pressure of 20 psig. Then a series of measurements were taken at a height of 2" at a series of delivery pressures ranging from 20 to 100 psig. These measurements were

then repeated with six holes (one spatially sinusoidal cycle) uncovered. This data is presented in Section 5.1.

Next a series of tests were performed with pulsing jets being produced. This was done to acquire an understanding of the effects of the unsteadiness in the delivery system and to observe the amount of turbulence present in a pulsing jet in the absence of a cross flow. First a single pulsating jet was observed over a frequency range from 500 to 4900 Hz., and the total pressure measured in the unsteady jet were recorded as a function of time. Traverses were made and instantaneous pictures of the pressures were reconstructed from the data at 10 fractional instants of the hole opening period. These tests were then repeated with six pulsing jets open. The results of these tests are discussed in Section 5.2.

The prototype injector was then set up in the wind tunnel. First, tests were run with a single steady jet in an effort to reproduce the classic steady single injected jet experiments. A single downstream distance of 11 jet diameters was selected and vertical traverses were made with the total pressure transducer to determine the jet penetration depths at wind tunnel speeds ranging from 37.9 to 60 mph and delivery pressures ranging from 5 to 20 psig. Then wind tunnel speed of 60 mph and a jet delivery pressure of 5 psig were selected and measurements were taken at a matrix of points in the transverse plane. From this data, contours of constant pressure were constructed. The results of

these tests are presented in Section 5.3.

It was discovered that upon inserting the Kulite pressure transducer into the tunnel flow, several seconds were required before the transducer output reached a relatively stable value. This behavior was due to thermal effects within the transducer. To isolate this effect from the data measurements, it was necessary to frequently record the transducer output voltage readings of the tunnel flow with no injected jet flow . These readings were used as the reference pressure P_∞ in the calculation of the pressure coefficient C_p. In this way, thermal drift effects were not allowed to accumulate, and essentially were subtracted out of the calculation of C_p.

The next step was to measure the total pressure of a single pulsing jet at a wind tunnel speed of 60 mph and a jet delivery pressure of 5 psig. Vertical traverses were taken at frequencies ranging from 500 to 4900 Hz. to reconstruct instantaneous pressure profiles. These measurements were repeated for mean flow speeds ranging from 37.9 to 60 mph and jet delivery pressures ranging from 5 to 20 psig at a jet pulsing frequency of 3200 Hz. to determine the penetration depths. Then measurements were taken at a complete matrix of points for a wind tunnel speed of 60 mph and a jet delivery pressure of 5 psi at a jet frequency of 715 Hz., and instantaneous pressure contours were reconstructed. The grid was 2" wide, centered on the jet, and 2.5" high. Finally, this test was repeated with six neighboring pulsing jets to obtain the

multijet pressure contours. This data is shown in Section 5.4.

4.3 Data Reduction and Analysis

During both benchtop and wind tunnel tests the output voltage from the pressure transducer was recorded with a two channel Nicolet^{tm} digital storage oscilloscope. The data was first passed through a low pass filter. The filter used was an A.P Circuit Corp. model AP-255-5, which has a four pole maximum flatness Butterworth type response, and falls off at a rate of 24 db/octave. Steady data was filtered with a 3000 Hz. cutoff frequency. Unsteady data was filtered with the cutoff frequency at least four times the jet pulsing frequency, and was stored simultaneously with the signal from the clock circuit. Care was taken so that at least two pulses in the clock signal were recorded. This was done since the time at which all data was taken was referenced to its relative time between the two clock pulses. Said another way, using the timing pulses as a time reference, it was possible to determine the drum angle corresponding to each data point.

In order to facilitate examination of the time history of a data trace, an ensemble averaging program was used on the data to construct an image of the average pulse. Data was examined between the two clock pulses. Since thirty jet pulses occur during each rotation of the drum, there are thirty jet pulses between any two clocking pulses. A computer program divided this

portion of the data into 600 "bins," or twenty bins per jet pulse. Other numbers of bins were examined, and it was decided that twenty bins provided sufficient resolution of the unsteadiness. Each data point was assigned to its proper bin, and then all the points in the first bin of each pulse were added together, those in the second were added together, etc. The totals were divided by the number of points assigned, and thus the average pulse was formed at each location from the ensemble average of thirty jet pulses. The standard deviation of each point of the average pulse was also calculated to obtain information on the variation of the pulses from the average pulse. As a result of this process, an ensemble averaged pulse as a function of time was available at every point measured.

In order to obtain an instantaneous spatial image of the flow field at any instant in time it is necessary to convert the pressure time history taken at individual points in space to pressure contours in space at individual instants in time. These contours of constant pressure or pressure profiles were constructed by collecting the values from the same bin (i.e. the same nondimensional time) from all the data traces from a certain set of test conditions. In this way, a series of instantaneous contours could be developed for successive times during a jet pulse. This collection of instantaneous contours portrays a time history of the pressure field characteristics.

The resulting data could be used to construct profiles or

complete contours of the pressure coefficient C_p. C_p is defined as:

$$C_p = \frac{P_t - P_\infty}{P_j - P_\infty} \tag{4.3}$$

where P_t is the total pressure measurement, P_j is the total pressure of the jet at its orifice, and P_∞ is the total pressure of the free stream. This quantity was originally defined by Jordinsen [8], and was used in this experiment to compare the single steady jet in a cross flow data with classic experiments to verify the validity of the experimental procedure. All data collected was reduced in terms of the pressure coefficient C_p. For the bench measurements, P_∞ was taken as the ambient static pressure.

In this chapter the experimental apparatus and setup was described. The testing procedure was outlined for all tests to be performed. Finally, the data reduction and analysis methods were presented.

5. Experimental Results

The results of the testing program outlined in Chapter 4 are presented and discussed in this chapter. The general objective of the testing program was to determine if a gas jet injector could be built which would be capable of exciting the aeroelastic modes of a high speed fan. The specific objective of the prototype testing program was to answer the four fundamental fluid mechanical questions posed in Chapter 2. These questions focused on: 1. Discovering if there is an acoustic limit to the jet pulsing frequency which can be obtained; 2. Determining if the pulsing jet gusts remain temporally discrete as they penetrate the flow; 3. Determining if the individual jets will interact to form a spatially sinusoidal pattern; and 4. Determining how the presence of unsteadiness in the jet affects its penetration distance.

Additionally, it is necessary to answer the questions concerning the practical design and implementation of the jet injector. These include: 1. Determining if the jets can be valved at the necessary high frequencies; 2. Determining if the jets can be phased properly to form a spatially sinusoidal excitation force; and 3. Determining if flexible tubing can be used to implement pneumatic logic to decrease the number of injector drums required.

The preliminary tests performed with steady jets in the

absence of a cross flow are discussed in Section 5.1. The results of the tests performed with unsteady pulsing jets in the absence of a cross flow are presented in Section 5.2. These tests were performed to discover if an acoustic limit to the attainable jet pulsing frequency exists. These tests also examined the ability of the injector design to valve the jets at high frequencies and investigated the effect of long flexible plenum tubing on the jet flow characteristics. In Section 5.3, the results of the tests with a steady jet injected into a cross flow are presented. These tests were performed to validate the testing procedure and to provide a comparison for the unsteady jet behavior. Finally, the tests of pulsing jets injected into a cross flow are discussed in Section 5.4. These results answer the remaining questions of gust pulse discreteness, gust spatial pattern formation, and jet penetration distance.

5.1 Steady Jets in the Absence of a Cross Flow

The testing program began with the observation of a single steady jet in the absence of a cross flow. The experimental set up is shown if Fig. 4.9. These tests were performed to compare the velocity profile and decay of a turbulent jet with classical analysis for a single steady turbulent jet. Typical jet profiles are shown in Fig. 5.1. Data was taken with the probe at the heights above the jet orifice and gas delivery pressures indicated in Fig. 5.1. A theoretical curve for the profile of a circular

jet is provided for comparison. This curve, presented by Schlichting [13], is based on Prandtl's mixing length theory. Schlichting originally presented this curve as the ratio of the jet velocity to the maximum jet velocity, $\frac{U}{U_{max}}$, as a function of the normalized distance, $\frac{Y}{Y(0.5 \cdot U_{max})}$. The data from the current investigation is presented as the ratio of the pressure coefficient C_p to the maximum value of C_p. Recall that C_p is defined as:

$$C_p = \frac{P_t - P_\infty}{P_j - P_\infty} \tag{4.3}$$

In Fig. 5.1, the curve representing Schlichting's analytical result has been modified to reflect the fact that for an incompressible jet:

$$\frac{C_p}{C_{pmax}} = \left[\frac{U}{U_{max}}\right]^2 \tag{5.1}$$

To be consistent, the appropriate normalized y coordinate is $\frac{Y}{Y(0.25 \cdot C_{pmax})}$. It can be seen that there is good agreement between the experimental data and the analytical model presented by Schlichting. These results verify that the prototype injector is producing nominal turbulent jets which behave as predicted by theory, and that the measurement method used in this study is capable of accurately measuring the jet behavior.

Next, the decay of the centerline velocity of a fully open jet was examined. The relationship between the pressure coefficient C_p and the measurement distance from the jet orifice normalized by the jet diameter, z/D, is shown in Fig. 5.2 on a

logarithmic plot. Schlichting [13] predicts a 1/z relationship between the jet velocity and the measurement distance from the jet orifice based on Prandtl mixing length theory. This corresponds to a $1/z^2$ relationship between the pressure coefficient C_p and the measurement distance from the jet orifice. Therefore, a line with a slope of -2 is shown in Fig. 5.2 for comparison. It can be seen that in the far field the data asymptotically approaches the prediction by Schlichting. The same data is presented in Fig. 5.3 on a linear scale. Here it can be seen that the experimentally measured value of C_p goes to unity at the jet orifice, by definition, and asymptotically approaches the curve $1/z^2$ as the measurement distance from the jet orifice is increased. So, once again, in the far field the measurements agree with the analytical model.

Tests were then performed to examine the ability of discrete jets to be superposed and to interact to form a spatially sinusoidal pattern. This was done by traversing with the pressure probe through the flow formed be six jets, with the injector drum fixed so that the third hole from the left was held fully open. Measurements were taken for nondimensional distances from the jet orifices z/D of 4, 8, 12, and 16 with a gas delivery pressure of 20 psig. The resulting pressure fields are shown in Fig. 5.4. The jet centerline decay, and diffusion with neighboring jets to form a smoother envelope at greater distances from the orifice can be seen.

Traverses were also made in a direction perpendicular to the row of jets in order to determine the flow behavior in the transverse plane and to discover the degree to which the total flow can be considered a superposition of individual jet flows. These cross-traverse measurements, taken at a distance of z/D = 12 above the jet orifice, are shown in Fig. 5.5, superimposed on a traverse over the row of jets. The horizontal axis is s/D, where s is taken to be x for the cross-traverses and y for the traverse along the row of jets. From this figure it can be seen that the pattern formed by multiple jets is basically a superposition of the patterns produced by individual jets, and that the jet profiles in the transverse plane are those of normal turbulent jets.

Static pressure measurements were made across a typical jet using the modifying attachment for the total pressure probe described in Section 4.1. The results indicated that the static pressure is equal to the atmospheric pressure everywhere, confirming the usual assumptions of jet theory.

The results of the tests performed on steady jets in the absence of a cross flow confirm that a the single jet produced by the injector behaves as a nominal turbulent jet. Secondly, the behavior of many jets is understandable in terms of the behavior of individual jets, in that the flows from single jets can be superposed to approximately obtain the behavior of the multijet flow.

5.2 Pulsing Jets in the Absence of a Cross Flow

Tests were next performed with pulsing jets in the absence of a cross flow in order to acquire a preliminary understanding of their behavior. The principal objective was to determine if there exists an acoustic limit to the jet pulsing frequency which can be achieved, and how this limit might depend on the plenum length, that is, the distance from the jet valve to the jet orifice.

First, the flow produced by six pulsing jets was examined with the shortest plenum length, L = .25". Figs. 5.6, 5.7, and 5.8 show the resulting pressure field distributions at successive instants in time for pulsing frequencies of 1044 Hz., 2618 Hz., and 4078 Hz. and a gas delivery pressure of 20 psig. Measurements were taken at a distance above the jet orifice z/D = 4. Comparing these waveforms with the steady multijet pressure distributions shown in Fig. 5.4, the similarity between both the waveforms and the amplitudes can be clearly seen, especially at lower frequencies. At higher frequencies, the waveforms decrease slightly in amplitude. These tests were repeated with measurements taken at a distance above the jet injector z/D = 12 and pulsing frequencies of 512 Hz., 2553 Hz., and 4071 Hz. These pressure distributions are shown in Figs. 5.9, 5.10, and 5.11. A distinct loss of both amplitude and discreteness of the jets can be clearly seen, especially in Fig. 5.11, the case with the

maximum measurement distance and pulsing frequency.

In Fig. 5.12 the ensemble average pulse shape as a function of time is shown for a point directly above the third jet from the left in the row of jets at a distance above the jet injector z/D = 4 for jet pulsing frequencies of 1044 Hz., 2618 Hz., and 4078 Hz. The value of the maximum pressure coefficient of a steady jet for this flow condition is shown for comparison. It can be seen that there is a slight decrease in the peak pressure as the pulsing frequency increases. A spectrum of each of these average pulses showing the relative magnitude of the component frequencies is shown in Figs. 5.13-5.15. These spectra are only reliable for the first few harmonics, but it can be seen clearly that the dominant frequency present is the pulsing frequency of the jet. Also, the spectra are all very similar in form.

The magnitudes of the first three harmonics of the spectra for the measurements made above the third jet from the left are shown at heights of z/D = 4, 8, and 12 in Figs. 5.16-5.18 as a function of the jet pulsing frequency. It can be seen that in all cases the magnitude of a given harmonic decreases as the jet pulsing frequency is increased.

A summary of the dependence of the maximum pressure on frequency is shown graphically in Fig. 5.19. Data from an additional measurement station of z/D = 8 has been shown. The ratio of the maximum pressure coefficient value to the steady pressure coefficient value at the corresponding measurement

station has been plotted against the jet pulsing frequency. The calculated fundamental acoustic frequency for a cylindrical cavity .25" long with open ends is approximately 27,100 Hz. The decrease in maximum pressure as the pulsing frequency increases can be clearly seen. However, since the pulses do remain discrete at high frequencies, there appears to be no acoustic limitation, and the reduction in pressure can be compensated for by increasing the gas delivery pressure.

Now that no acoustic limit has been found for the shortest plenum length, it is desirable to discover if it is possible to use a longer plenum. If so, the engineering of the jet injector will be simplified. The next set of tests were performed to study the effect of jet plenums of various lengths on the flow characteristics. The jet plenum length was varied using two different methods. The first method involved the addition of plates to the top of the injector which had holes drilled to match the jet locations. This method is shown in Fig. 5.20, and was used to produce plenum lengths of L = 0.75", 1.25", 1.75", 2.25", and 2.75". The second method involved using an attachment consisting of two plates with holes drilled to match the jet locations, separated by two inches. The holes in the two plates were connected by flexible tubes with an inner diameter of .125", and lengths varying from 2" to 6". This method is illustrated in Fig. 5.21, and was used to produce plenum lengths of L = 3.25", 4.25", 5.25", 6.25", and 7.25"

All measurements for the plenems of various length were made at a distance from the jet orifice of z/D = 4. A few representative ensemble averages of the pressure profiles are shown in Fig. 5.22 for a plenum length of 3.25". Comparing these to the ensemble average time histories shown in Fig. 5.12 for a plenum length of .25", it can be seen that the only apparent difference is a decrease in the peak pressure. The results of these tests with varying plenum length are summarized in Fig. 5.23, where the ratio of the maximum pressure coefficient to the steady jet pressure coefficient is plotted as a function of frequency for the various jet plenum lengths. It can be seen clearly that the pressure coefficient decreases slightly as the jet plenum length is increased. Also, it can be seen that the data appears to form two different families of curves. The data composing the lower curve consists of the cases where longer flexible tubes were used which were curved to fit between the two metal plates. Evidently the curving the connector tubes caused a greater decrease in the peak pressure.

Spectra of jet time history are shown in Figs. 5.24 and 5.25 for jet pulsing frequencies of 578 Hz. and 4902 Hz. for the case of L = 3.25". This case was of special interest because the fundamental resonant frequency for a tube of this length with open ends is approximately 2100 Hz. Thus the two cases shown represent data taken well below and above the fundamental resonance. It can be seen that the jet pulsing frequency is still the primary

component of both spectra, and that the pulses do not appear to be attenuated at higher frequency. The magnitude of the first three harmonics of the spectra for the measurements made at z/D = 4 for jet plenum lengths of L = 3.25" and 7.25" are shown in Figs. 5.26 and 5.27. As before, the magnitude of the fundamental harmonic decreases as the jet pulsing frequency is increased, while the magnitudes of the higher harmonics are essentially unchanged.

Overall these results indicate that there is not a strong second order acoustic behavior of the jet flow in the plenums. Neither resonances nor strong attenuation above the fundamental resonance are found. Therefore flexible tubes may be used to connect the jet injector to the wind tunnel wall without losing the discrete peak in pressure or the harmonic character of the pulsing jet.

5.3 Steady Jet in the Presence of a Cross Flow

Before studying the interaction of multiple unsteady jets with a cross flow, it was desirable to examine steady jet interactions. In order to verify the testing procedure and develop a data base for comparison with classical steady jet measurement, the behavior of a single steady jet was first observed. The experimental wind tunnel setup is shown in Fig. 4.6 and discussed in Section 4.1.

The first tests performed involved taking steady total pressure measurements in a plane at x/D = 11, i.e. 11 jet

diameters downstream. The measurements were taken at a matrix of points in the y-z plane to construct contour plots of constant pressure. These measurements were performed with both the Kulite pressure transducer and with a standard pitot-static probe. This was done to establish the reliability of the Kulite transducer. The resulting contours for a wind tunnel speed of 60 mph and a jet delivery pressure of 5 psig are shown in Fig. 5.28. These values for wind tunnel speed and jet delivery pressure were chosen by using isentropic flow relations to match the velocity ratio used for results reported by Jordinson [8]. Jordinson reports results for a velocity ratio $\frac{U_j}{U_\infty} = 8$. The pressure contour plot developed by Jordinson for this downstream plane and jet velocity ratio is also shown in Fig. 5.29 for comparison. As can be seen, the pressure contours taken with the Kulite (after correction for temperature drift as discussed in Section 4.2) and the contours taken with the pitot static probe agree quite well. Thus the Kulite total pressure probe gives accurate steady measurements of the flow.

Comparison of the current data with results obtained by Jordinson show qualitative agreement in size and shape of the pressure disturbance, but show a quantitatively smaller C_P excess and a corresponding larger deficit. Thus the C_P data of Jordinson is shifted slightly by an algebraic factor. Despite several attempts to reconcile these measurements, the fact that the Kulite

and pitot-static probe measurements agree quite well indicates that the most likely source of discrepancy is in the measurement of P_∞, the free stream total pressure.

The wind tunnel speed and the jet gas delivery pressure were then varied and the jet penetration distance, i.e. the z location of the greatest total pressure, was determined. The results as measured at x/D = 11 are shown in Fig. 5.30 for a range of delivery pressures from 5 to 20 psig. The jet penetration depths calculated from equation 3.3 are also shown. The penetration depth measurements agree well with the predicted values.

As a prelude to understanding the behavior of a pulsing jet, a series of vertical traverses of the flow were made with the jet opening set fully open, two-thirds open, one-third open, and fully closed. Note that this corresponds to drum rotations of 2°, 4°, and 6° from the fully open position. The pressure coefficient profiles, i.e. vertical surveys in z at a y position directly downstream of the jet, and at x/D = 11 are shown in Fig. 5.31. The measurements were made for U_∞ = 60 mph and a jet delivery pressure of 5 psig. The penetration depth calculated for the partially open jets is designated on the diagrams. These calculations were performed by calculating the jet open area and assuming the jet was a circular jet with a diameter producing the same area. These predictions closely match the measured penetration depths.

The important results for a steady jet in terms of

penetration depth and pressure contour have now been reproduced. With this verification of the experimental procedure the effects of an unsteady jet injected into a cross flow can now be examined.

5.4 Pulsing Jets in the Presence of a Cross Flow

So far it has been shown that the injector is capable of producing a nominal turbulent jet, that there is no acoustic limitation to the jet pulsing frequency which can be obtained, and that the experimental method obtains valid wind tunnel measurements. Now the remaining questions concerning the effects of unsteadiness can be addressed.

The behavior of pulsing jets in a cross flow was first examined by making vertical traverses of the flow at x/D = 11 and a jet delivery pressure of 5 psig for jet frequencies of 200 Hz., 655 Hz., 1160 Hz., 3323 Hz., and 5200 Hz. at a wind tunnel speed of 60 mph. The resulting pressure profiles are shown in Fig. 5.32-5.36 for 10 instant in time over a single jet period. The instant during which the jet is totally open has been indicated on the diagram. For low jet pulsing frequencies, the appearance and disappearance of the pressure excess and deficit due to a single jet pulse can be clearly seen. Comparison of the unsteady measurements made at K_x = 0.85 (655 Hz.) with the steady measurements with partially open holes reveals the quasi-steady nature of the flow at this low reduced frequency. At higher jet pulsing frequencies the behavior is more complex. The effects of

several jet pulses combine to create less distinct periods of velocity excess and defect. Thus, these plots illustrate the importance of the reduced frequency K_x. If K_x is less than unity, the pulsing jet is essentially quasi-steady. If K_x is greater than unity, the flow behavior is more complex, and the pulsing jet gusts do not remain discrete at the downstream plane of the measurement. Therefore the second of the fundamental fluid mechanical questions has been answered. The rotor will experience discrete gusts due to the injected jets provided the reduced frequency based on the downstream distance, K_x, is less than unity.

Next measurements were taken at a complete matrix of points at x/D = 11. The y/D measurements ranged from -3.78 to 3.78 and z/D ranged from 2 to 20. A jet pulsing frequency was chosen to give a value of K_x = 0.93, a value high in the quasi-steady range. The resulting pressure coefficient contours at successive instants in time are shown in Fig. 5.37.

The jet valve is completely open in frame 3, but the resulting pressure excess is seen in frame 2. The jet pulse begins to appear in frames 10 and 1, reaches its maximum value in frame 2, and then decreases in frames 3 and 4. In frames 5, 6, and 7, the jet is not in evidence and only turbulence associated with the breakup of the jet and its convection past the measurement station can be seen. In frames 8 and 9 the flow is largely unaffected by the jet. The cycle then repeats.

The growth and decay of the jet and its wake can be seen in these traces, showing that the jet pulses remain discrete at the measurement station. This reinforces the conclusion that if $K_x < 1$, discrete gusts are sensed at the rotor.

In order to answer the third fundamental question, that of interaction of several jets to form a spatially sinusoidal pattern, measurements of the unsteady pressure were then made on the same matrix to examine the pressure fields produced when six adjacent jets are pulsing. Since the jets are spaced three jet diameters apart, this resulted in three jets being within the field of measurement. It is unnecessary to measure the flow over the entire y/D range since the behavior should be periodic in y/D, since the jets are all identical except for a phase shift in time. The resulting pressure coefficient contours at successive instants in time are shown in Fig. 5.38 for x/D = 11, U_∞ = 60 mph, and the jet delivery pressure is 5 psig. The growth and decay of the jet pulse can still be seen, but the additional effects of neighboring jets can also be noted.

The left hand jet (jet 1) reaches its fully open state in frame 3, the center jet (jet 2) reaches its fully open position in frame 4, and the right hand jet (jet 3) is fully open in frame 6. The jet pulse from jet 1 begins to appear in frame 2 and grows in frame 3. The pulse from jet 2 appears in frame 4 as the jet 1 pulse begins to fade. The pulse from jet 2 grows in frame 5 and decreases in frame 6 as the pulse from jet 3 begins to appear.

The pulse from jet 3 grows in frame 7 as jet 2 continues to fade, and then in turn begins to fade in frames 8 and 9. In frames 10 and 1 there is essentially no influence from the jets, and then the cycle repeats.

The jets do appear to be interacting to form the desired sinusoidal envelope. Therefore the third fundamental question is answered. Even at this high interjet phase angle, the jets interact to form a smooth spatial envelope of the wake structure.

Finally, in order to investigate the effects of unsteadiness on the jet penetration depth, a series of jet penetration measurements were made. The jet pulsing frequency was set at 1600 Hz. while the jet delivery pressure ranged from 5 to 20 psig and the wind tunnel speed was set at 37.9 mph, 50.2 mph, and 60 mph. The penetration depths were also obtained from the data presented in Fig. 5.32-5.36. The results are shown in Fig. 5.39 for the penetration depth z/D as a function of the effective velocity V_e. In this case the exit jet velocity was calculated using a quasi-steady model of the isentropic flow in the plenum. The steady jet penetration depths predicted by equation 3.3 are also shown. The results indicate that the jet penetration depth is not substantially affected by the jet frequency or the existence of pulsing flow. Equation 3.3 can therefore be used to accurately predict the penetration depth of a pulsing jet over the range of K_x and K_D investigated. Thus the fourth fundamental question has been answered. Pulsing jets can penetrate into the

mean flow far enough to produce a sufficiently deep wake to excite vibrations in a rotating fan.

6. Conclusions

The results of this study indicate that injecting pulsing jets into the flow is a feasible method of exciting the aeroelastic modes of a rotating fan. The answers to the four fundamental fluid mechanics questions and the three practical implementation questions all substantiate this conclusion.

The first fundamental fluid mechanics question involved the possible presence of an acoustical limit to the jet pulsing frequency which can be obtained. The testing results presented in Section 5.2 indicate that there is be no simple acoustical limit to the jet pulsing frequency which can be produced. It was possible to detect discrete, largely unattenuated gusts at the jet orifice even at frequencies well above the fundamental frequency of the plenum.

The results presented in Section 5.4 answer the second fundamental fluid mechanical question, that of the ability of the jet pulses to remain discrete in time as they mix with the cross flow, and to produce periodic gusts at the downstream location of the fan. The experimental results show that the gusts created by the jet pulses remain discrete at the fan location if the reduced frequency based on the downstream distance (K_x) is less than unity. Under these conditions the gust disturbance created by one pulsed jet has been completely convected by the rotor prior to the appearance of the gust created by the succeeding jet pulse. Above

this reduced frequency, a much more complex downstream pressure disturbance is created. For the experiment to be performed at the NASA Lewis Research Center, the maximum reduced frequency of injection will be slightly greater than one. Therefore coherent discrete gusts will be felt by the rotor as a result of the upstream jet injection.

The results of this investigation also answer the third fundamental concern, that of the ability of the discrete jets to form a spatially sinusoidal pattern. The results presented in Section 5.4 indicate that the individual jets will interact to form the spatially sinusoidal wake which is necessary to excite pure aeroelastic traveling wave modes in the rotating fan.

The last fundamental fluid mechanical question is satisfactorily answered by the results in Section 5.4. These results show that the transverse penetration distance of a pulsing jet is essentially the same as that of a steady jet. Therefore, the empirically derived equation for the penetration depth of a steady jet can be used to calculate the penetration depth of a pulsing jet. Thus it is possible to design a jet injection system which produces a wake which penetrates deep enough into the flow to successfully excite vibrations in a rotating fan.

The three practical implementation problems involved with producing high frequency pulsing jets have also been resolved by this study. First, it has been shown that it is possible to

successfully produce a jet at high frequency by operating a drum valve operating at high speeds. Second, it has been shown in this study that the individual jets can be phased properly to form a spatially sinusoidal pattern. Finally, since there appears to be no problem inherent in using flexible tubes for the jet plenums, it is not necessary to use an injector which is directly coupled to the tunnel wall. Flexible tubes can be used to keep all the jet plenums the same length. This in turn allows a single drum to be used to excite more than one aeroelastic vibration mode through the use of pneumatic logic. The design relations for the location and number of injected jets have also been determined and are summarized in Fig 2.4.

References

1. Srinivasan, A.V., and Fulton, G.B., "Advanced Turboprop Vibratory Characteristics", United Technologies Research Center, NASA CR 174708, Apr. 1984.

2. Srinivasan, A.V., and Cutts, D.G., "Aerodynamically Excited Vibrations of a Part-Span Shrouded Fan", ASME Journal of Engineering for Gas Turbines and Power, Vol. 107, No. 2, Apr. 1985.

3. Jay, R.L., and Burns, D.W., "Characteristics of the Diametrical Resonant Response of a Shrouded Fan Under a Prescribed Distortion", to be presented at the ASME Tenth Biennial Conference on Mechanical Vibration and Noise, Sept. 1985.

4. Crawley, E.F., "Aerodynamic Damping Measurements in a Transonic Compressor", ASME Journal of Engineering for Power, Vol. 105, Jul. 1983, pp. 575-584.

5. Crawley, E.F., and Hall, K.C., "Optimization and Mechanisms of Mistuning in Cascades", ASME Journal of Engineering for Gas Turbines and Power, Vol. 102, No. 2, Apr. 1985.

6. Hoyniak, D., and Fleeter, S., "The Effect of Aerodynamic and Structural Detuning on Turbomachine Supersonic Unstalled Torsional Flutter", Proceedings of the 26th Structures, Structural Dynamics, and Materials Conference, Part 2, Orlando, Florida, Apr. 15-17, 1985.

7. Callaghan, E.E., and Ruggeri, R.A., "Investigation of the Penetration of an Air Jet Directed Perpendicularly to an Air Stream," NACA TN-1615, 1948.

8. Jordinson, R., "Flow in a Jet Directed Normal to the Wind," R. & M. 3074, British A.R.C., 1956.

9. Kamotani, Y., and Greber, I., "Experiments on a Turbulent Jet in a Cross Flow," AIAA Journal, Vol. 10, No. 11, Nov. 1972.

10. Margason, R.J., "The Path of a Jet Directed at Large Angles to the Free Stream," NASA TN D-4919, Nov. 1968.

11. Curtet, R.M., and Girard, J.P., "Visualization of a Pulsating Jet," Symposium on the Joint Meeting of the ASME Fluids Engineering Division and the Applied Mechanics Division, June 1973.

12. Kovasnay, L.S.G., Fujita, H., and Lee, R.L., "Unsteady Turbulent Puffs," Proceedings of a Symposium on Turbulent Diffusion in Environmental Pollution, Apr. 1973.

13. Schlicting, H., "Boundary Layer Theory," McGraw-Hill, New York, 1968.

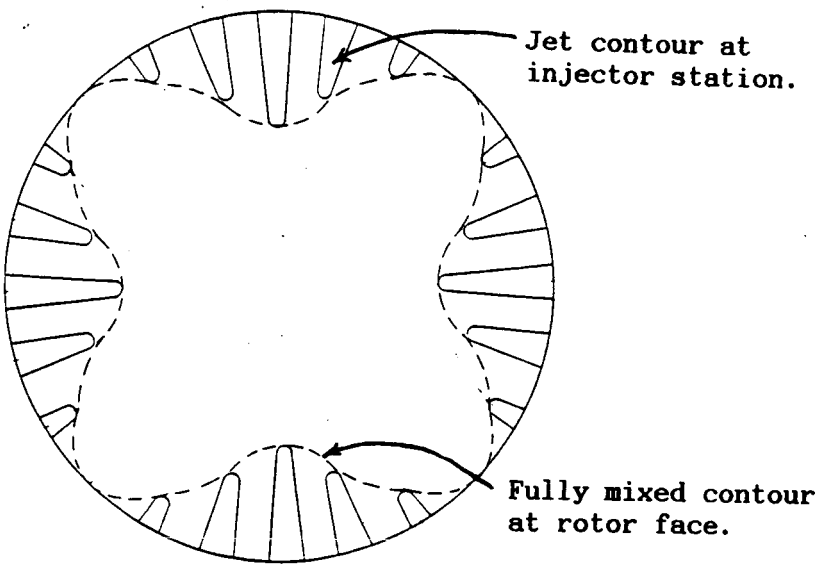

Fig. 2.1 A two nodal diameter spatially sinusoidal velocity defect produced by the mixing of properly phased discrete jets.

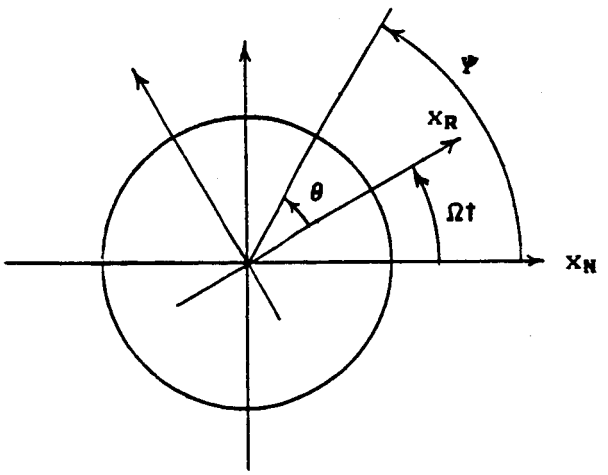

Fig. 2.2 Transformations from the rotating to nonrotating coordinate system.

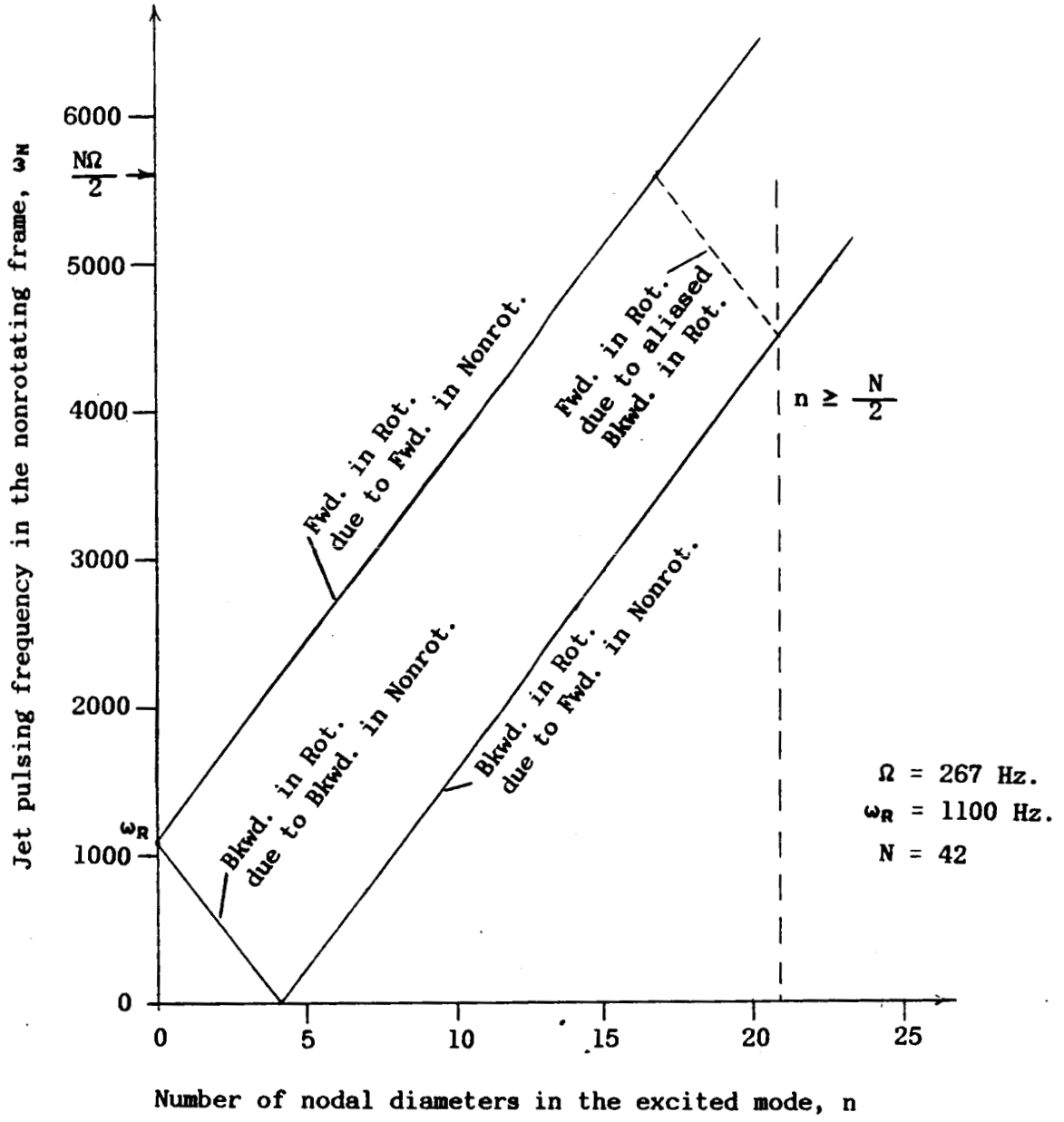

Fig. 2.3 Relationship between jet pulsing frequency, ω_N, and number of nodal diameters n in the excited mode for a fixed rotation speed, Ω, and desired excitation frequency of the fan, ω_R.

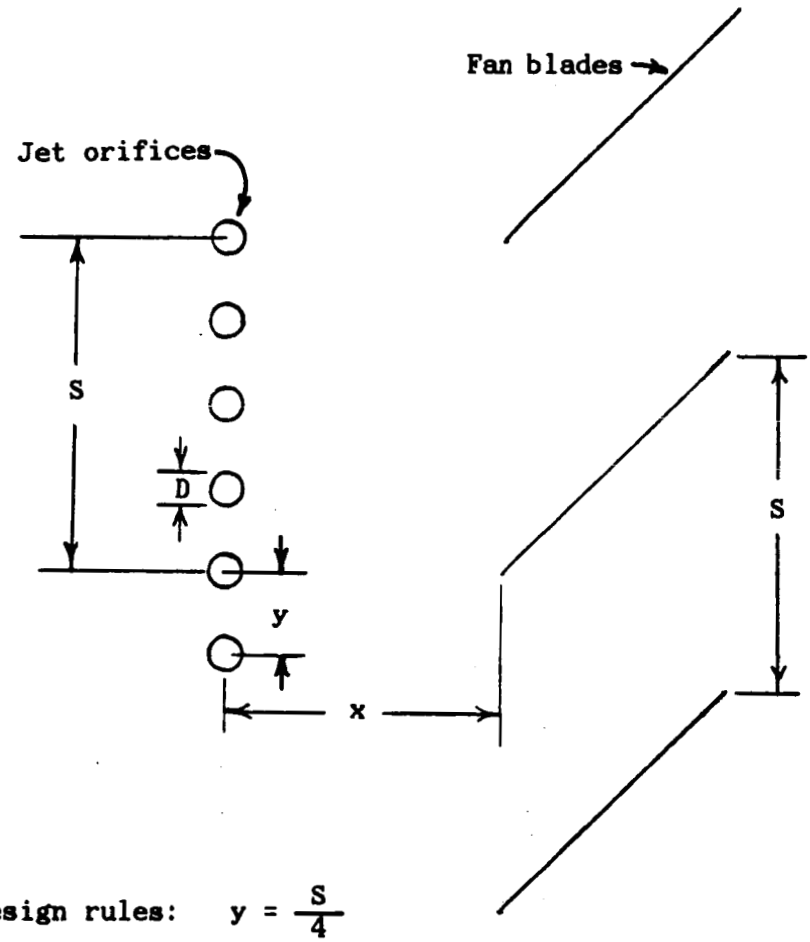

Design rules: $y = \frac{S}{4}$

$D = \frac{y}{3}$

$x = 10D$ to $12D$

Fig. 2.4 Design rules for geometry of the jet spacing relative to the cascade geometry at the fan tip.

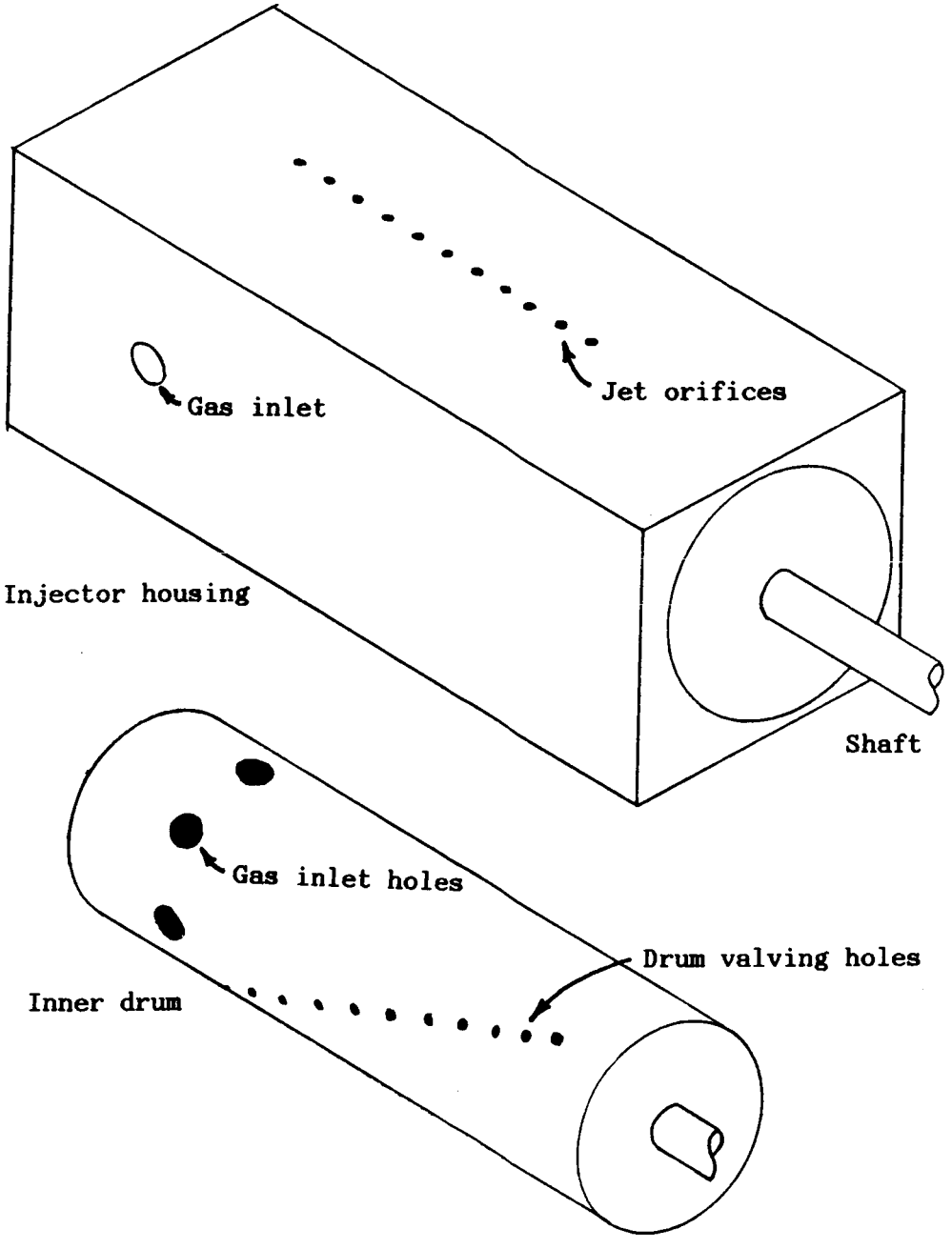

Fig. 2.5 Housing and inner drum of proposed jet injector design.

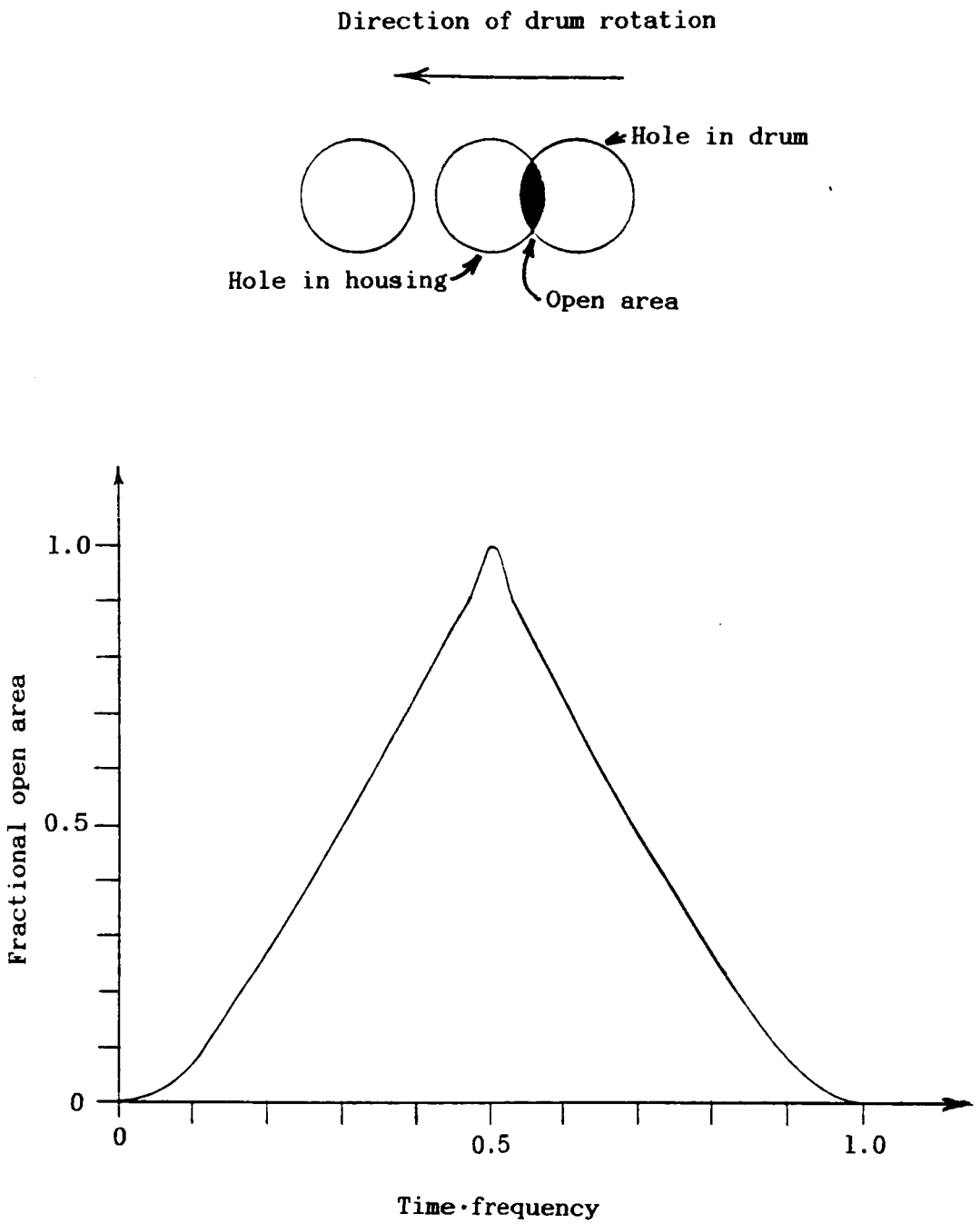

Fig. 2.6 Time history of the fractional open area of a single jet valve as a function of jet pulsing period.

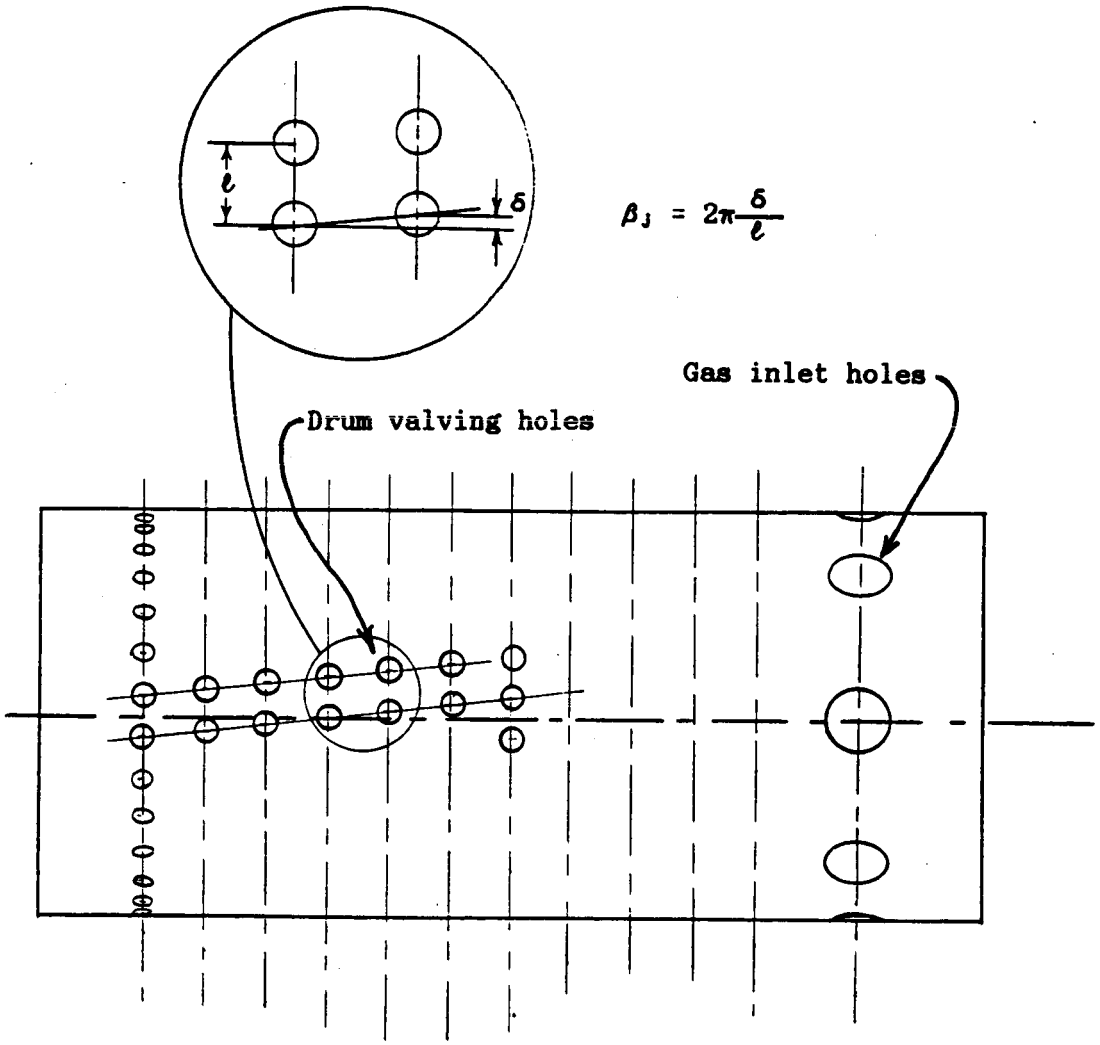

Fig. 2.7 Layout of the injector drum, showing multiple circumferential sets of holes and relative phase, β_j, between adjacent sets of holes.

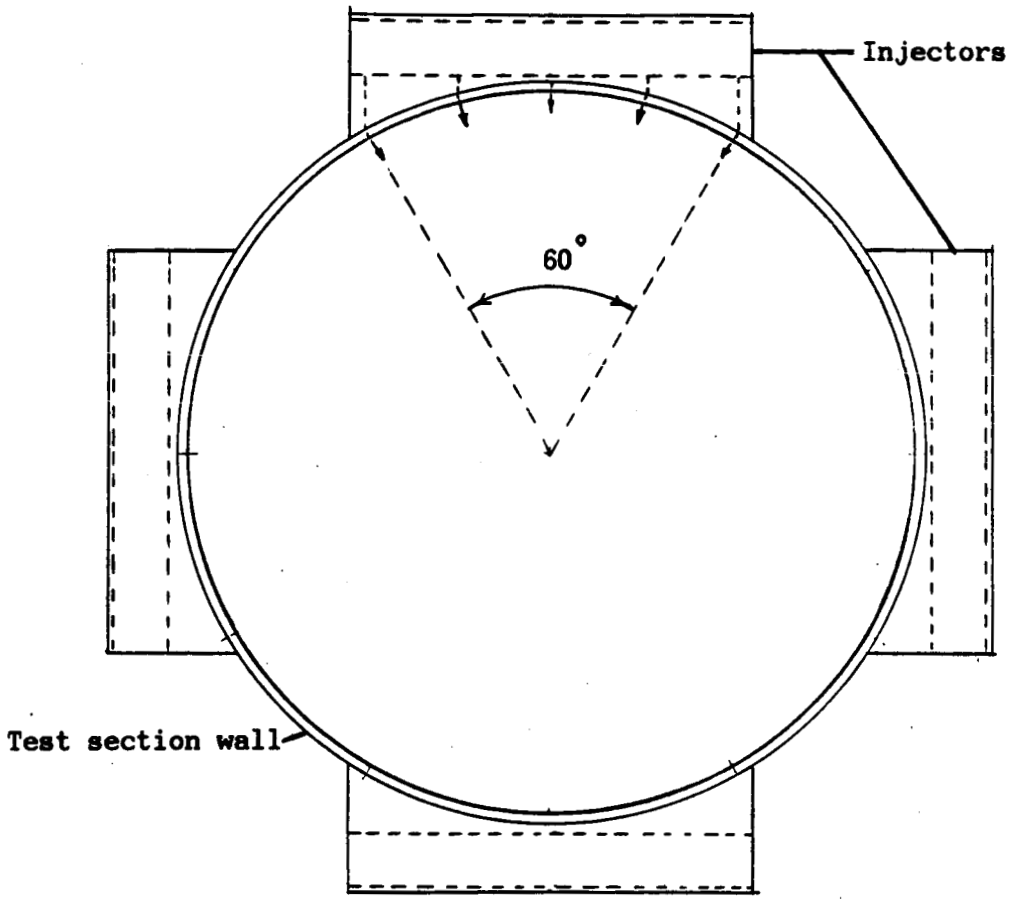

Fig. 2.8a Injectors closely coupled to test section wall, covering four 60° segments of the test section wall.

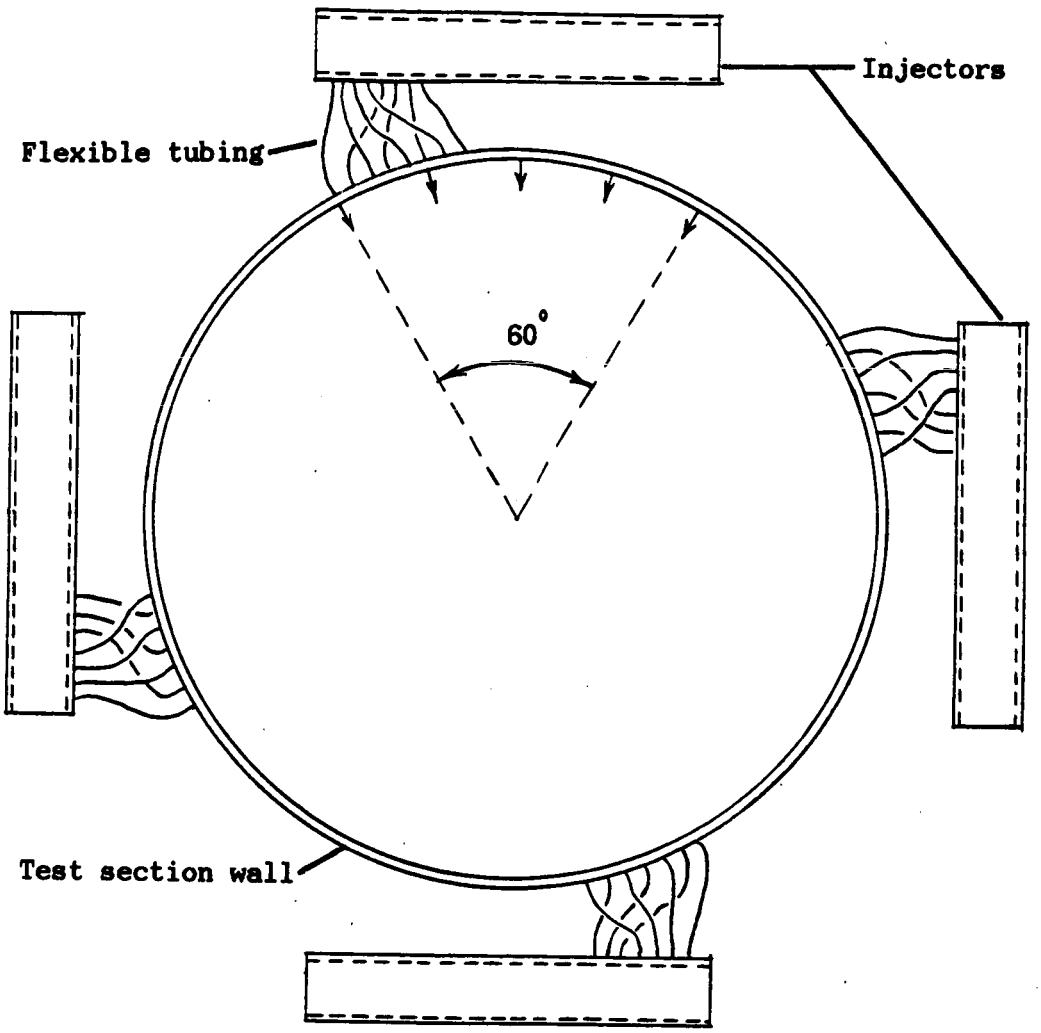

Fig. 2.8b Injectors set away from test section wall, and connected by flexible tubing, which allows rearrangement of hole pulsing pattern by "pneumatic logic."

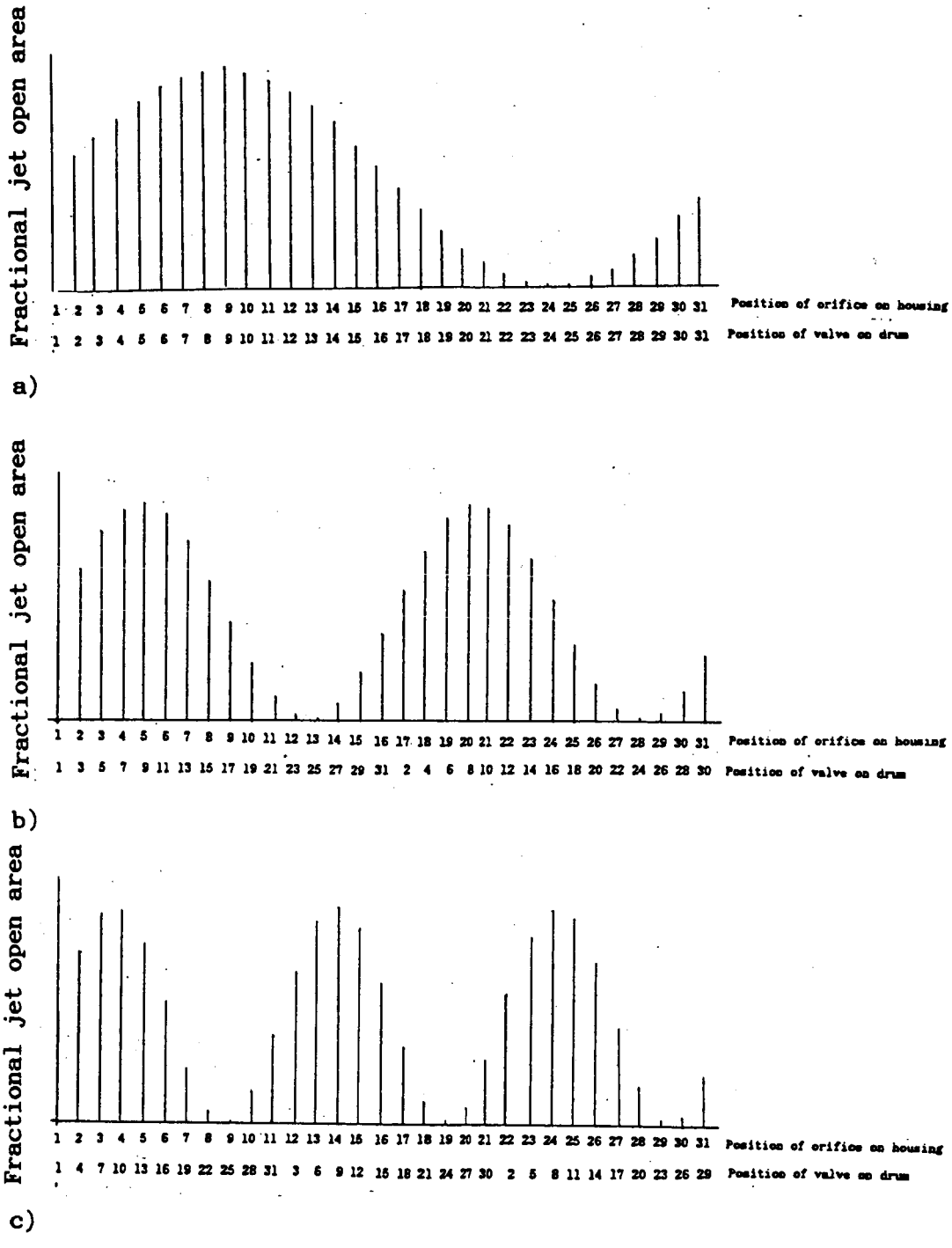

Fig. 2.9 Graphical illustration of the jet pattern created at a single instant using pneumatic logic. The logic arranged to create a) the fundamental mode b) the second harmonic and c) the third harmonic.

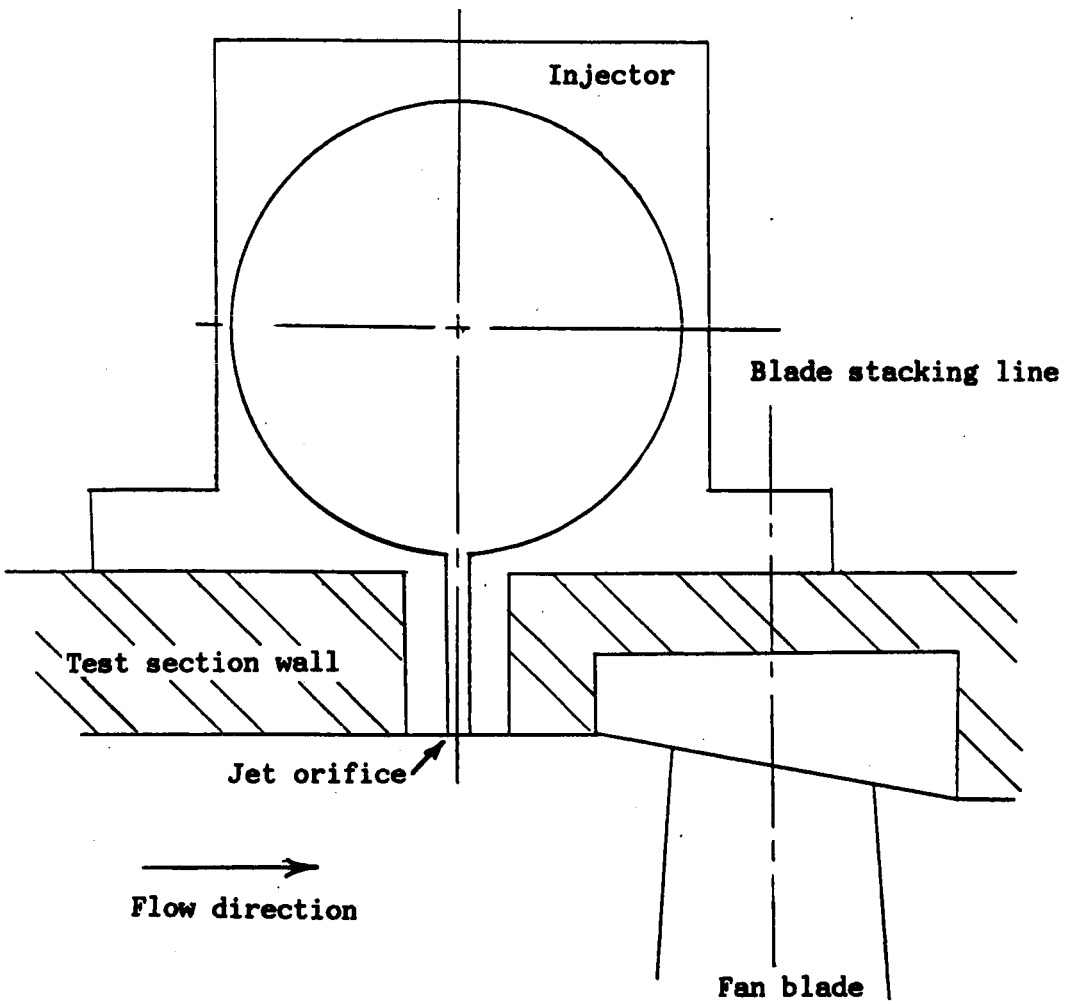

Fig 2.10 Placement of a close coupled injector in NASA Lewis Research Center Multistage Compressor Test Facility (W8).

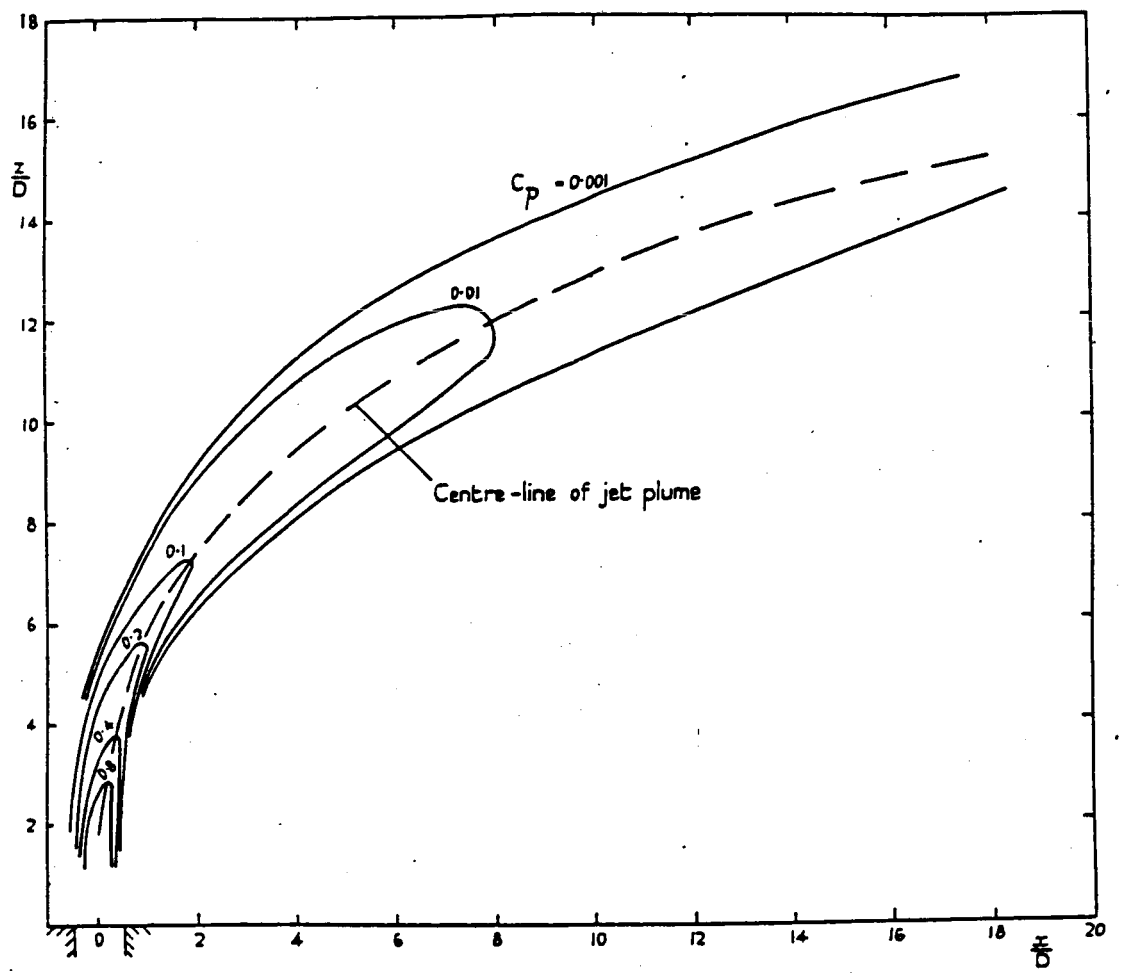

Fig. 3.1 Contours of constant pressure for a jet injected into a cross flow (after Jordinson [8]).

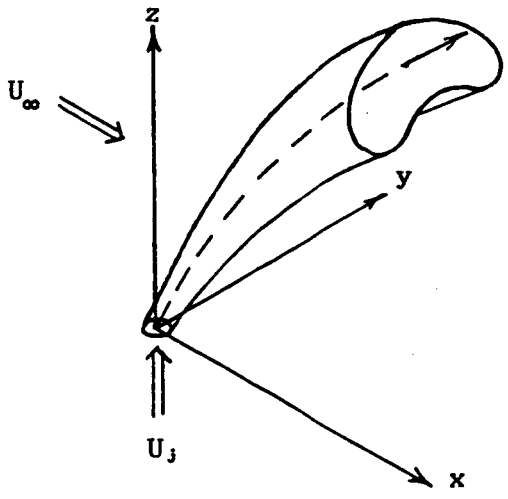

Fig. 3.2 The deformation of an injected jet in a cross flow showing the evolution of the horseshoe shape.

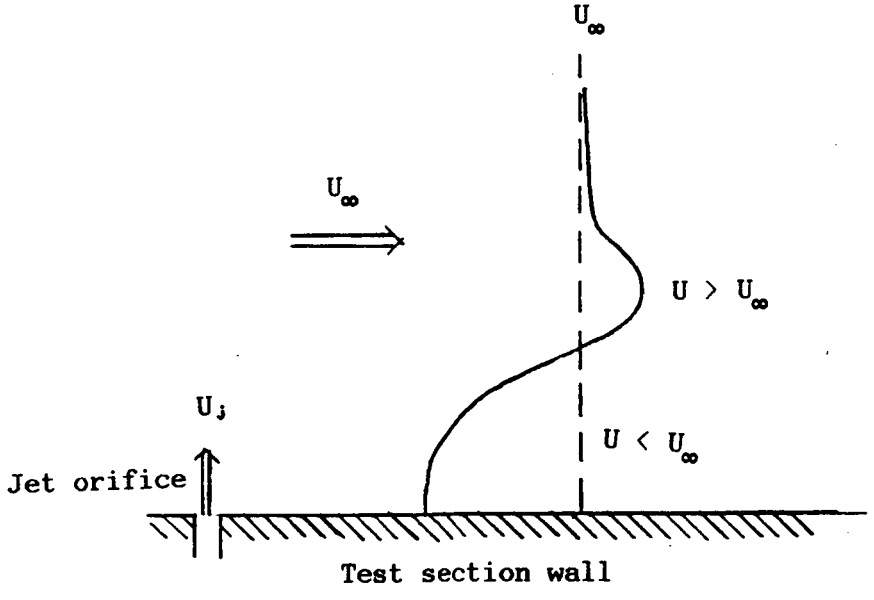

Fig. 3.3 Velocity excess and defect produced downstream by an injected jet.

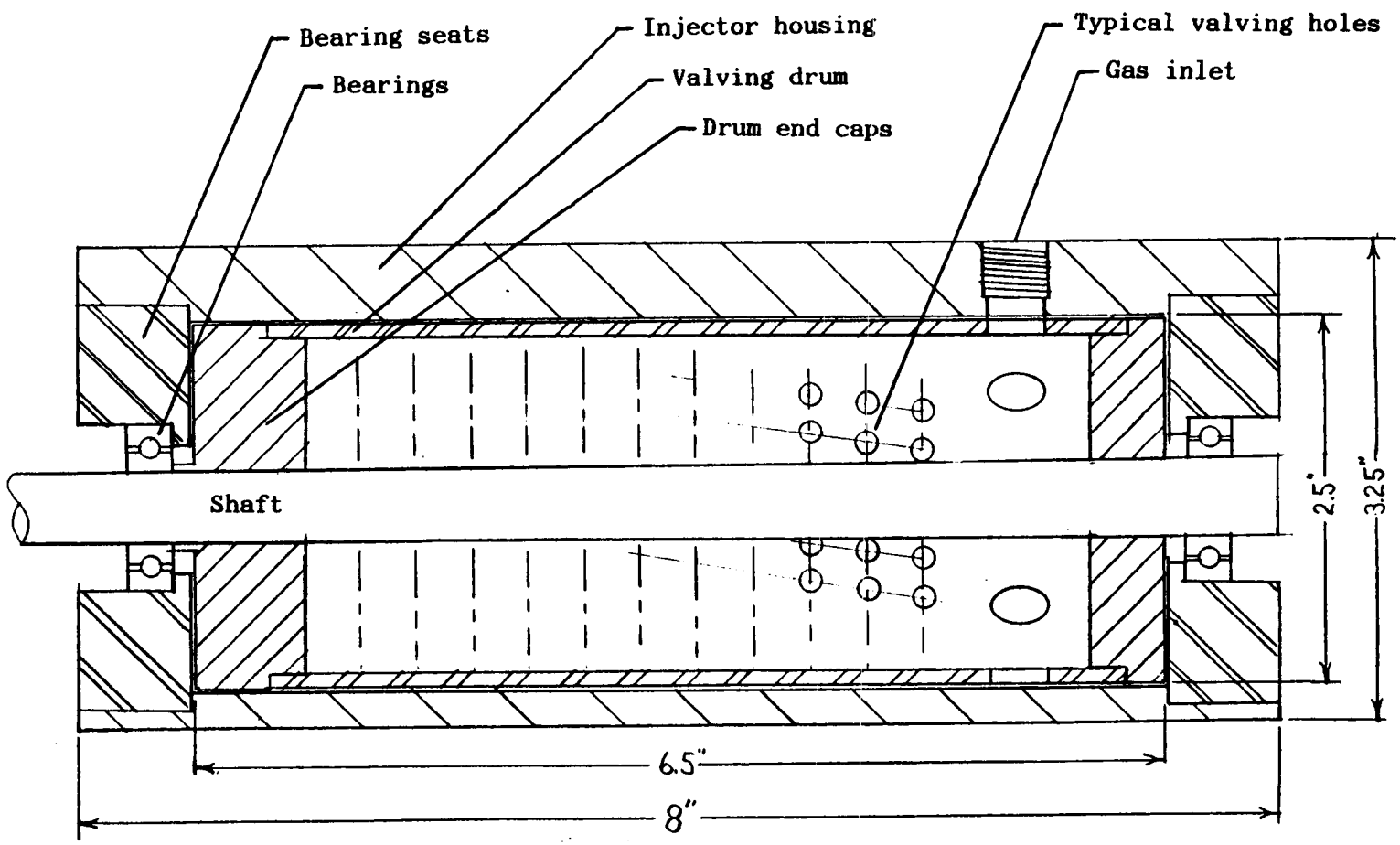

Fig. 4.1 Cutaway of the prototype injector design.

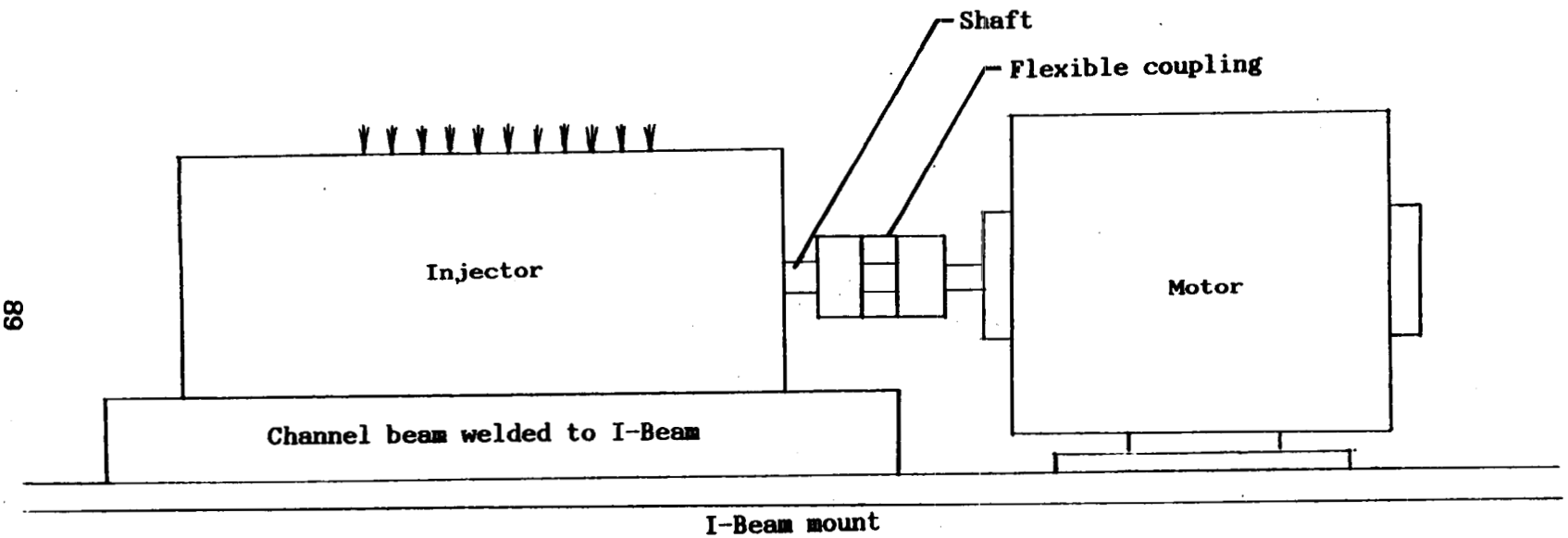

Fig. 4.2 Assembled view of prototype injector showing coupling to drive system.

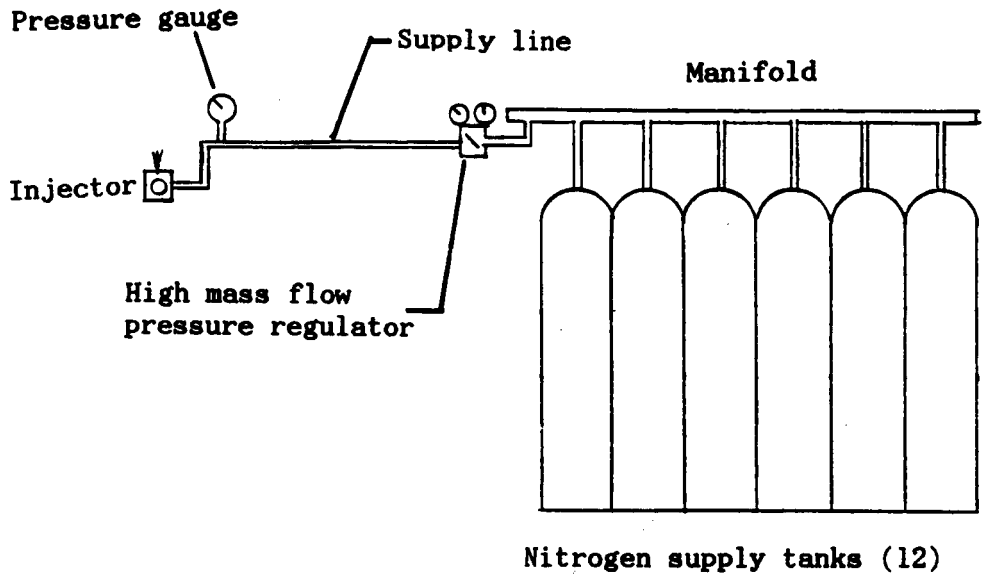

Fig. 4.3 Schematic of gas delivery system.

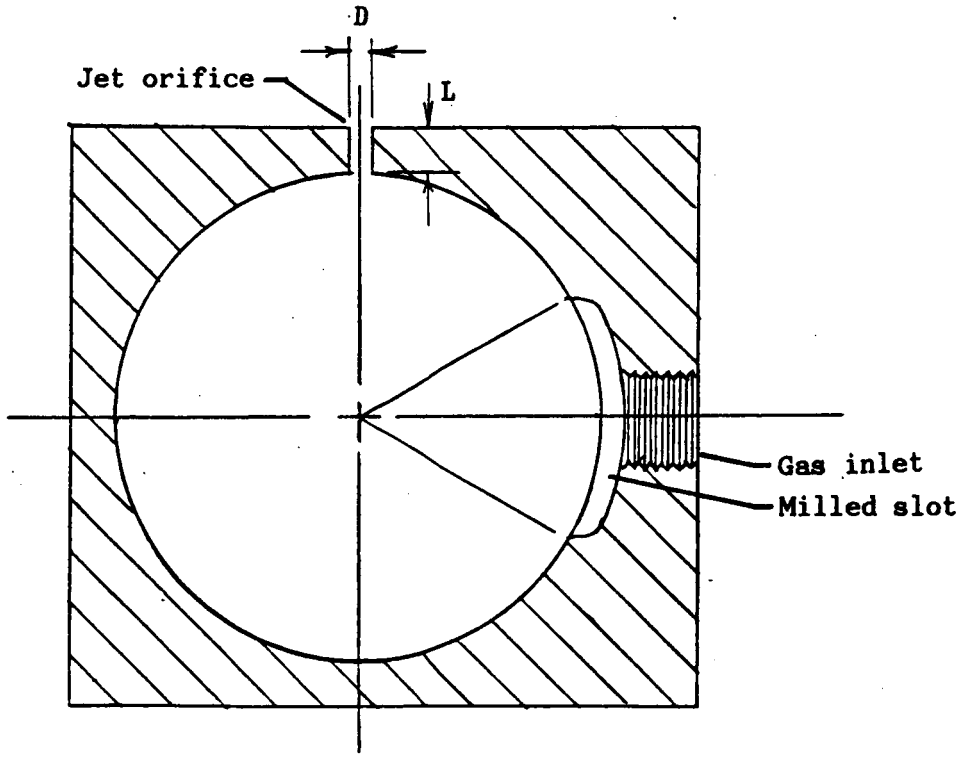

Fig. 4.4 Section of the injector housing at the axial location of the gas inlet.

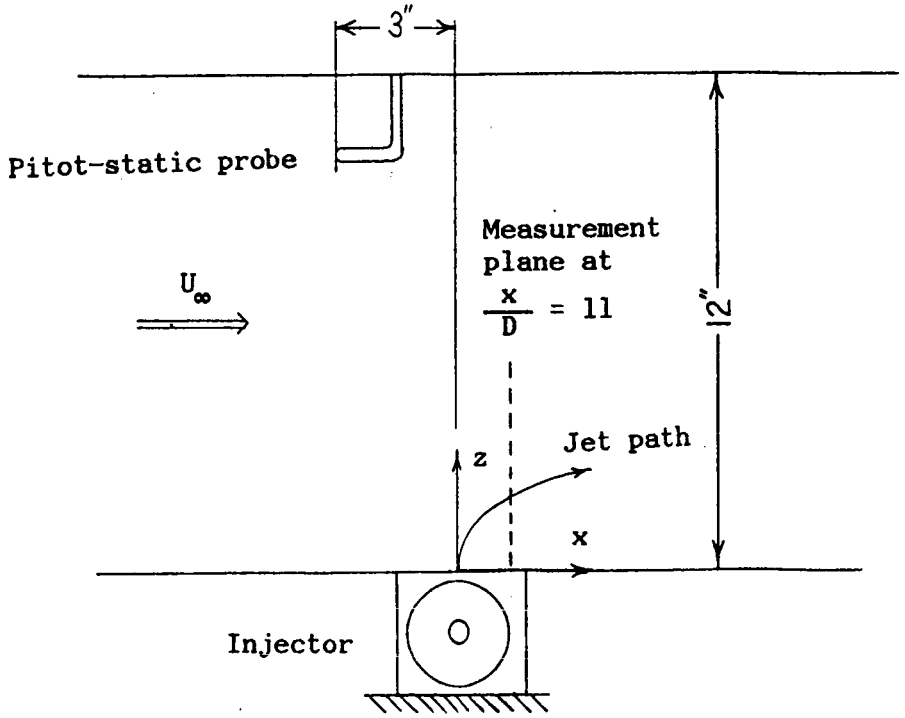

Fig. 4.5 Test section arrangement during testing in the MIT Low Turbulence Wind Tunnel.

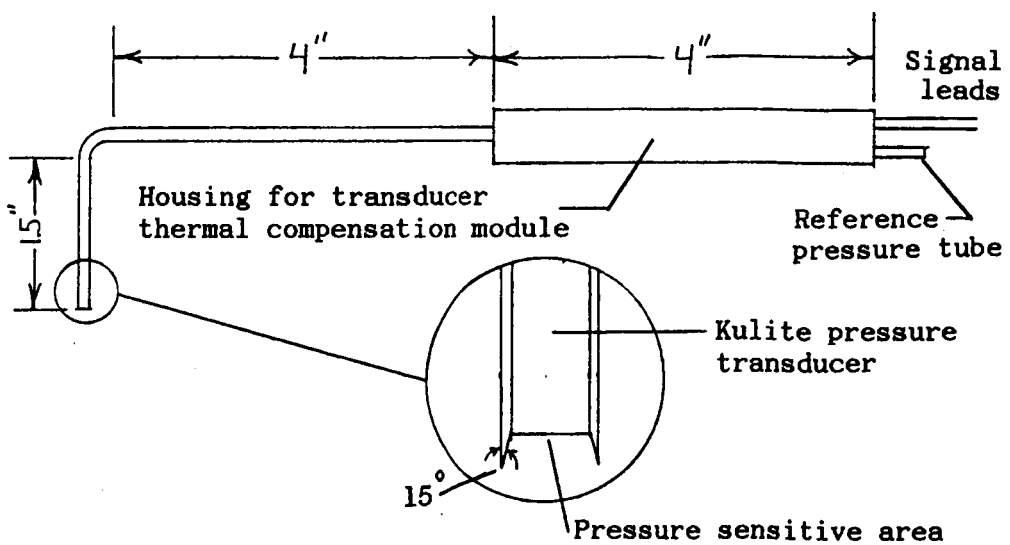

Fig. 4.6 Kulite total pressure probe.

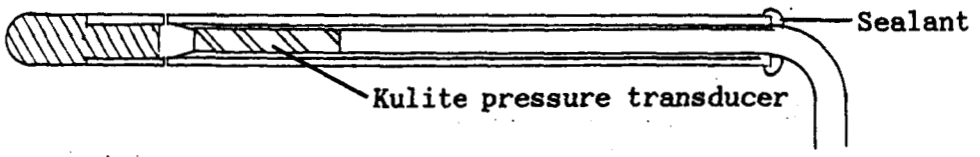

Cross section of attachment
showing mounting on total pressure probe.

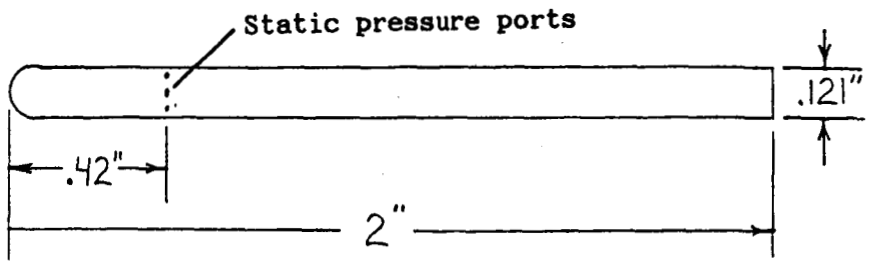

Fig. 4.7 Attachment for converting a Kulite total pressure probe to a static pressure probe.

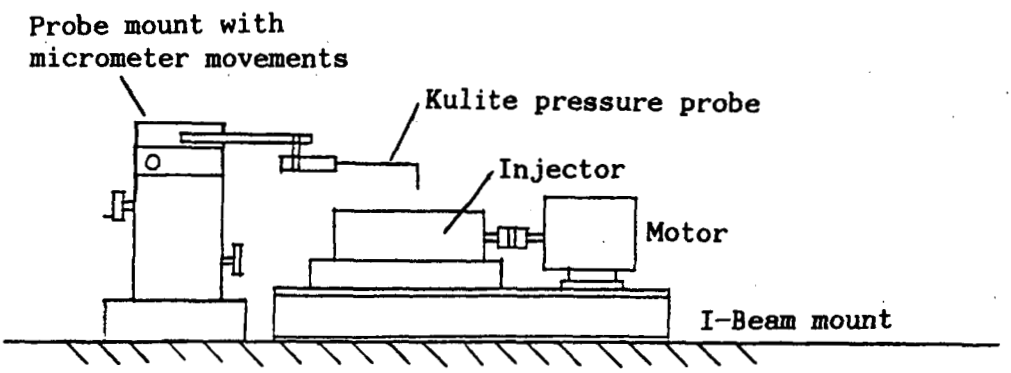

Fig. 4.8 Bench top testing arrangement.

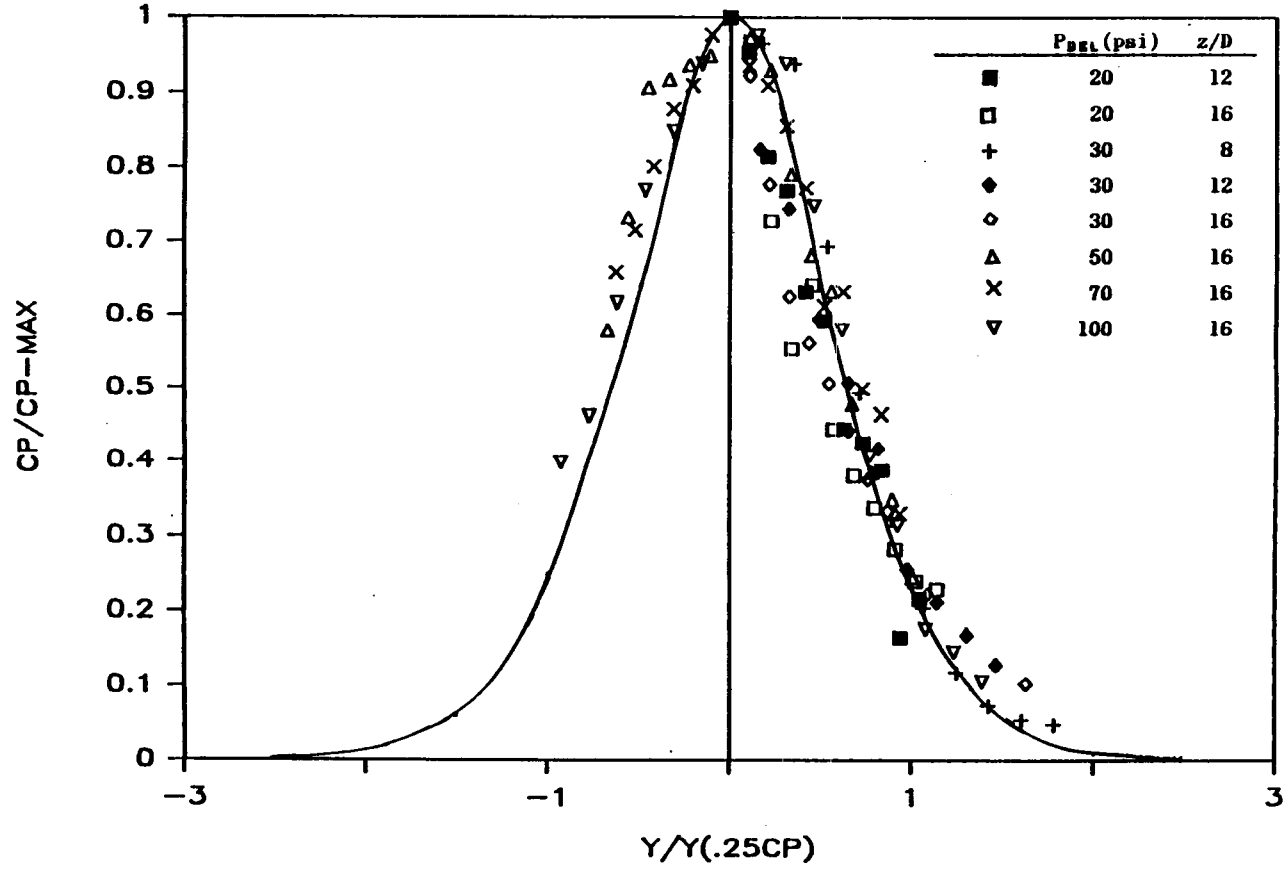

Fig. 5.1 Measured jet pressure profiles compared with the analytical model of Schlicting [13].

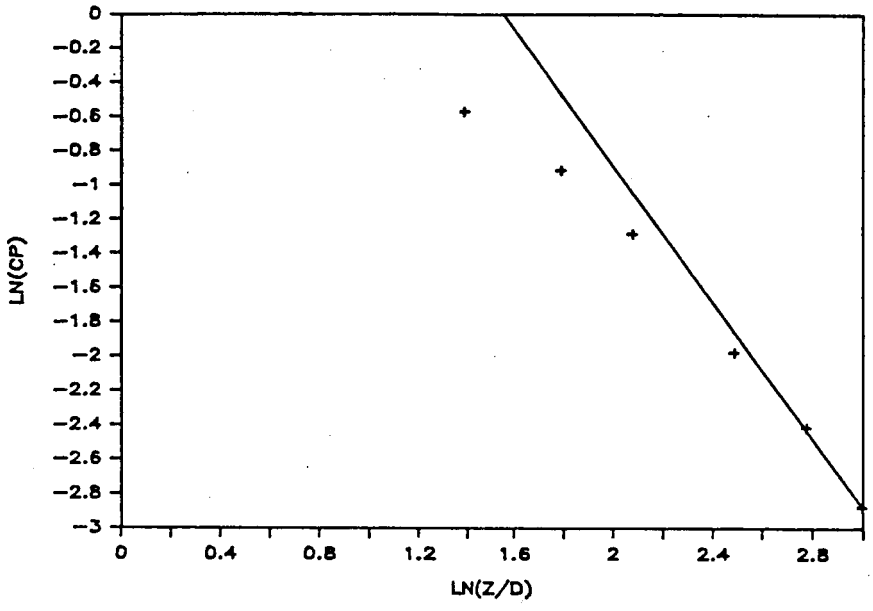

Fig. 5.2 Logarithmic plot of the decay of the centerline jet pressure measurement of a fully open jet, compared with the $1/z^2$ prediction of Schlicting [13].

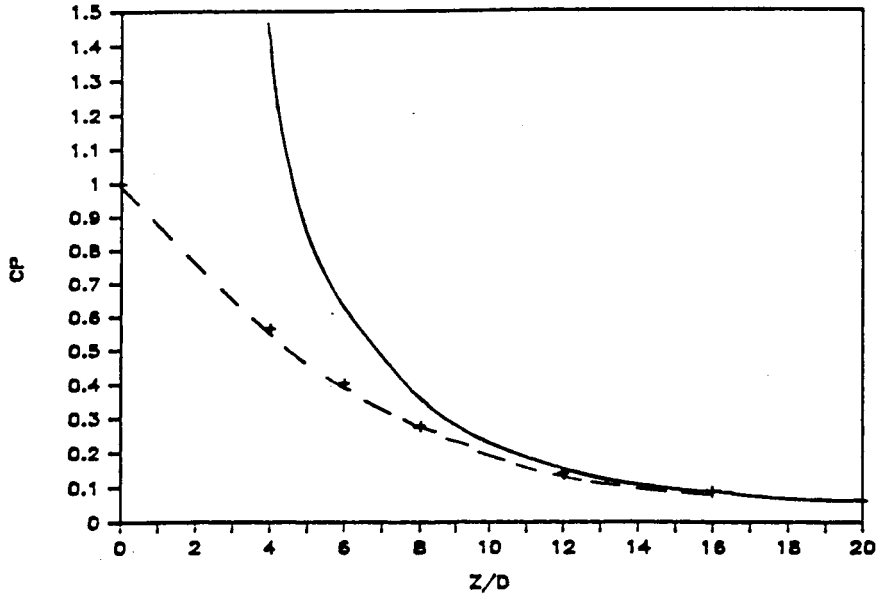

Fig. 5.3 Linear plot of the decay of the centerline jet pressure measurement of a fully open jet, compared with the $1/z^2$ prediction of Schlicting [13].

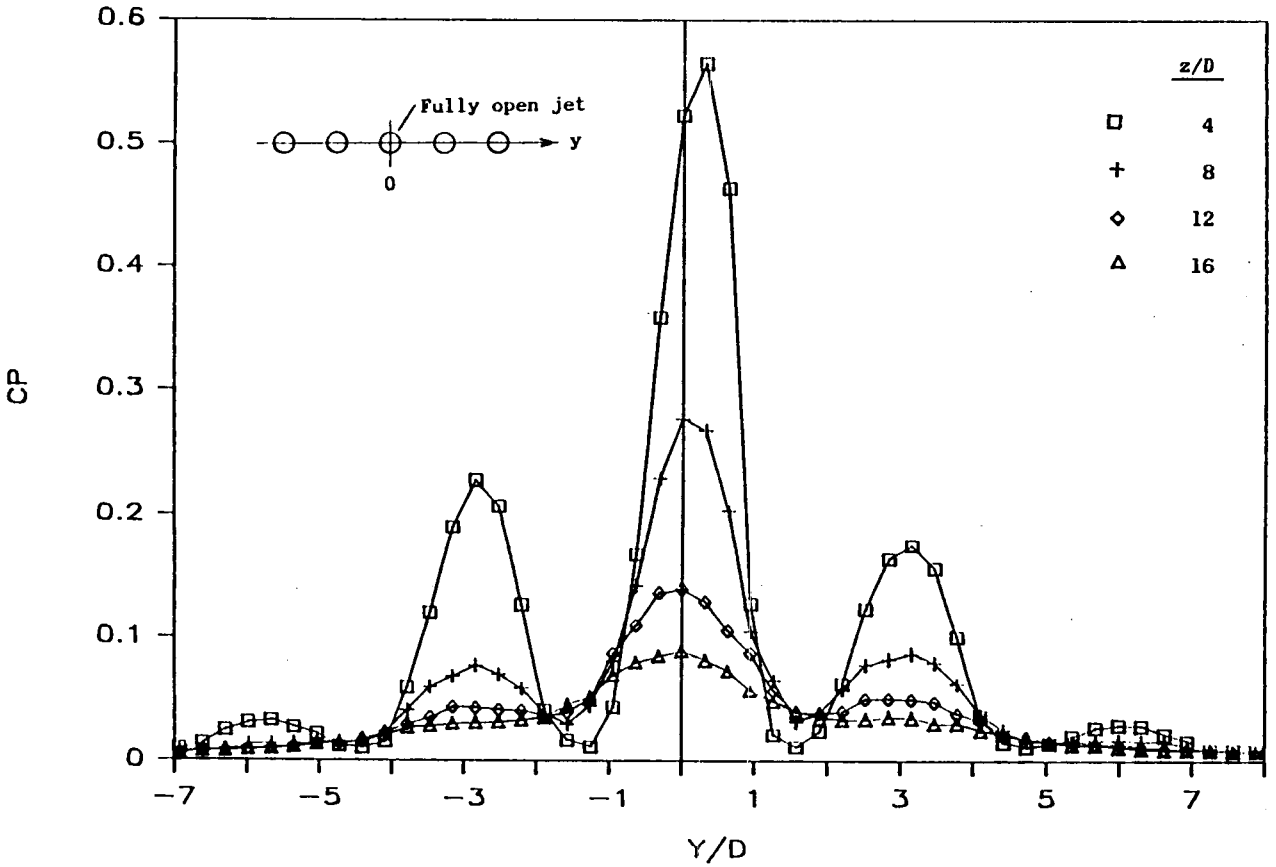

Fig. 5.4 Pressure distribution measured along a line over the jets (y), for a multiple jet pattern with the center jet fully open with 20 psig delivery pressure.

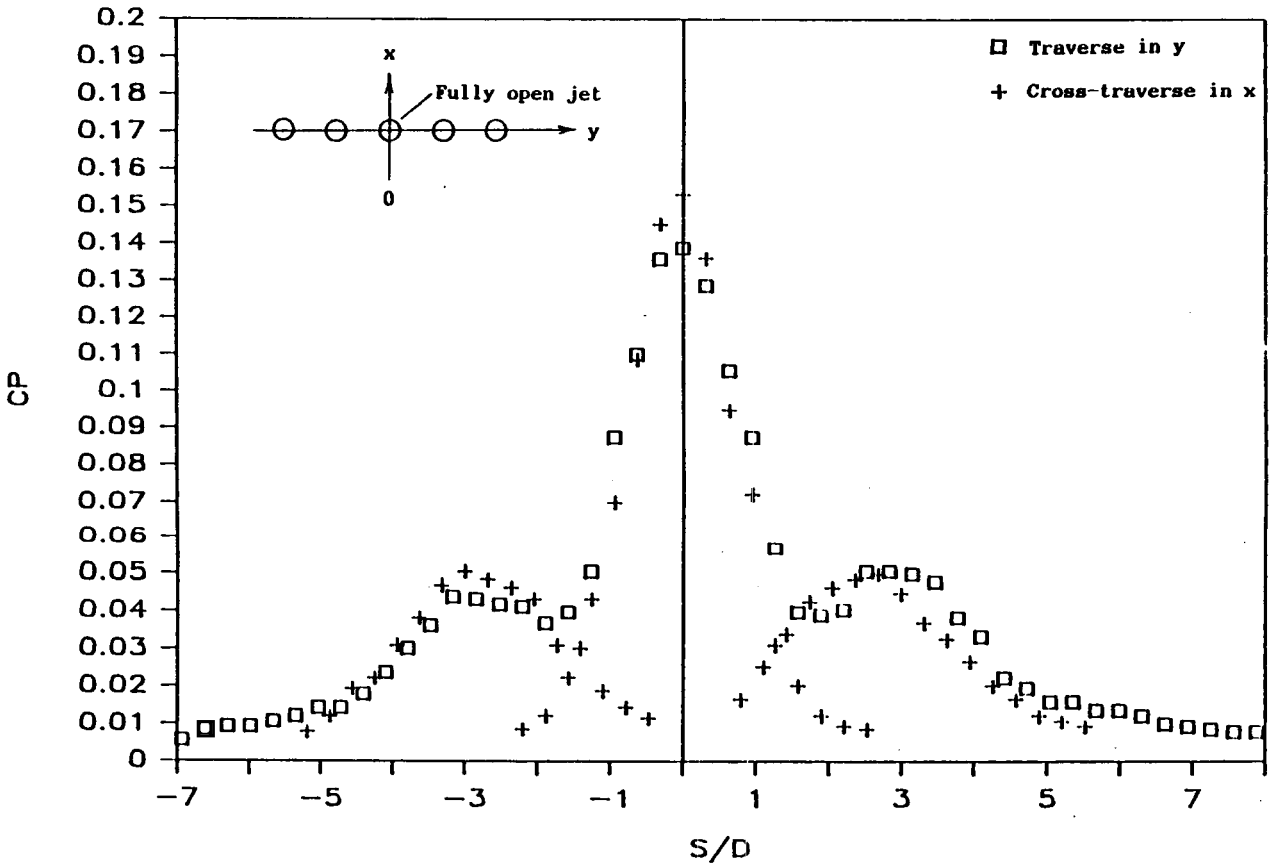

Fig. 5.5 Pressure distribution measured in the transverse (x) direction superimposed on those measured along the jets (y) for 20 psig delivery pressure at 12 jet diameters above the jet orifice.

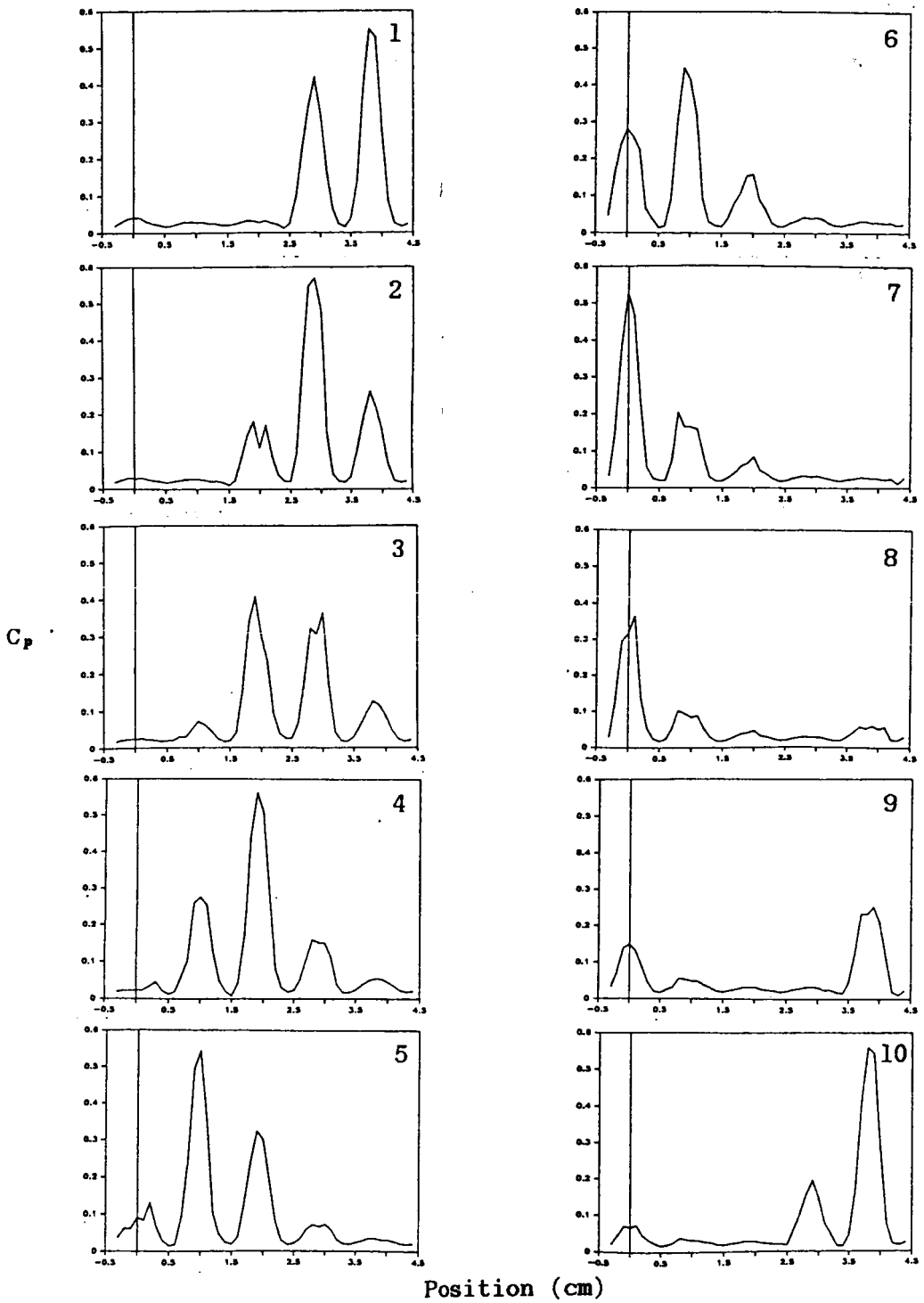

Fig. 5.6 Time history of multiple pulsing jets shown for 10 evenly spaced instants in a jet period, 20 psig delivery pressure, z/D = 4, L = .25", 1044 Hz. pulsing frequency.

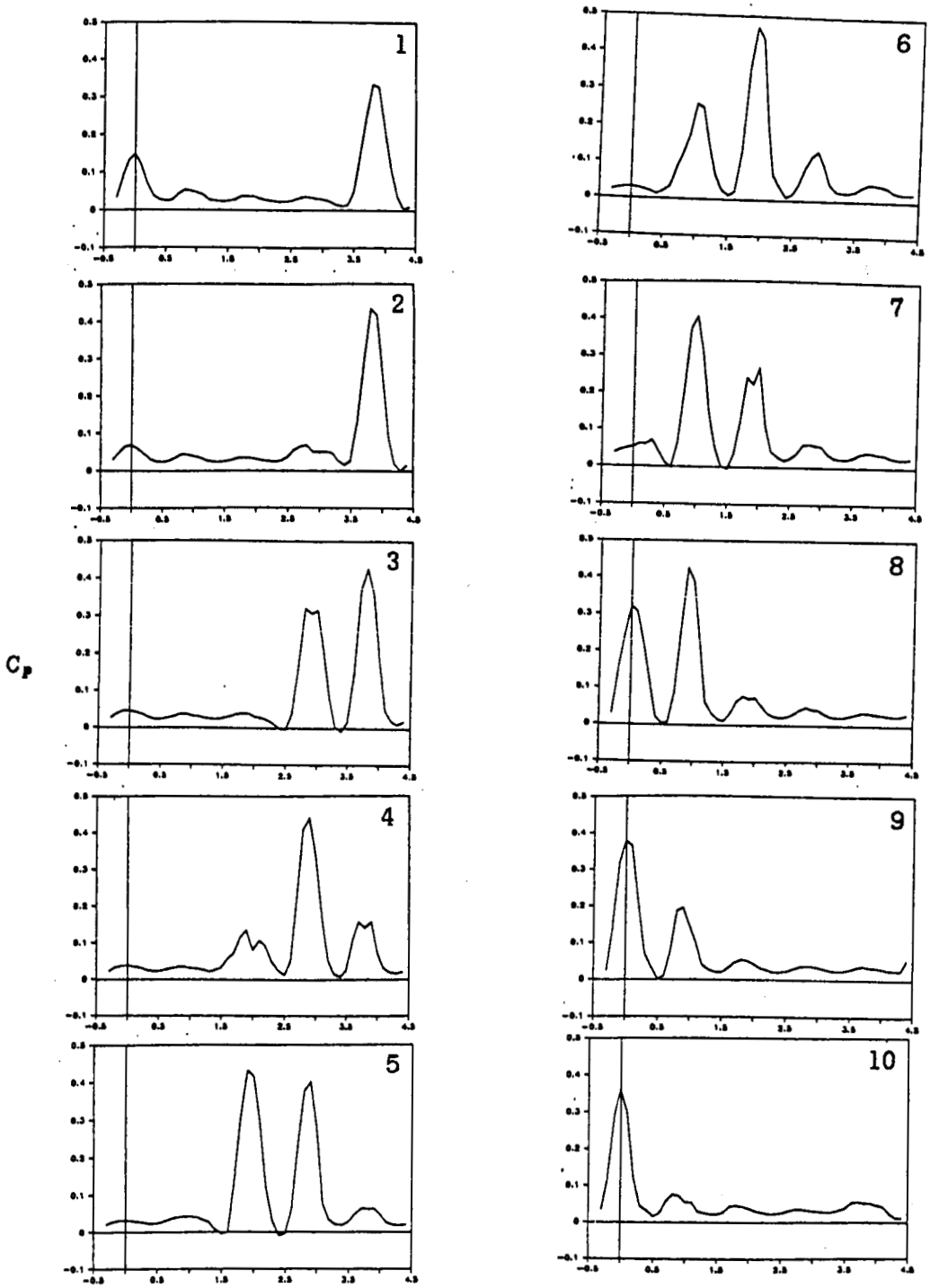

Fig. 5.7 Time history of multiple pulsing jets shown for 10 evenly spaced instants in a jet period, 20 psig delivery pressure, z/D = 4, L = .25", 2618 Hz. pulsing frequency.

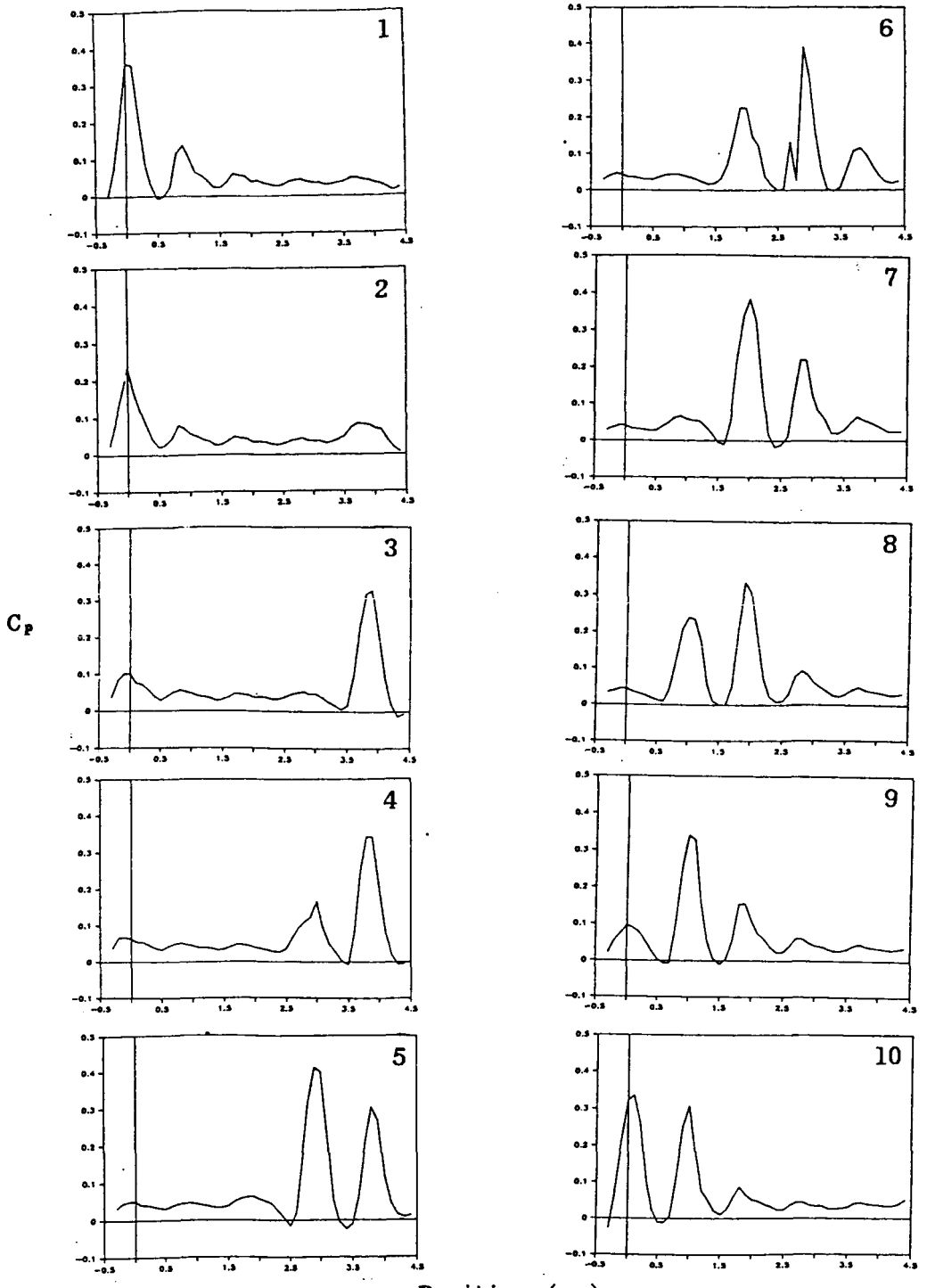

Fig. 5.8 Time history of multiple pulsing jets shown for 10 evenly spaced instants in a jet period, 20 psig delivery pressure, z/D = 4, L = .25", 4078 Hz. pulsing frequency.

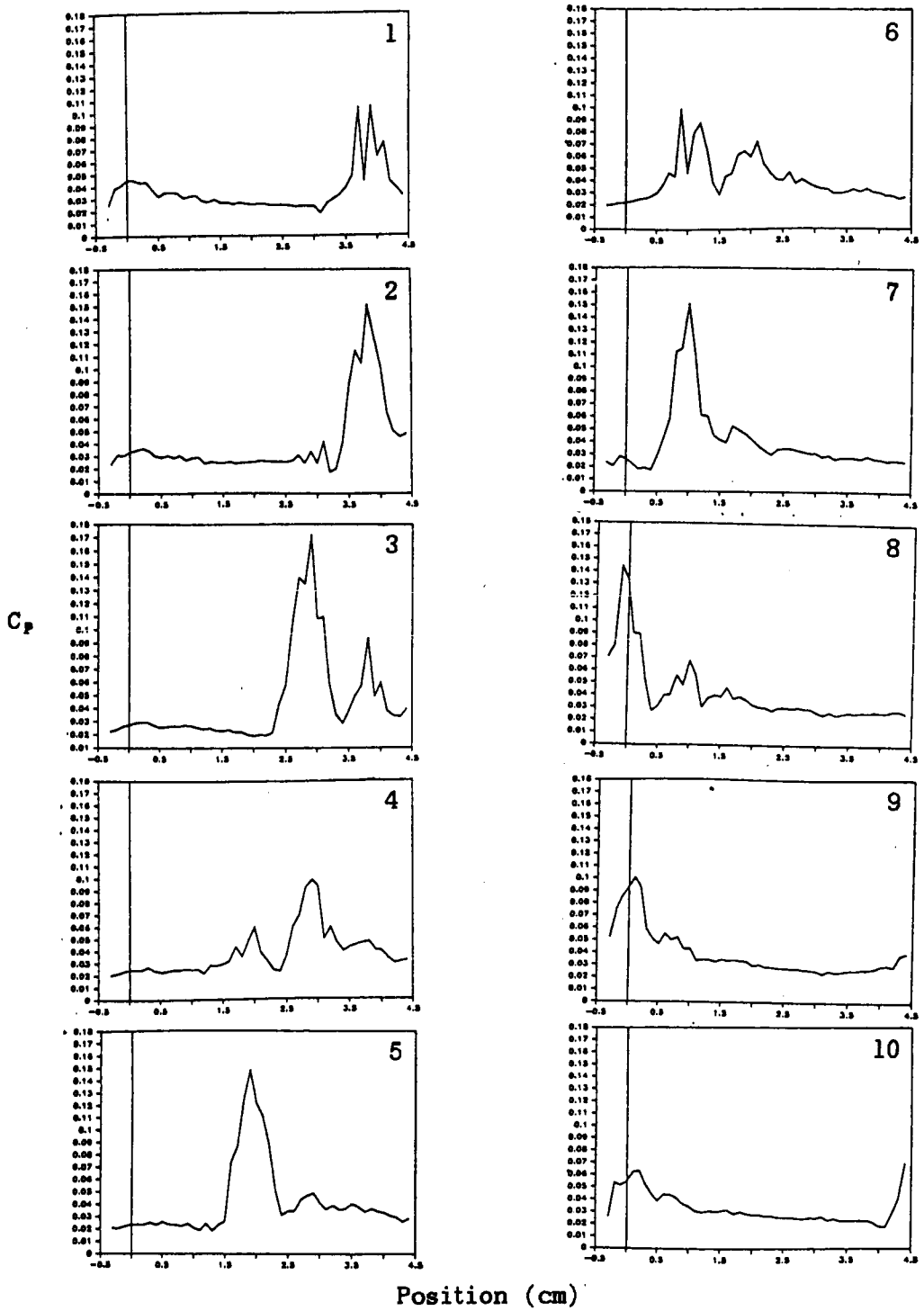

Fig. 5.9 Time history of multiple pulsing jets shown for 10 evenly spaced instants in a jet period, 20 psig delivery pressure, z/D = 12, L = .25", 512 Hz. pulsing frequency.

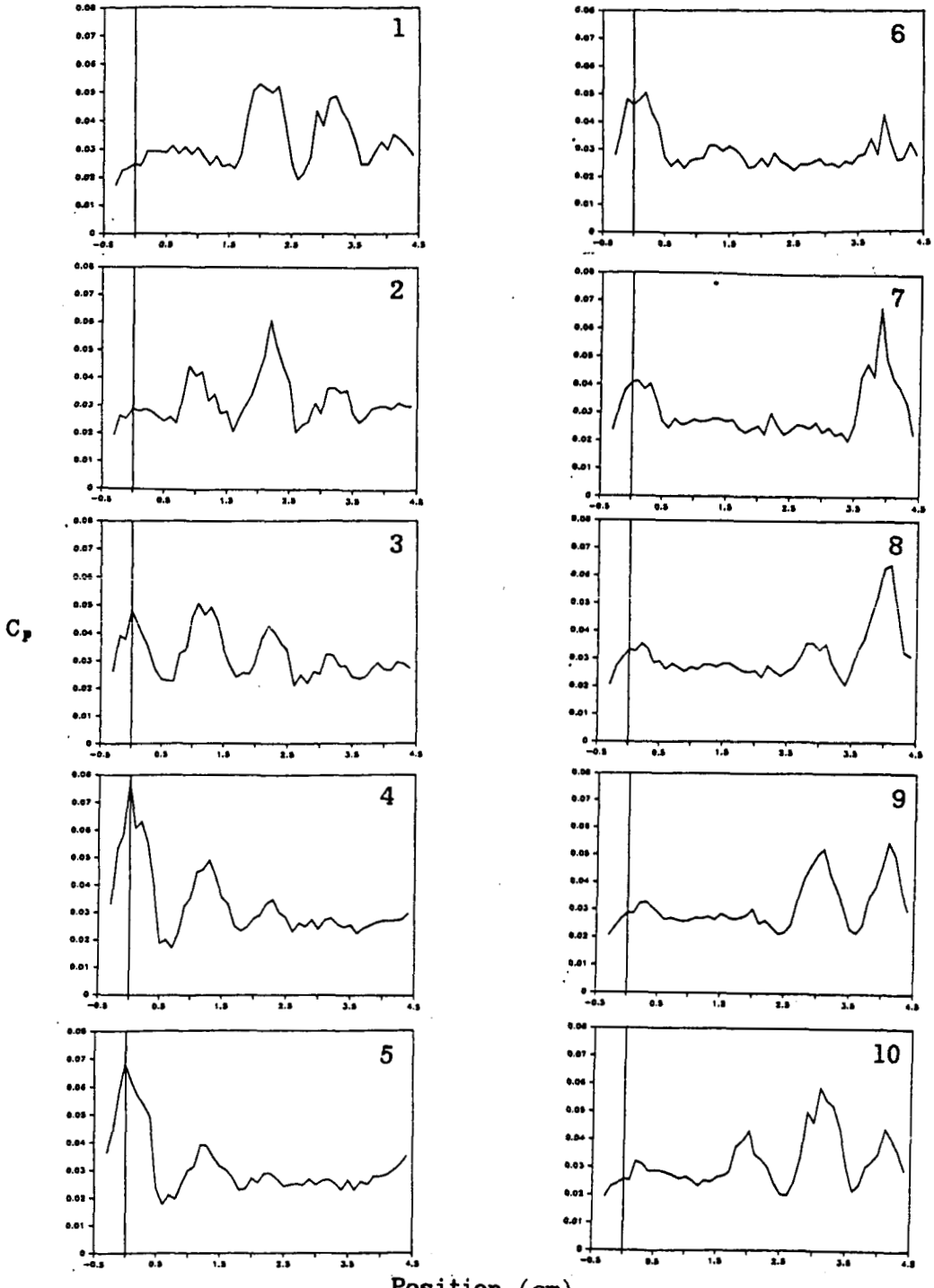

Fig. 5.10 Time history of multiple pulsing jets shown for 10 evenly spaced instants in a jet period, 20 psig delivery pressure, z/D = 12, L = .25", 2553 Hz. pulsing frequency.

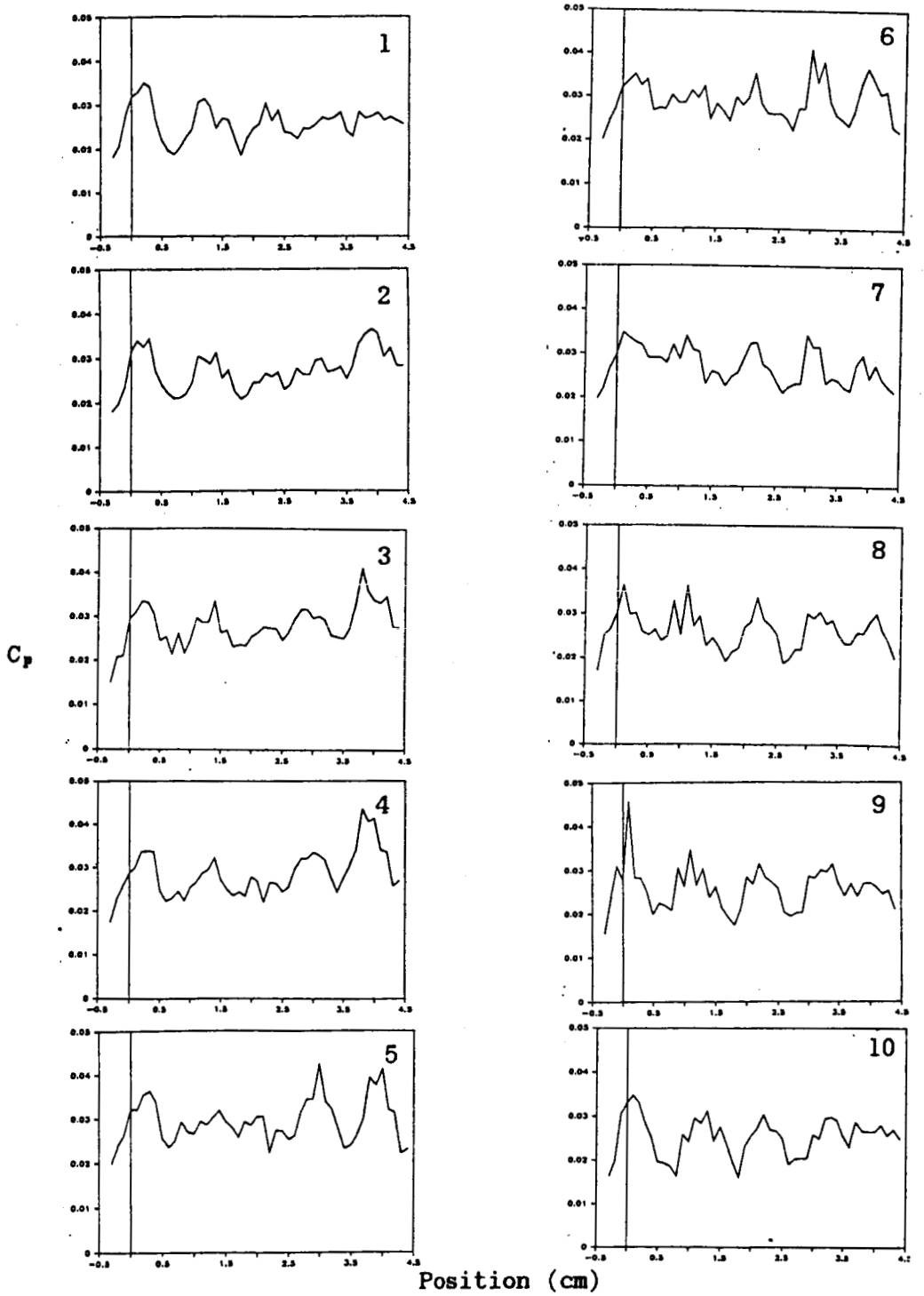

Fig. 5.11 Time history of multiple pulsing jets shown for 10 evenly spaced instants in a jet period, 20 psig delivery pressure, z/D = 12, L = .25", 4071 Hz. pulsing frequency.

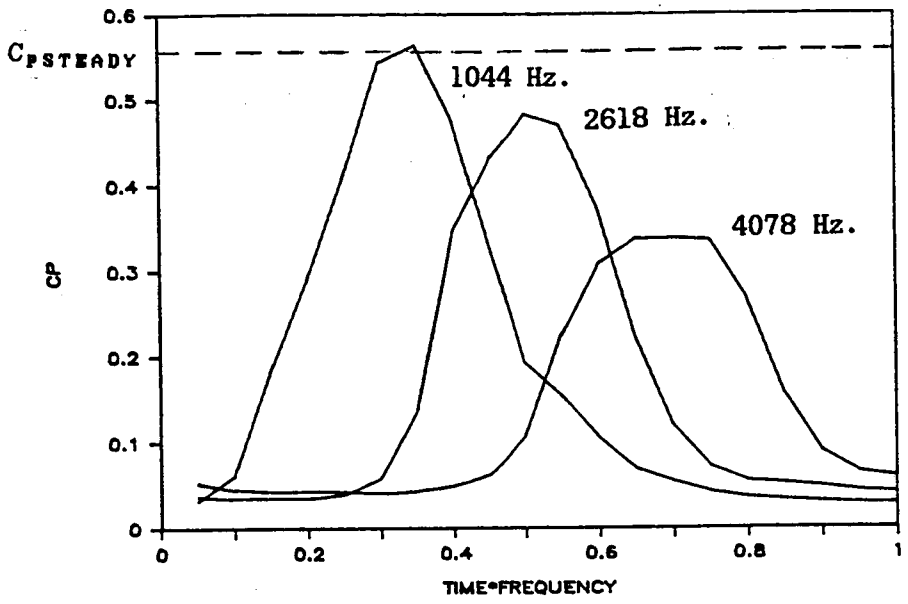

Fig. 5.12 Ensemble averaged pressure pulse shape, z/D = 4, 20 psig delivery pressure, z/D = 4, L = .25", for the indicated frequencies.

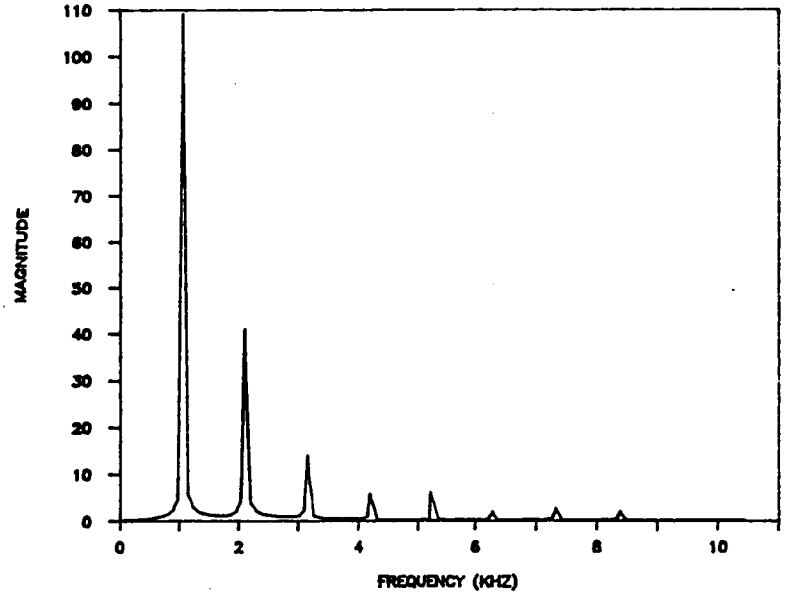

Fig. 5.13 Spectrum of ensemble averaged pulse shape, 20 psig delivery pressure, z/D = 4, L = .25", 1044 Hz. pulsing frequency.

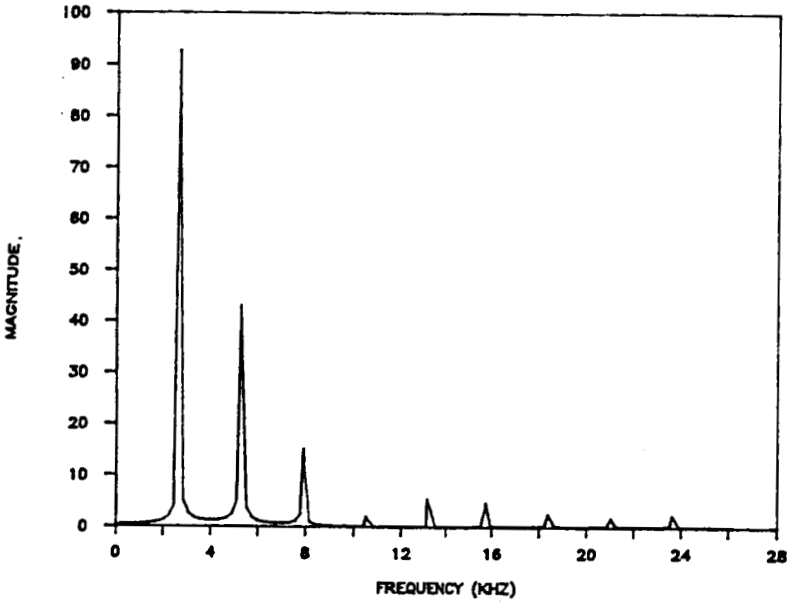

Fig. 5.14 Spectrum of ensembled average pulse shape for 20 psig delivery pressure, z/D = 4, L = .25", 2618 Hz. pulsing frequency.

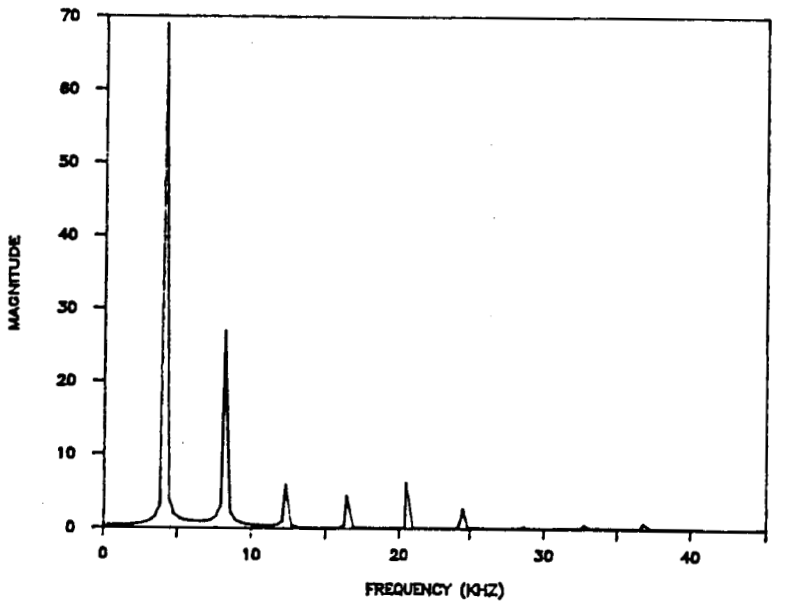

Fig. 5.15 Spectrum of ensembled average pulse shape for 20 psig delivery pressure, z/D = 4, L = .25", 4078 Hz. pulsing frequency.

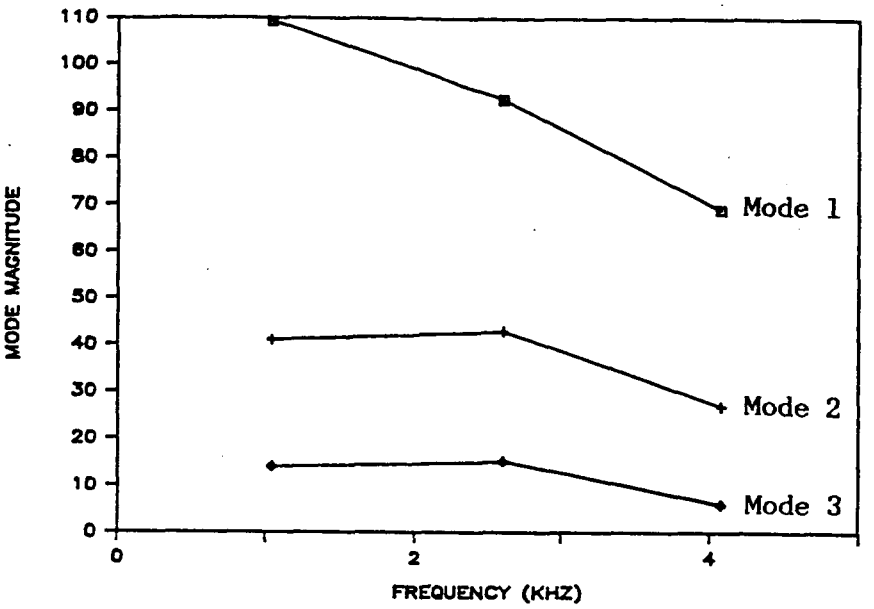

Fig. 5.16 Magnitudes of the first three harmonics of the ensembled average pressure as a function of jet pulsing frequency, 20 psig delivery pressure, z/D = 4, L = .25".

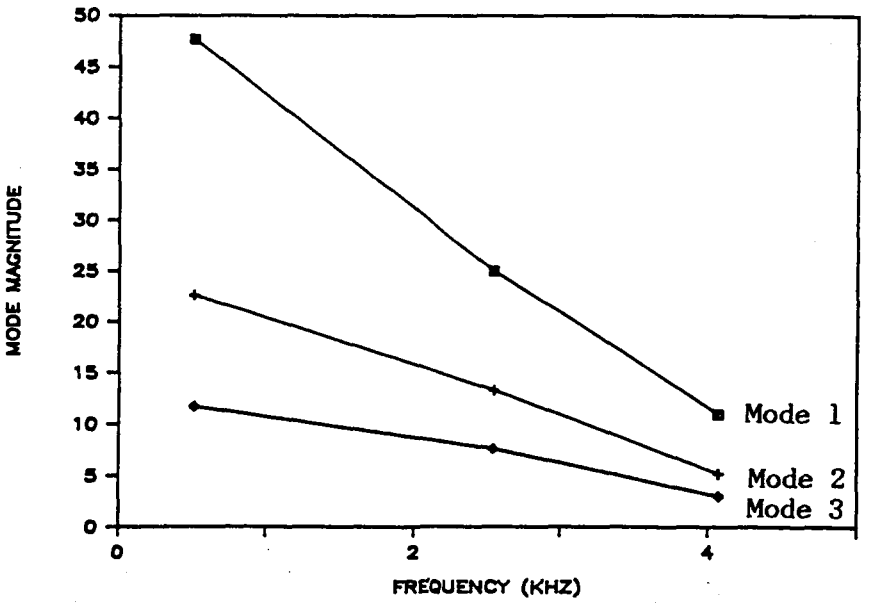

Fig. 5.17 Magnitudes of the first three harmonics of the ensembled average pressure as a function of jet pulsing frequency, 20 psig delivery pressure, z/D = 8, L = .25".

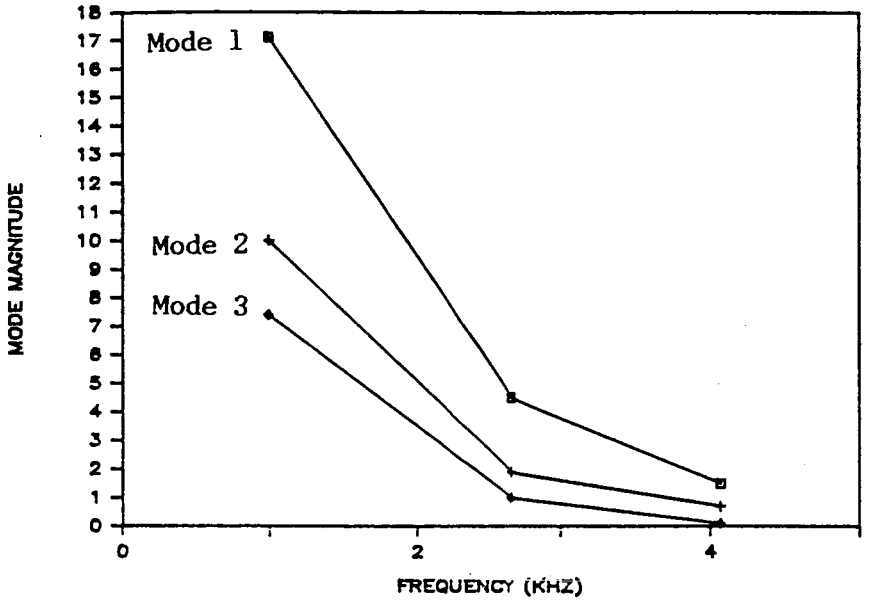

Fig. 5.18 Magnitudes of the first three harmonics of the ensembled average pressure as a function of jet pulsing frequency, 20 psig delivery pressure, z/D = 12, L = .25".

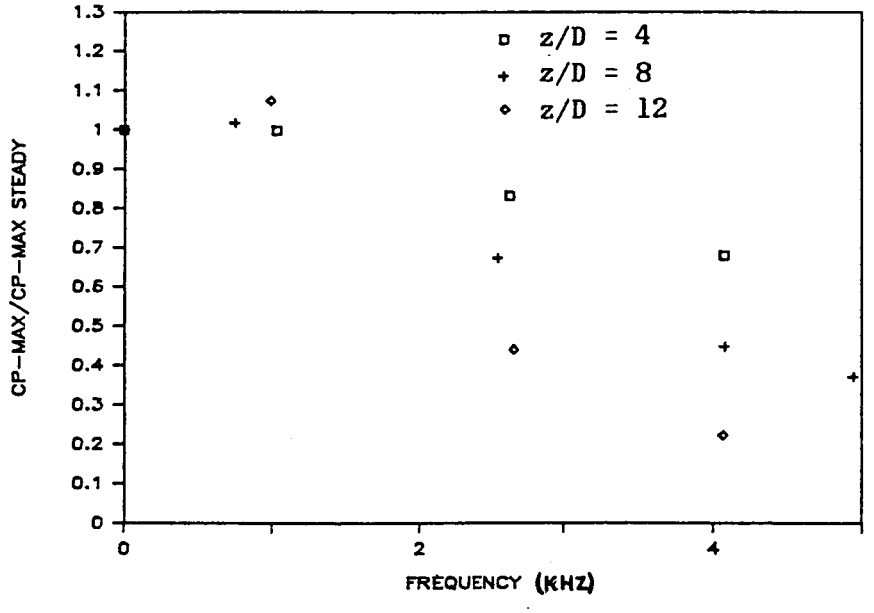

Fig. 5.19 Maximum pressure in the average pulse as a function of jet pulsing frequency, 20 psig delivery pressure L = .25"

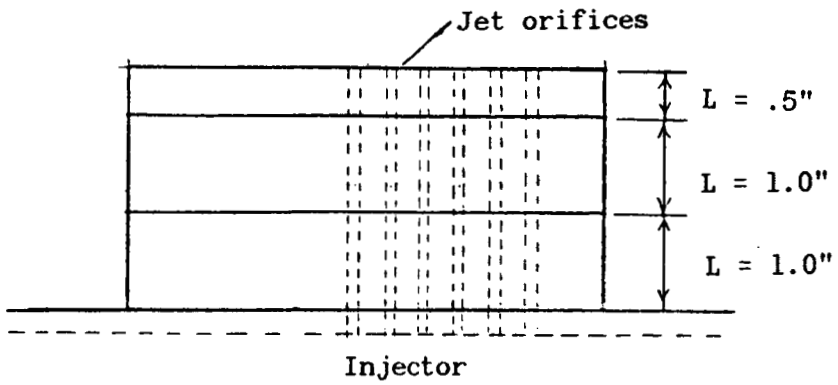

Fig. 5.20 Injector attachment to produce jet plemums of lengths L = .75" to 2.75".

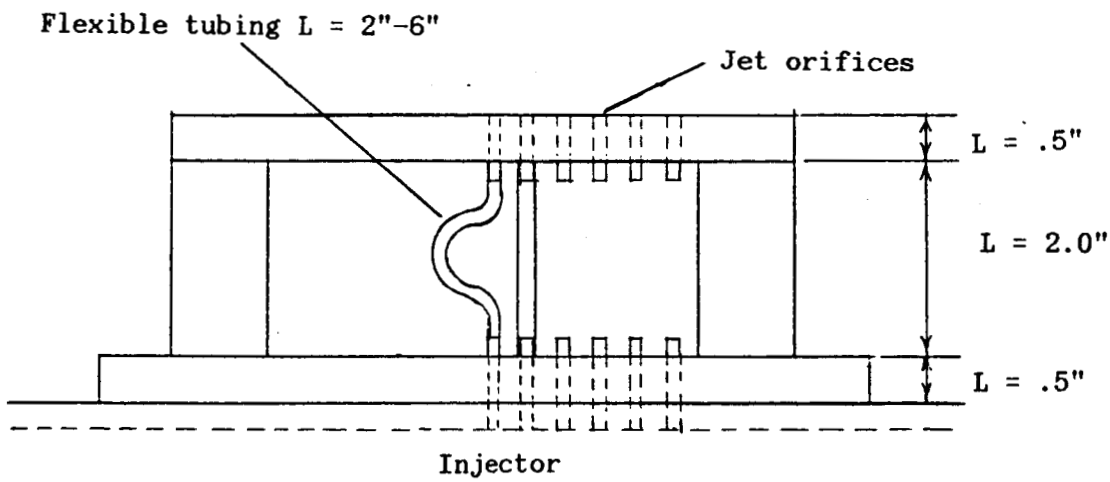

Fig. 5.21 Injector attachment to produce jet plenums of lengths L = 3.25" to 7.25"

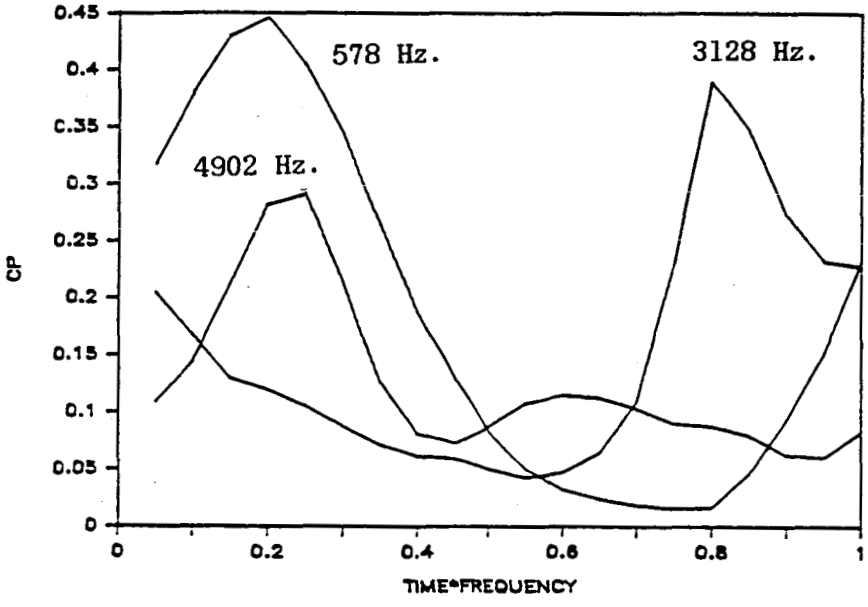

Fig. 5.22 Ensemble averaged pressure pulse shape, z/D = 4, 20 psig delivery pressure, z/D = 4, L = 3.25", for the indicated frequencies.

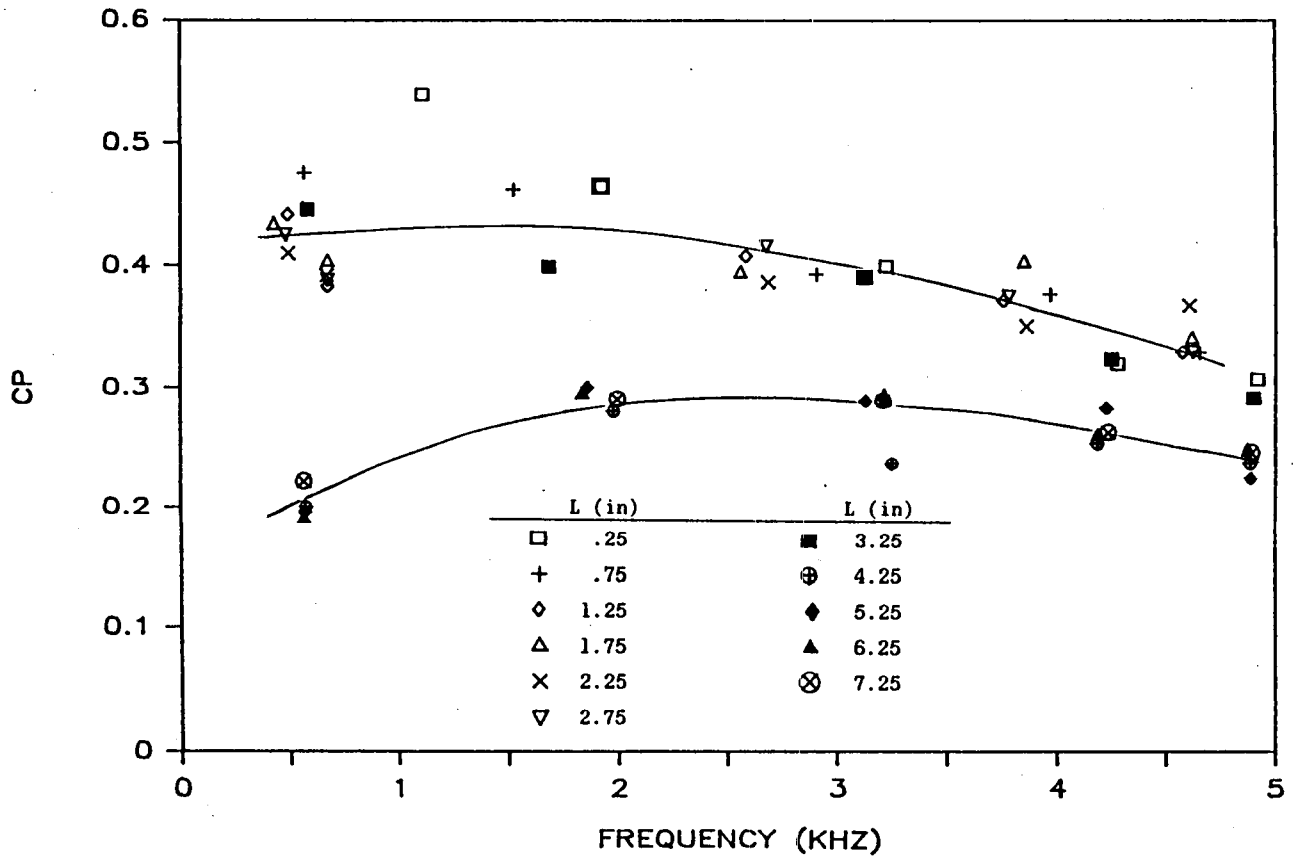

Fig. 5.23 Maximum pressure in the average pulse as a function of jet pulsing frequency, for a variety of plenum lengths, 20 psig delivery pressure, z/D = 4.

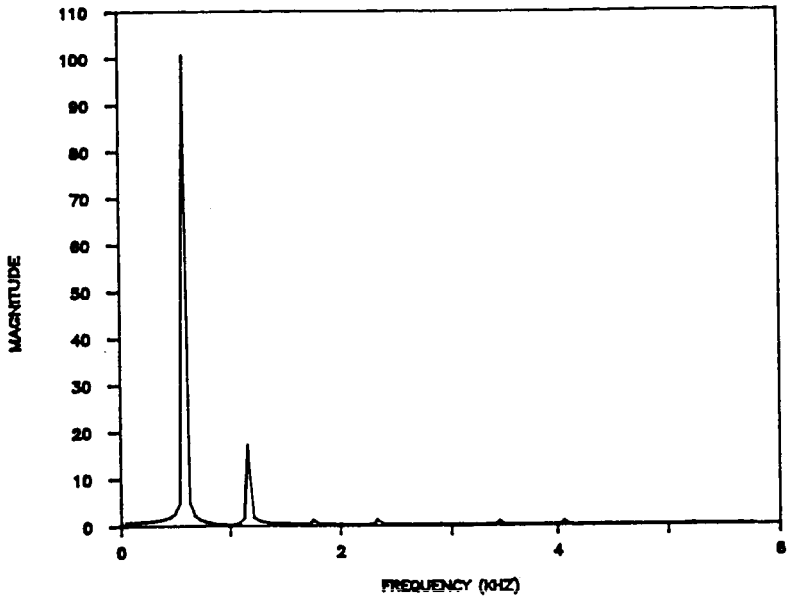

Fig. 5.24 Spectrum of ensemble averaged pulse shape, 20 psig delivery pressure, and z/D = 4, L = 3.25", 1044 Hz. pulsing frequency.

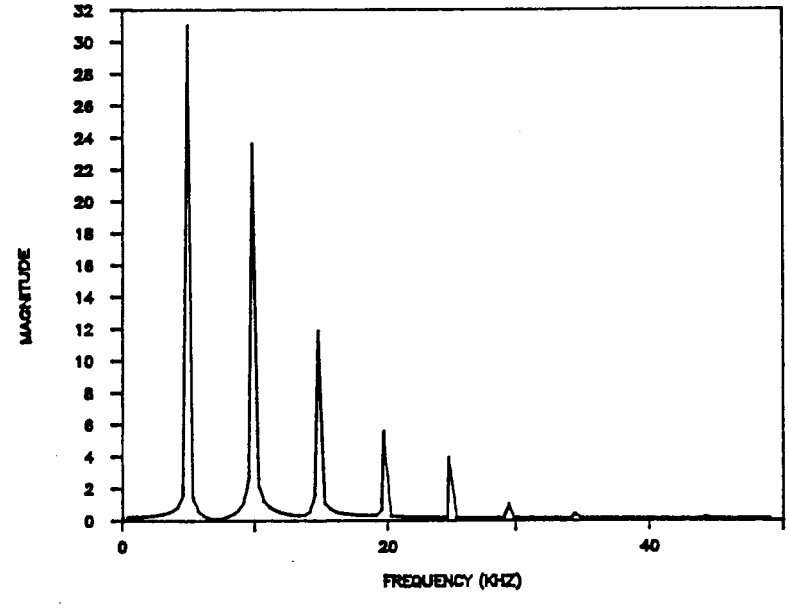

Fig. 5.25 Spectrum of ensemble averaged pulse shape, 20 psig delivery pressure, and z/D = 4, L = 3.25", 4902 Hz. pulsing frequency.

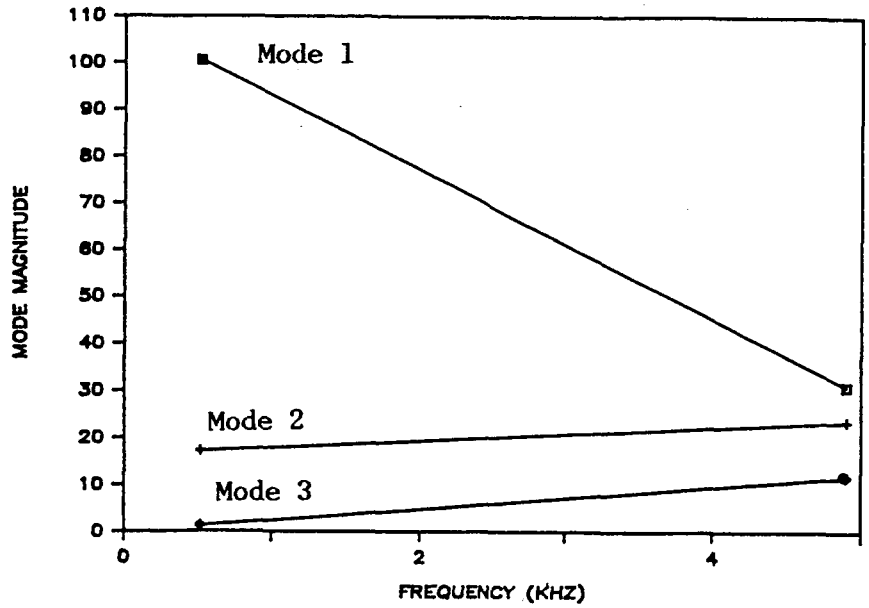

Fig. 5.26 Magnitudes of the first three harmonics of the ensembled average pressure as a function of jet pulsing frequency, 20 psig delivery pressure, z/D = 4, L = 3.25".

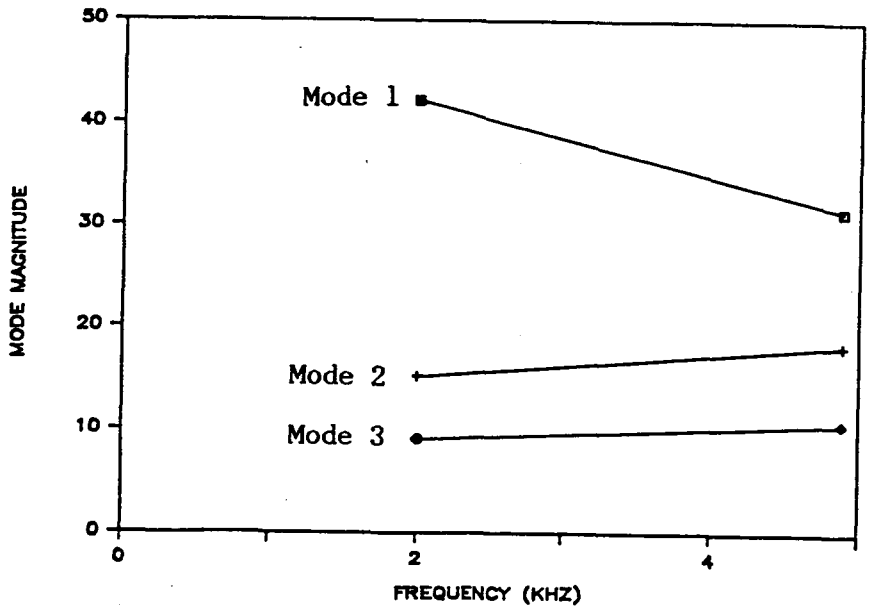

Fig. 5.27 Magnitudes of the first three harmonics of the ensembled average pressure as a function of jet pulsing frequency, 20 psig delivery pressure, z/D = 4, L = 7.25".

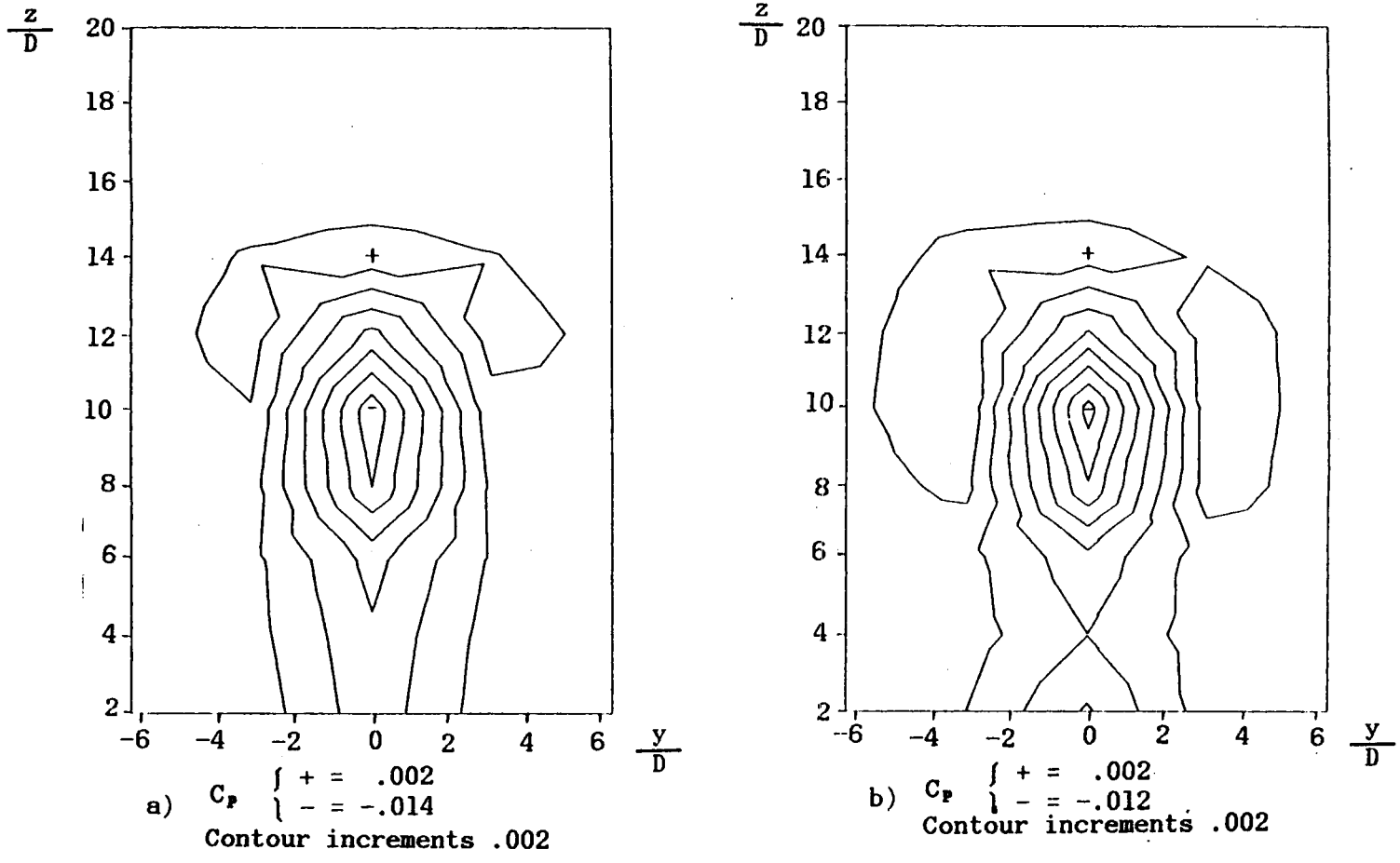

Fig. 5.28 Contours of constant pressure in a y-z plane at x/D = 11, U_∞ = 60 mph, and 5 psig delivery pressure, taken with a) Kulite pressure probe and b) standard pitot-static probe.

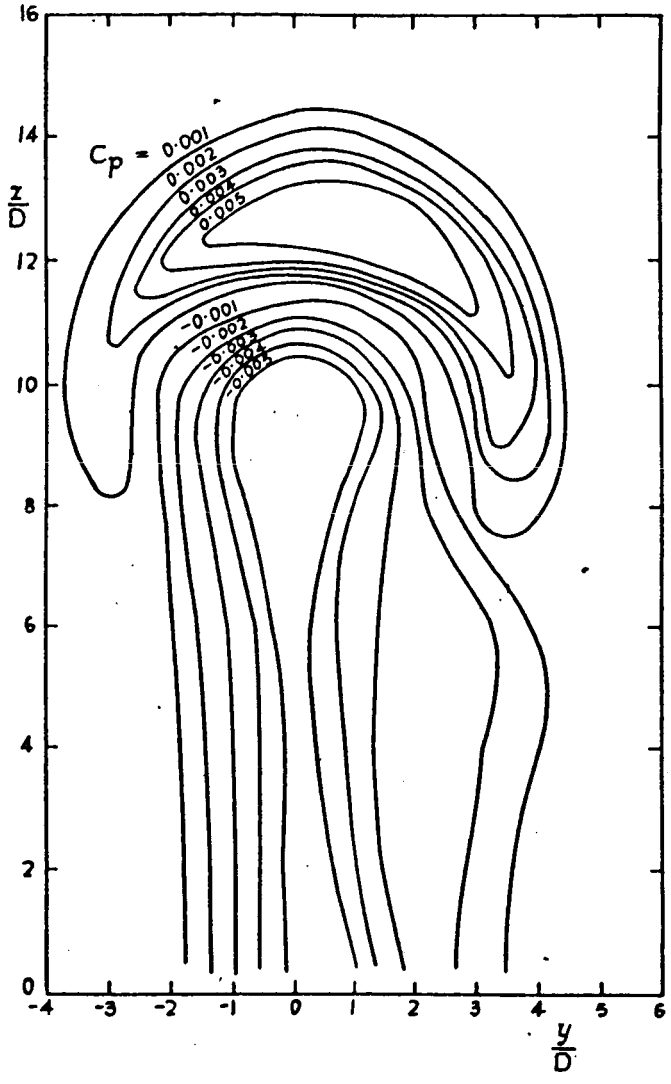

Fig. 5.29 Contours of constant pressure in a y-z plane at x/D = 11, U_j/U_∞ = 8, after Jordinson [8].

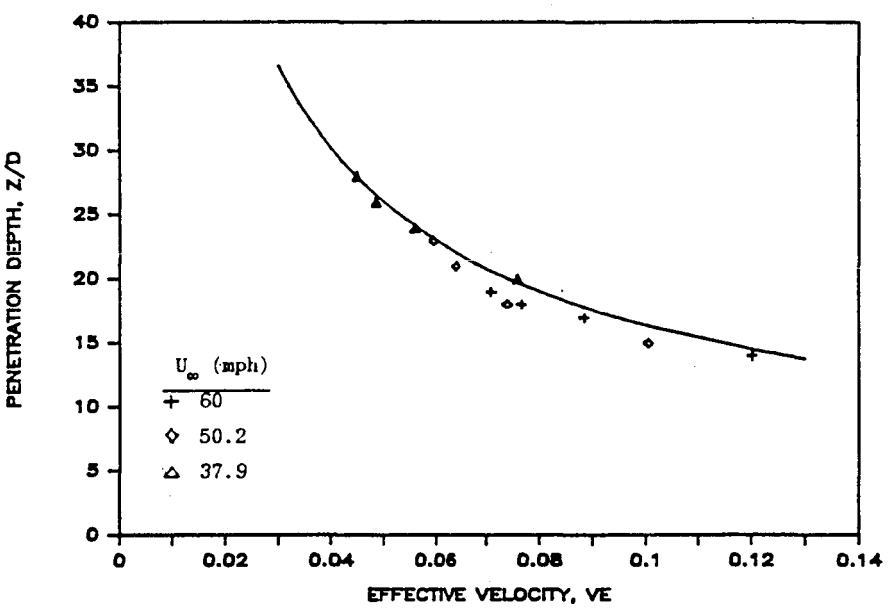

Fig. 5.30 Measured penetration depth of a single steady jet as a function of V_e, compared to Equation 3.3.

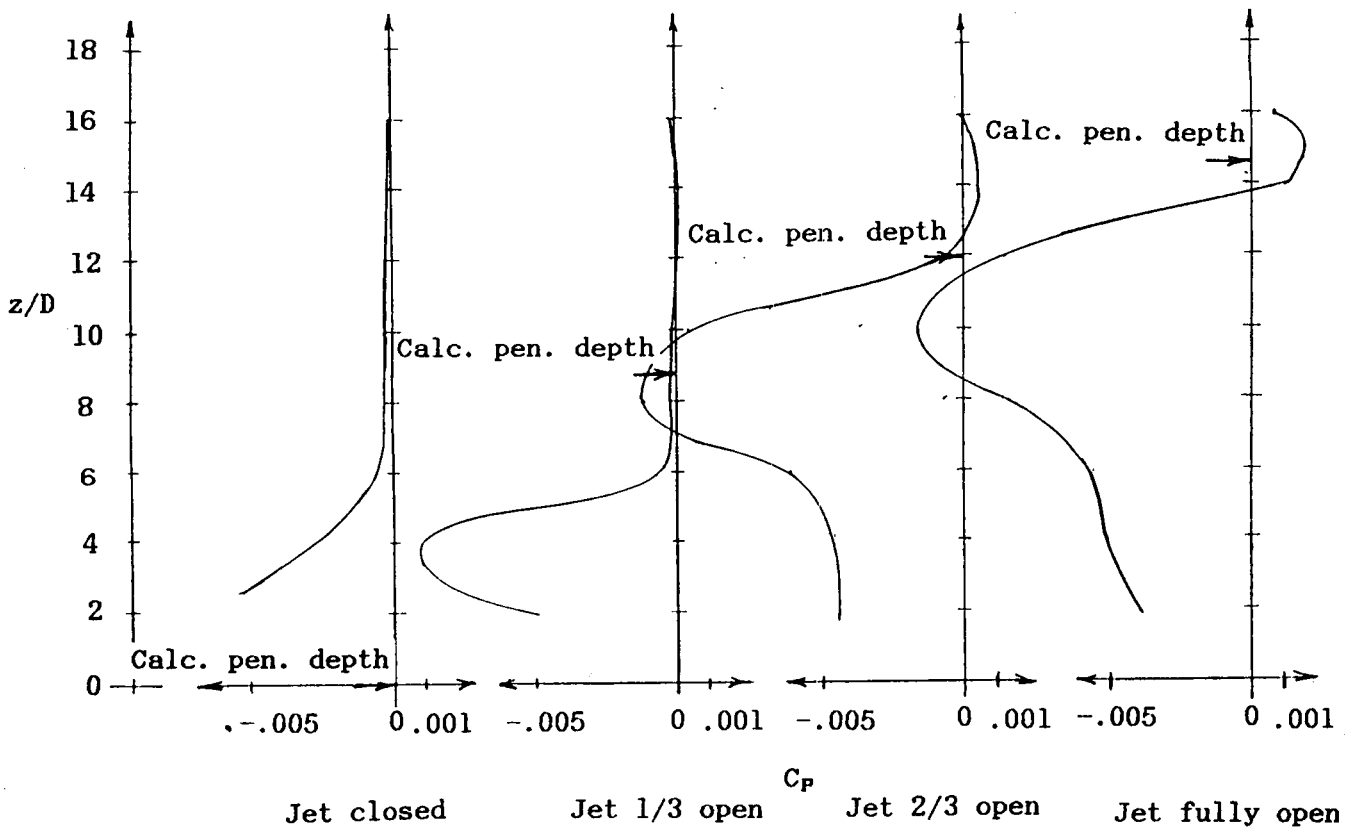

Fig. 5.31 Pressure profiles of a single steady jet at various jet valve settings, x/D = 11, U_∞ = 60 mph, 5 psig delivery pressure.

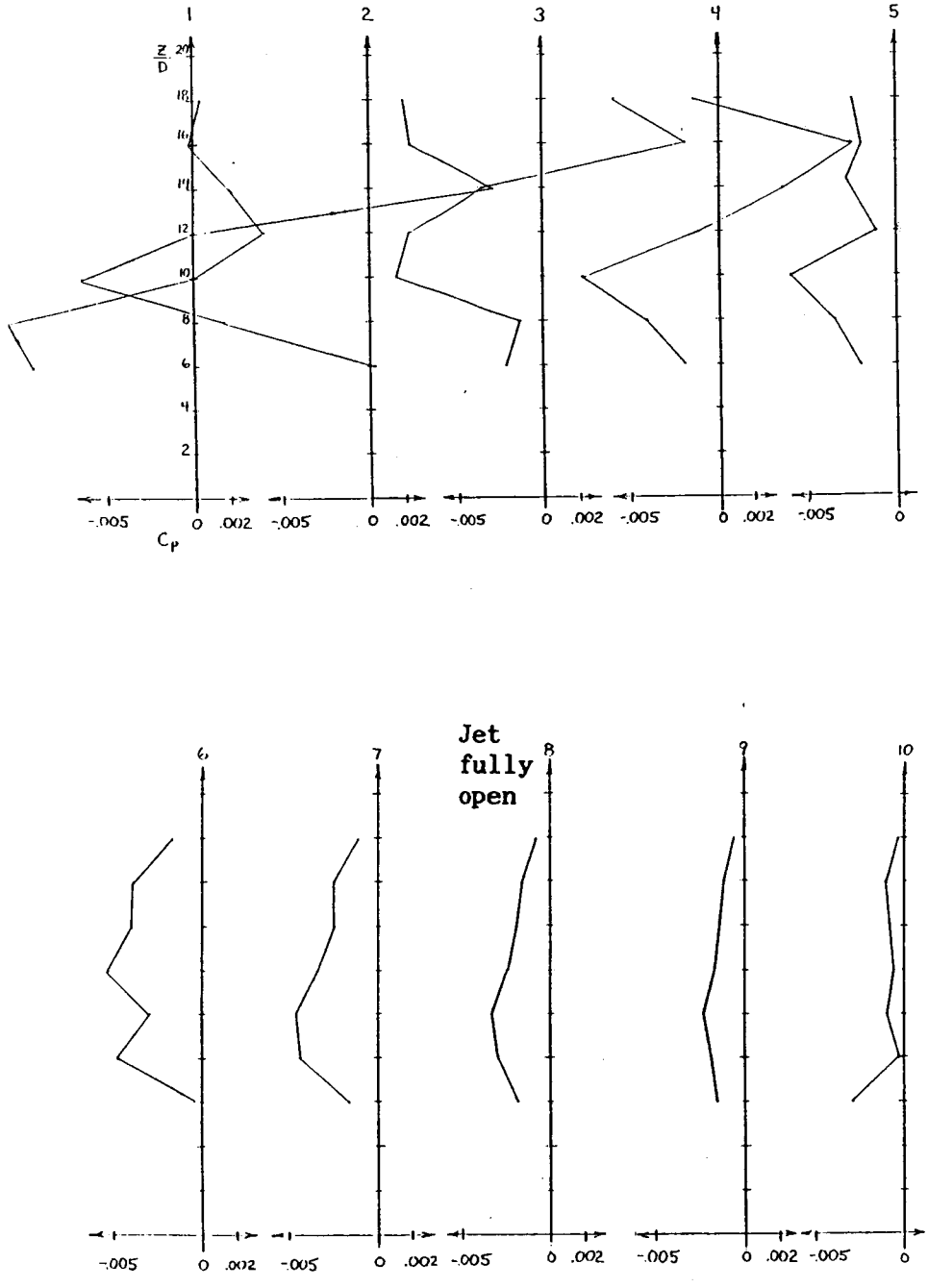

Fig. 5.32 Pressure profiles of a single pulsing jet at 10 evenly spaced instants in a jet period, x/D = 11, U_∞ = 60 mph, 5 psig delivery pressure, and a jet pulsing frequency of 200 Hz.

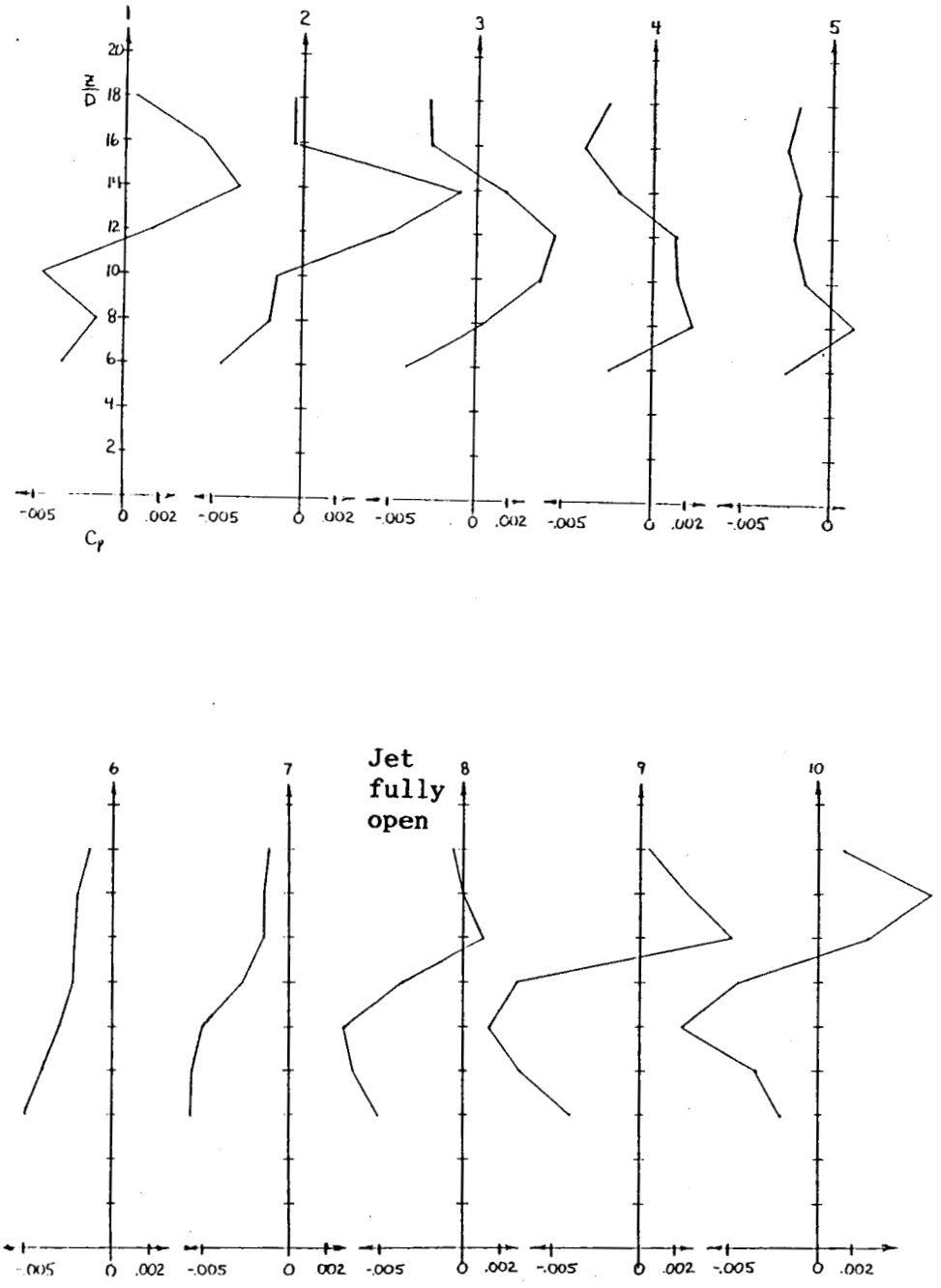

Fig. 5.33 Pressure profiles of a single pulsing jet at 10 evenly spaced instants in a jet period, x/D = 11, U_∞ = 60 mph, 5 psig delivery pressure, and a jet pulsing frequency of 665 Hz.

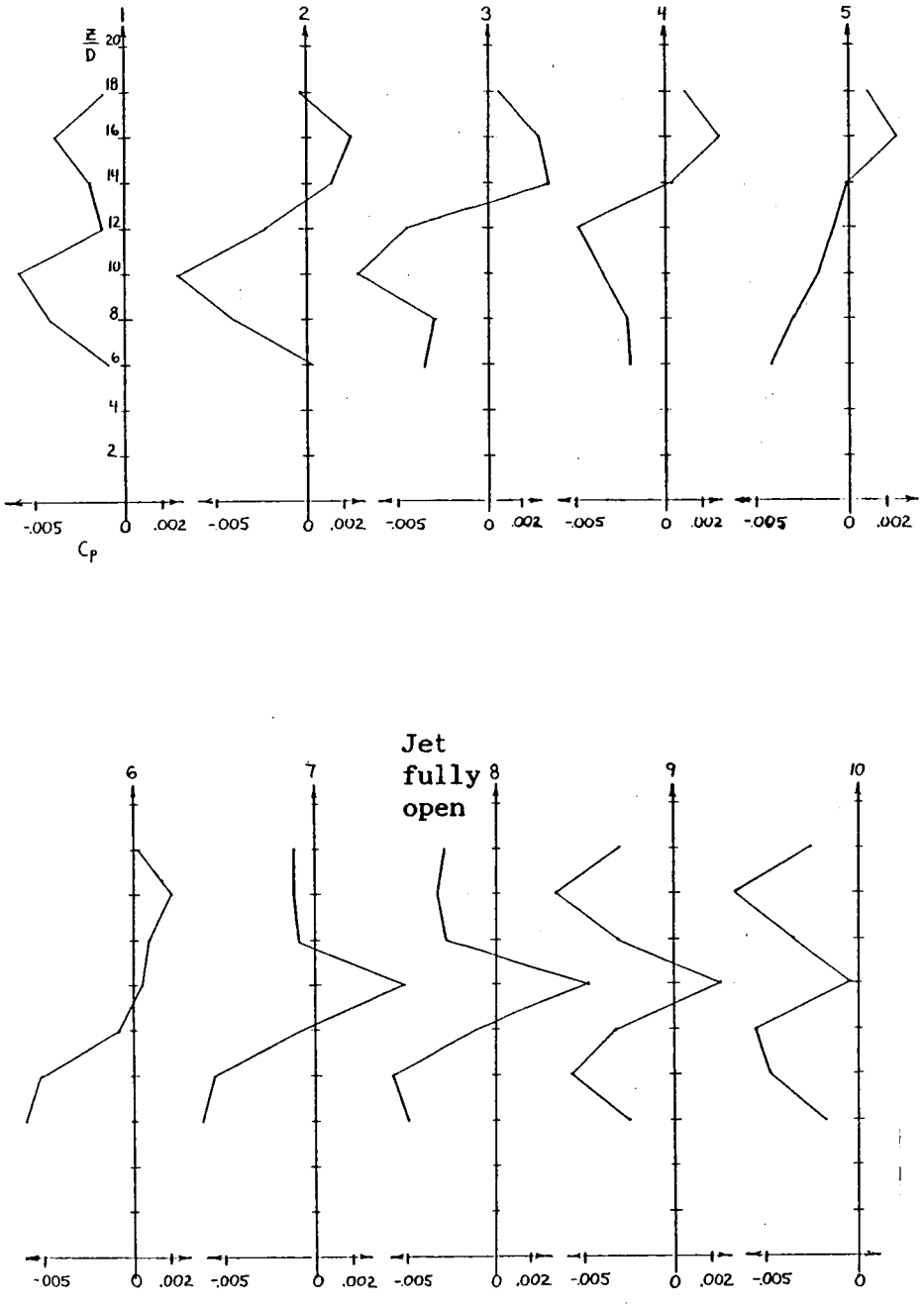

Fig. 5.34 Pressure profiles of a single pulsing jet at 10 evenly spaced instants in a jet period, x/D = 11, U_∞ = 60 mph, 5 psig delivery pressure, and a jet pulsing frequency of 1160 Hz.

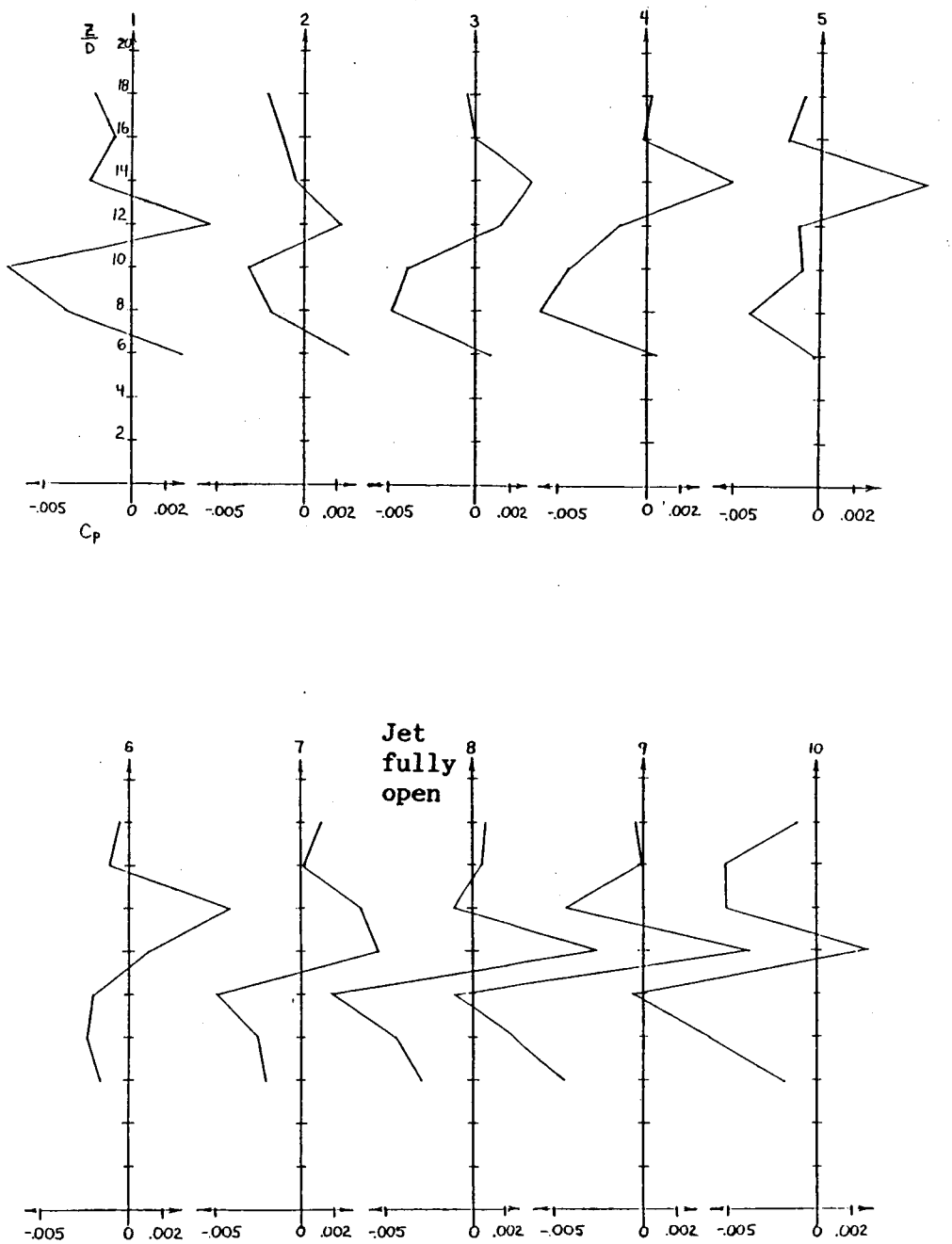

Fig. 5.35 Pressure profiles of a single pulsing jet at 10 evenly spaced instants in a jet period, x/D = 11, U_∞ = 60 mph, 5 psig delivery pressure, and a jet pulsing frequency of 3323 Hz.

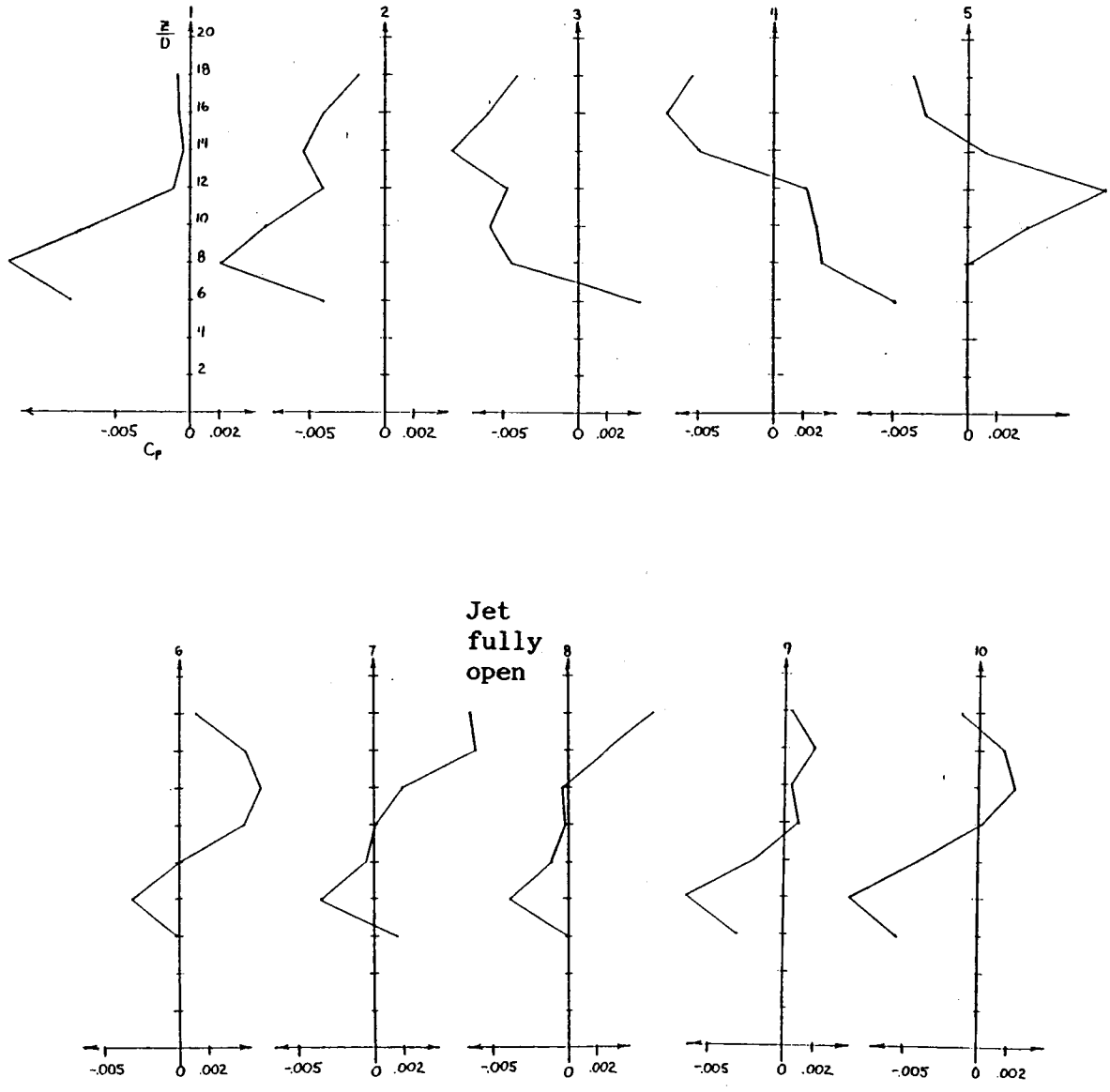

Fig. 5.36 Pressure profiles of a single pulsing jet at 10 evenly spaced instants in a jet period, x/D = 11, U_∞ = 60 mph, 5 psig delivery pressure, and a jet pulsing frequency of 5200 Hz.

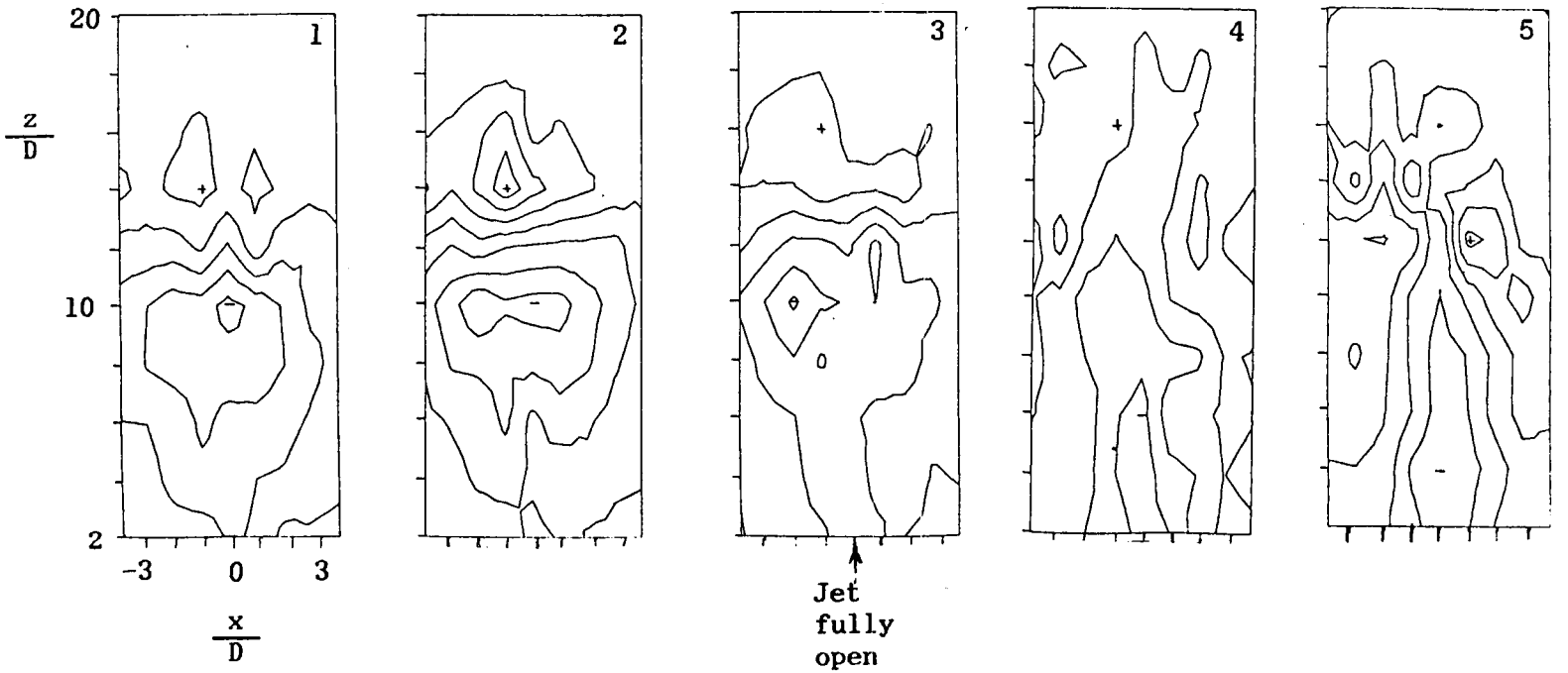

Fig. 5.37 Constant pressure contours of a single pulsing jet, x/D = 11, U_∞ = 60 mph, 5 psig delivery pressure, and a jet pulsing frequency of 715 Hz.

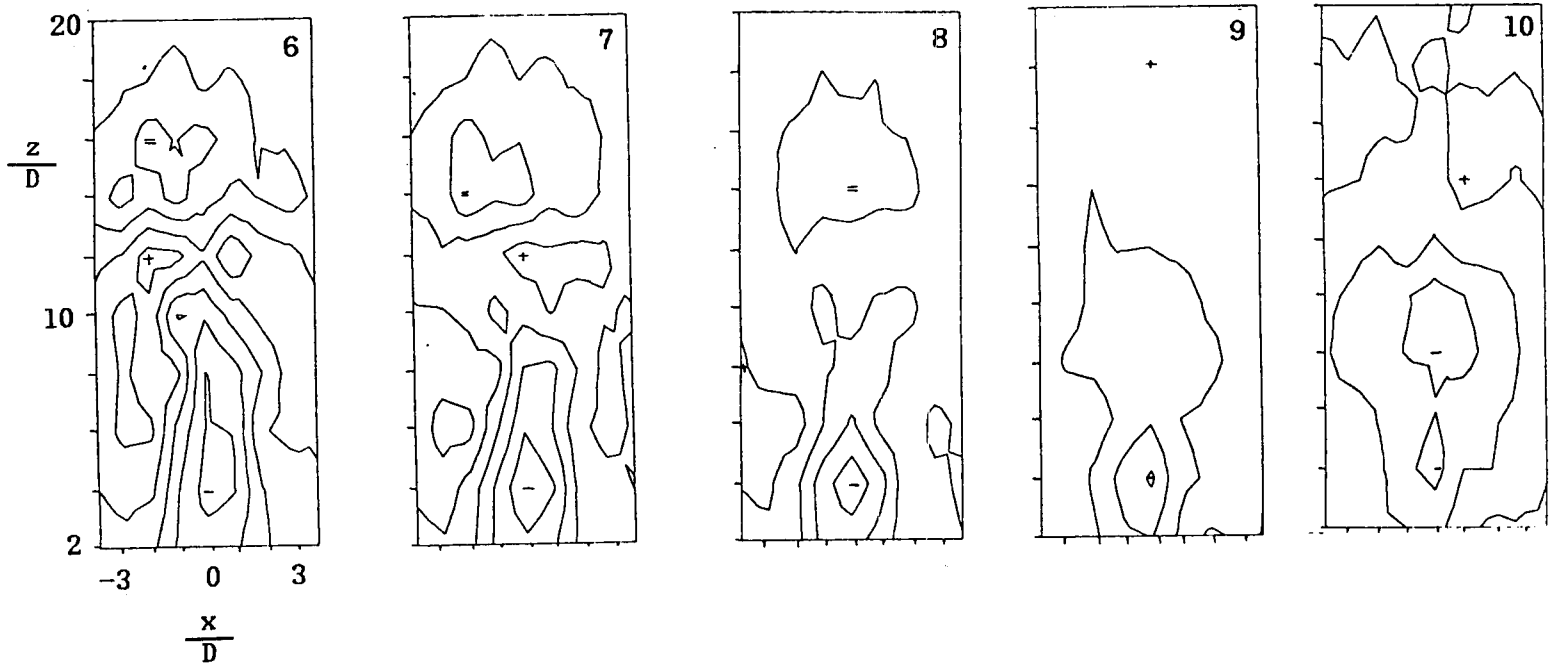

C_p { = = −.005, + = .003, − = −.007 | = = −.006, + = .001, − = −.008 | = = −.003, + = .0002, − = −.007 | + = −.0005, − = −.006 | + = .0005, − = −.005

Contour increments .002

Fig. 5.37 (cont.) Constant pressure contours of a single pulsing jet, x/D = 11, U_∞ = 60 mph, 5 psig delivery pressure, and a jet pulsing frequency of 715 Hz.

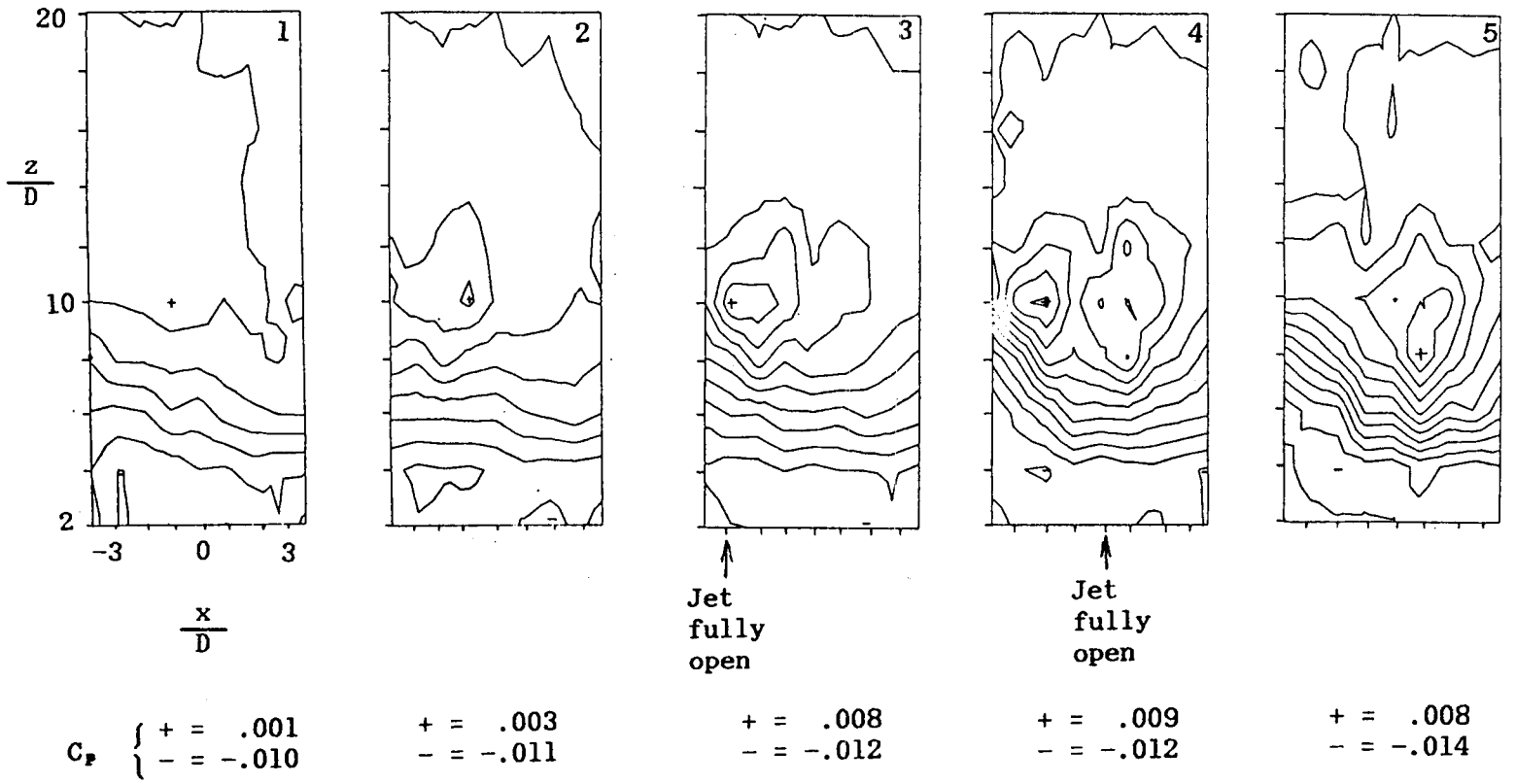

Fig. 5.38 Constant pressure contours of multiple pulsing jets, at x/D = 11, U_∞ = 60 mph, 5 psig delivery pressure, and a jet pulsing frequency of 715 Hz.

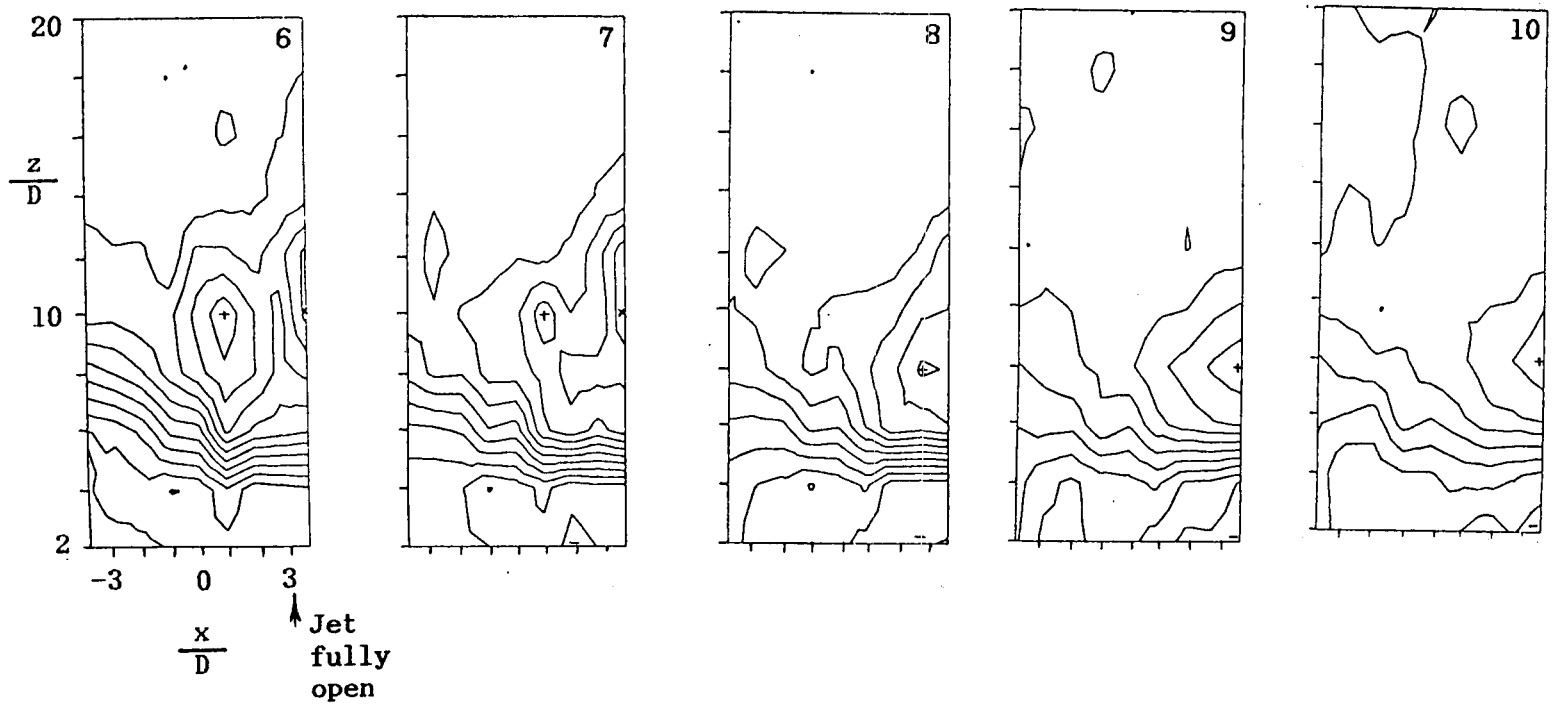

Fig. 5.38 (cont.) Constant pressure contours of multiple pulsing jets, at x/D = 11, U_∞ = 60 mph, 5 psig delivery pressure, and a jet pulsing frequency of 715 Hz.

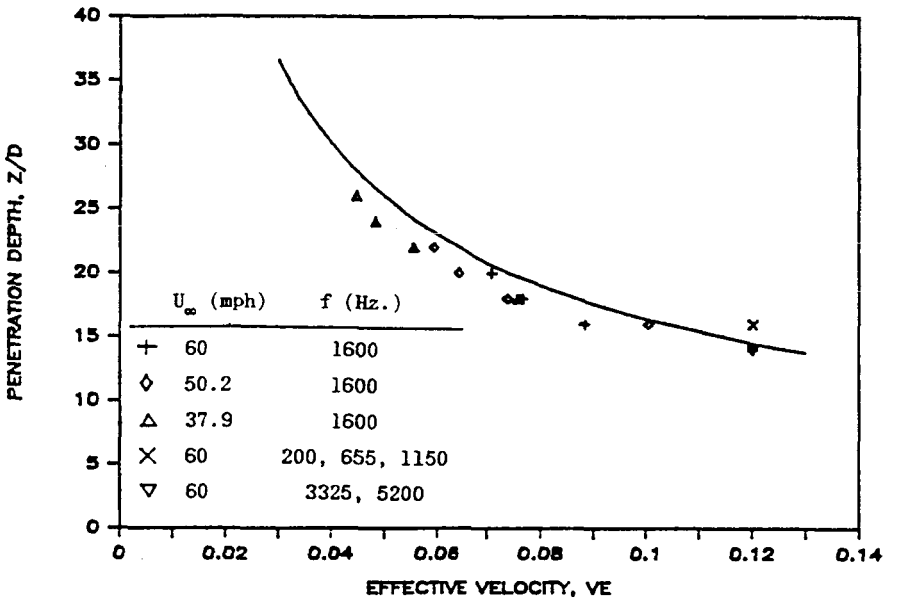

Fig. 5.39 Measured penetration depth of a single pulsing jet as a function of V_e, compared to Equation 3.3.